EFFECT OF ELECTROLYTE-TO-SULFUR RATIO ON THE PERFORMANCE OF LITHIUM-SULFUR BATTERIES WITH DIFFERENT ELECTROLYTE SYSTEMS

by

Ayça Fırtın

B.S., Chemical Engineering, Gazi University, 2015

Submitted to the Institute for Graduate Studies in
Science and Engineering in partial fulfillment of
the requirements for the degree of
Master of Science

Graduate Program in Chemical Engineering
Boğaziçi University

2023

ACKNOWLEDGEMENTS

Even though this journey seemed short for 2.5 years, it was not for me because there were many struggles, beyond this study. On this journey, I realized once again how important it is to be determined for a goal and never give up till the end. As my advisor said, being determined is important on this journey. I learned this through experience. There are many people whom I felt supported by and would like to thank.

First of all, today, if I am an engineer and engage in science as a woman, I owe these to him, Mustafa Kemal Atatürk, and this republic that he founded. Therefore, first, I would like to express my deepest gratitude to Atatürk. When I feel hopeless, he has always been a source of inspiration and hope to me, and he will always be. I will always continue to follow this path that he enlightens. Also, I would like to mention the words that Türkan Saylan said and affected me deeply; ‘‘Every educated woman owes a debt to this Republic.’’ So, I hope I can pay this debt by engaging in science.

I would like to express my gratitude to my advisor Assoc. Prof. Damla Eroğlu Pala, for including me in her research group. I would like to thank her for her knowledge, patience, support, kindness, guidance, and understanding. Her speech, advice, and encouragement always make me feel better when I feel stressed and down. I am very fortunate to study with her and take a place in her research group.

I am very grateful to my thesis committee members Prof. Ramazan Yıldırım and Assoc. Prof. Burak Ülgüt for accepting to be on my committee and reading and commenting on my thesis.

In addition, I would like to express my deepest pleasure to my parents, Recep and Mübeccel Fırtın, my sisters Alev Sürekbakan and Ayla Yalçın, and my brother-in-law Nazmi Sürekbakan and Fatih Yalçın whom I see as brothers. Also, thanks to my lovely nephew and niece, Umut Sürekbakan and Deniz Yalçın. I always feel their support in every aspect of my life, and I am very lucky to have this great family.

I would like to thank the members of the EChemE research group. At first, I am very thankful, especially to Kağan Yüksel for friendship, his support, and patience with my questions because he always shared his experience. I also thank Ayşegül Karakuş Kılıç and Atakan Ayhan for their friendship and support.

I think the best chance of my life might be to have great friends like them. I would like to thank Merve Yüce and Fethiye Kıyga, who are my childhood and best friends, for supporting me, and for always being with me at every time of my life. Also, I would like to thank Gül Dilara Saraylı, Ezgi Yıldırım Karakoyun, and Güliz Nil Varlı very much for their continued friendship regardless of time and place.

I also thank my friends Seymen İlke Kaykanat, Ayşe Korkut, and Duygu Kaya for their friendship and for sharing their experiences with me. Also, thanks to Destina Ekingen Genç for entertaining me with her funny life stories and being a great housemate. In addition, I thank Merve Yazar, who was my dormmate, for her friendship and also for sharing with me her playlist.

Finally, I would like to thank the Scientific and Technological Research Council of Turkey (TUBITAK), Grant No: 220N164 for financial support.

ABSTRACT

EFFECT OF ELECTROLYTE-TO-SULFUR RATIO ON THE PERFORMANCE OF LITHIUM-SULFUR BATTERIES WITH DIFFERENT ELECTROLYTE SYSTEMS

Lithium-sulfur (Li-S) batteries, one of the most promising alternatives for next-generation battery systems, have been a top research topic due to their high theoretical specific capacity and energy density. In Li-S batteries, battery performance is closely tied to certain materials and cell design parameters, particularly electrolyte design, due to the complex mechanisms in the cell. Herein, the effect of the electrolyte-to-sulfur (E/S) ratio, a critical electrolyte design parameter, on the performance of the Li-S batteries is investigated with various electrolyte systems. In order to understand the effect of the design parameters on battery performance, at first, experimental characterization is conducted by using galvanostatic cycling and electrochemical impedance spectroscopy (EIS). In the experimental study, seven different types of electrolytes with four different E/S ratios of 6 μL/mg, 9 μL/mg, 16 μL/mg, and 23 μL/mg are used. In general, the lowest E/S ratio, 6 μL/mg, has a better performance compared to the highest E/S ratio because the high amount of electrolyte escalates the polysulfide shuttle mechanism, affecting the battery performance adversely. In addition, EIS characterization is used to investigate the resistance of cells with an E/S ratio of 6 μL/mg and 9 μL/mg. Then, zero-dimensional and one-dimensional electrochemical models are developed to mechanistically study the effect of the E/S ratio on the discharge profile. The 0-D model can capture the expected trend of the variance of the discharge profile with changing E/S ratio; the capacity decreases significantly with decreasing E/S ratio. To model the impact of the E/S ratio on the discharge profile of Li-S for different electrolyte systems, selected model parameters were changed systematically. At the different values of k_{S8}, both the 0-D and 1-D models predict other trends for the dependence of discharge profiles on the E/S ratio. Consequently, both models can capture the effect of the E/S ratio on the discharge behavior for different electrolyte systems implicitly through the variation of k_{S8}. It is seen clearly from this study that the impact of the electrolyte amount on battery performance changes according to the types of electrolytes.

ÖZET

FARKLI ELEKTROLİT SİSTEMLERİNDE ELEKTROLİT-SÜLFÜR ORANININ LİTYUM-SÜLFÜR BATARYA PERFORMANSINA ETKİSİ

Yeni nesil batarya sistemleri için umut vadeden alternatiflerden biri olan lityum-sülfür (Li-S) bataryaları, yüksek teorik enerji yoğunluğu ve kapasitesi nedeniyle yoğun araştırma konusu olmuştur. Kompleks mekanizması nedeniyle Li-S bataryalarının performansı malzeme ve hücre tasarım parametreleriyle, özellikle de elektrolit tasarımı ile yakından ilişkilidir. Bu çalışmada da , elektrolit tasarım parametresi olarak farklı elektrolit sistemlerinde elektrolit-sülfür (E/S) oranının batarya performansına olan etkisi incelenmiştir. Tasarım parametrelerinin batarya performansına olan etkisini inceleyebilmek için ilk olarak galvanostatik döngüleme ve elektrokimyasal empedans spektroskopi (EIS) yöntemleri kullanılarak deneysel karakterizasyon yapılmıştır. Deneysel çalışmada yedi farklı elektrolit tipinde 4 farklı E/S oranı (6 µL/mg, 9 µL/mg, 16 µL/mg ve 23 µL/mg) kullanılarak galvonastatik döngüleme metodu ile batarya performansı incelenmiştir. Genel olarak, yüksek elektrolit miktarı batarya kapasitesini olumsuz etkileyen polisülfid mekik mekanizmasını arttırdığı için yüksek E/S oranına sahip pillerde performans iyi değilken düşük E/S oranı olan 6 µL/mg, daha iyi performans gözlemlenmiştir. Ayrıca EIS metodu ile iki farklı E/S oranın, 6 µL/mg ve 9 µL/mg, batarya resistansına etkisi incelenmiştir. Deneysel çalışmanın yanı sıra, E/S oranının batarya performansına olan etkisini mekanistik olarak anlayabilmek için sıfır boyutlu tek boyutlu elektrokimyasal modeller geliştirilmiştir. Sonuç olarak 0-D modeli ile elektrolit miktarının etkisi teorik olarak beklenileni karşılamaktadır; E/S oranın azalmasıyla birlikte kapasite de azalır. Farklı elektrolit sistemlerinde E/S oranın etkisini inceleyebilmek için, belirlenen model parametreleri sistematik bir şekilde değiştirilmiştir. Her iki modelde de farklı k_{S8} değerlerinde E/S oranın değişmesiyle farklı trendler elde edilmiştir. Sonuç olarak iki model de k_{S8} değişimi ile farklı elektrolit sistemleri için E/S oranın batarya deşarj davranışına olan etkisi yakalayabilmektedir. Bu çalışmadan da anlaşılacağı üzere elektrolit miktarını batarya performansına olan etkisi elektrolit tipine göre farklılık göstermektedir.

TABLE OF CONTENTS

LIST OF FIGURES

LIST OF TABLES

LIST OF SYMBOLS

a	Electrochemically active area
a_0	Electrochemically active area parameter
b	Bruggeman's coefficient
C_i	Concentration of components, i
$C_{i,,ref}$	Reference concentration of components, i
D_i	Diffusion coefficient of species i
$D_{i,0}$	Diffusion coefficient of species i in bulk
E_j	Standard potential of electrochemical reaction *j*
E_j^0	Standard open circuit potential of electrochemical reaction *j*
F	Faraday's constant
i_e	Liquid phase current density
i_j	Current density of electrochemical reaction j
$i_{j,ref}^0$	Exchange current density of jth electrochemical reaction
i_s	Solid phase current density
$I_{applied}$	Applied current density
k_{Li_2S}	precipitation rate constant of k_{Li_2S}
k_{S_8}	precipitation rate constant of k_{S_8}
K_{sp,Li_2S}	Solubility product of precipitate Li_2S
K_{sp,S_8}	Solubility product of precipitate S_8
L	Cathode thickness
n_j	The number of electrons transferred
N_i	Flux of species, i
$p_{i,j}$	Anodic reaction order of species *i* in electrochemical reaction *j*
$q_{i,j}$	Cathodic reaction order of species *i* in electrochemical reaction *j*

R	Universal gas constant
R_k	The production/consumption rate of the solid species
$s_{i,j}$	Stoichiometric coefficient of species i in electrochemical reactions, j
t	Time
T	Temperature
z_i	Charge number of species i
V_{cell}	Cell voltage
$\tilde{V}_k$	Molar volume of precipitate k
α_{a_j}	Transfer coefficient of anodic reaction *j*
α_{C_j}	Transfer coefficient of cathodic reaction, *j*
ε	Cathode porosity
ε_{Binder}	Binder volume fraction
ε_{Carbon}	Carbon volume fraction
$\varepsilon_{initial}$	Initial cathode porosity
$\varepsilon_{Li_2S_{(s)}}$	Li_2S volume fraction
$\varepsilon_{Li_2S_{(s)},initial}$	Initial S volume fraction
ε_{ref}	Refence cathode porosity
$\varepsilon_{S_{8(s)}}$	$S_{8(s)}$ volume fraction
$\varepsilon_{S_{8(s)},initial}$	Initial $S_{8(s)}$ volume fraction
η_j	Overpotential of electrochemical reaction *j*
ξ	An empirical morphology parameter of the precipitates
ρ_{Binder}	Binder density
ρ_C	Carbon density
$\rho_{Cathode}$	Cathode density
$\rho_{Electrolyte}$	Electrolyte density

ρ_S	Sulfur density
σ	Electrolyte conductivity
Φ_e	Liquid phase potential
Φ_s	Solid phase potential
ω_s	Sulfur weight fraction
ω_B	Binder weight fraction

1. INTRODUCTION

In today's world, technology is developing day by day, and almost every day, new types of electric devices are released or improved by adding new applications. Therefore, the demand for energy is also increasing along with these innovations in electric devices, especially electric vehicles that have been widely used recently. At this point, batteries as energy storage systems have a significant role in supplying this demand. Even though Li-ion batteries, which are widely used in commercial applications, have high energy and power density and long life, they have high costs and limited capacity for newly emerging technologies such as electric vehicles [1–3].

Consequently, researchers seek new battery systems with longer cycle life, higher capacity, and safer than commercial batteries. Lithium-sulfur (Li-S) batteries have recently been one of the top research topics on next-generation energy storage technologies [4]. This is because Li-S batteries have a high theoretical specific energy that is 3-5 folds (nearly 2600 Wh/kg) of Li-ion batteries. They have a high theoretical specific capacity,1675 mAh/g as well [5–9]. In addition to this, elemental sulfur used as the active cathode material is low-cost, naturally abundant, non-toxic, and has a wide operation temperature range [10–13]. Due to these features, Li-S batteries are a great option to meet the increasing energy demand and diminish emissions.

Li-S batteries mainly consist of a Li metal anode, a polymer-based separator, a sulfur-carbon cathode, and an organic electrolyte. In addition, copper foil (Cu foil) and Aluminum foil (Al foil) are used as current collectors at the anode and cathode sides of Li-S batteries, respectively. Figure 1.1 illustrates the typical Li-S battery schematic description [14,15]. The overall redox reaction with a standard potential of U_0= 2.2 V taking place in Li-S batteries is given as [16,17]

$$16\mathrm{Li} + \mathrm{S_8} \longrightarrow 8\mathrm{Li_2S}, \tag{1.1}$$

$$\mathrm{Li} \longrightarrow \mathrm{Li^+} + \mathrm{e^-}. \tag{1.2}$$

In contrast to this simple overall reaction occurring in the Li-S batteries, the mechanism is more complicated than seen. During discharge, lithium metal is oxidized at

the anode, the negative electrode (Equation (1.2)). Li^+ ions produced at the anode move toward the cathode, the positive electrode, through the electrolyte and the separator. In the meantime, the electrons move to the cathode via the external circuit, generating the electrical current. Then, sulfur is reduced at the cathode side, reacting with Li^+ ions through a multi-step mechanism, producing the end discharge product Li_2S. During charge, the reverse of these steps occurs [18–20].

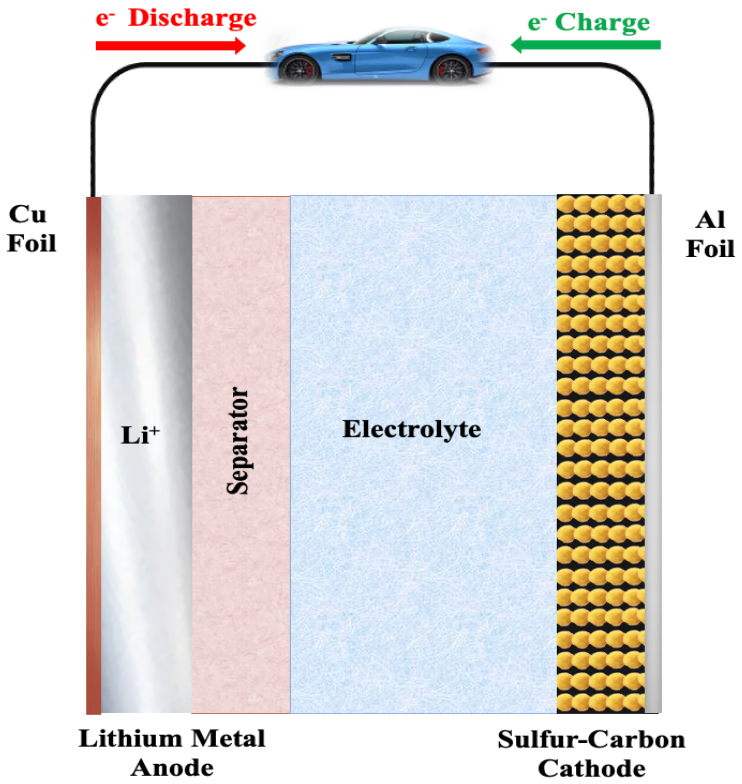

Figure 1.1. Schematic description of lithium-sulfur (Li-S) batteries.

There are two voltage plateaus, the low and the high, in the typical discharge profile of Li-S batteries given in Figure 1.2. The discharge profile may be divided into four regions where several complex reactions occur in each region.

Elemental sulfur first dissolves in the electrolyte and is then reduced forming Li_2S_8, and Li_2S_8 dissolves into the electrolyte in Region I in which the reactions are

$$\frac{1}{2}S_{8(l)} + e^- \rightleftharpoons \frac{1}{2}S_8^{2-}, \tag{1.3}$$

$$2Li^+ + S_8^{2-} \rightleftharpoons Li_2S_8. \tag{1.4}$$

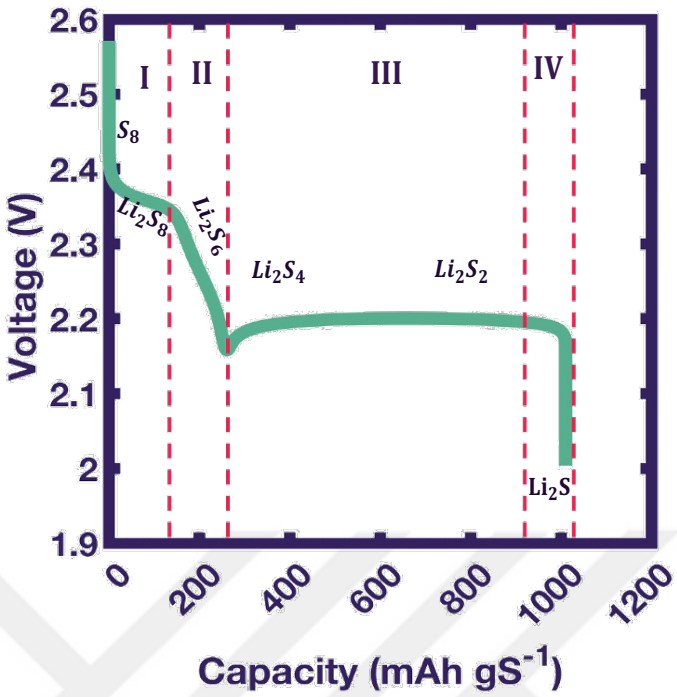

Figure 1.2. Illustration of the discharge profile of Li-S batteries.

In Region II, the reduction reaction of Li_2S_8 to a lower-order polysulfide chain occurs. Meanwhile, the cell voltage decreases sharply, and the electrolyte viscosity increases because of the rising the concentration of the polysulfide anions and the diminishing length of the sulfur chain. In this region, reactions are

$$\frac{3}{2}S_8^{2-} + e^- \rightleftharpoons 2S_6^{2-}, \tag{1.5}$$

$$2Li^+ + S_6^{2-} \rightleftharpoons Li_2S_6. \tag{1.6}$$

In Region III, low-order polysulfides, Li_2S_4 and Li_2S_2 form. In this region, the voltage of the battery stays almost constant, and the low voltage plateau appears, promoting the capacity of the cell and the reactions are

$$S_6^{2-} + e^- \rightleftharpoons \frac{3}{2}S_4^{2-}, \tag{1.7}$$

$$2Li^+ + S_4^{2-} \rightleftharpoons Li_2S_4, \tag{1.8}$$

$$\frac{1}{2}S_4^{2-} + e^- \rightleftharpoons S_2^{2-}, \tag{1.9}$$

$$2Li^+ + S_2^{2-} \rightleftharpoons Li_2S_{2(s)}. \tag{1.10}$$

In the last region, the end discharge product Li_2S is produced. This part has slow kinetics and high polarization arising from the non-conductivity and insolubility of both Li_2S_2 and Li_2S. Reactions in this, region are

$$\frac{1}{2}S_2^{2-} + e^- \rightleftharpoons 2S^{2-}, \tag{1.11}$$

$$2Li^+ + S^{2-} \rightleftharpoons Li_2S_{(s)}. \tag{1.12}$$

Although Li-S batteries are highly promising due to their positive aspects like high theoretical specific capacity and energy density, there are several challenges that need to be handled before commercialization. One of the biggest problems is the shuttling of the polysulfides (LiPSs) produced by the complex reactions inside the cell. LiPSs migrate to the anode side, causing unwanted side reactions with Li, and then move back to the cathode side during cycling. This back-and-forth transport of the LiPSs within the cell is called the polysulfide shuttle mechanism [12], [21–23]. The polysulfide shuttle mechanism leads to crucial problems. Firstly, the LiPSs can react with the lithium easily, causing the deterioration of the anode [24]. Secondly, it results in capacity fading due to the loss of sulfur at the cathode surface [25]. And also, the solubility and mobility of the LiPSs cause self-discharge, resulting in deficient coulombic efficiency and short cycle life [12]. The second main problem seen in Li-S batteries is the low electronic conductivity of S and Li_2S. The precipitation of Li_2S passivates the cathode surface, hindering the reaction kinetics and thus declining capacity [26]. In addition, the unsteadiness of Li metal causes grooving dendrites on the anode, decreasing active Li material and giving rise to safety issues. Another problem is volumetric growth during cycling due to the considerable difference between Li_2S and S densities [27–30].

There are different approaches in the literature to overcome these challenges. One of the most common approaches is engineering the cathode. By the modification of the cathode material, the electronic conductivity of the cathode can be improved, and the dissolution of the LiPSs can be diminished. LiPSs can be caught by the porous structure of the cathode by tailored adsorption abilities [5], [31–34]. Another approach is the use of a protective layer on the anode surface in order to protect the anode surface [35–37]. In addition, the separator may be modified with an extra layer in order to mitigate the LiPSs migration and hinder the polysulfide shuttle mechanism [38–42].

One of the most critical approaches to improve battery performance is electrolyte design, as the electrolyte type, properties, and amount control the dissolution of the polysulfides and, thus, the reaction and polysulfide shuttle mechanisms. First of all, the selection of the components of the electrolyte is highly important for the performance of the battery. The salt used in the electrolyte should have high ionic conductivity and not lead to unwanted side reactions with the LiPSs. Next, the properties of solvents, such as viscosity, solubility, and stability against lithium and LiPSs, are also crucial for performance [42]. The final component used in electrolytes to decrease the shuttle effect and self-discharge rate is additives; an additive such as $LiNO_3$, the most common additive used in Li-S cells, improves the coulombic efficiency and battery life because it reacts with the lithium and leads to a protective SEI layer on the surface of the lithium, which hinders the side reactions between Li and polysulfides and dendrite growth [41], [43,44].

Another electrolyte design parameter is the concentration of the electrolyte. A high concentration of electrolyte stabilizes the Li metal, resulting in high coulombic efficiency and improvement of the SEI layer. Furthermore, high concentrations suppress the polysulfide shuttle mechanism. On the other hand, low salt concentrations in the electrolyte lead to low viscosity and correspondingly better wettability [41], [45,46].

The electrolyte-to-sulfur ratio (E/S) is one of the most crucial factors for electrolyte design because it considerably affects the electrochemical performance and system- and cell-level specific energy and energy density of the Li-S cells. In addition, the electrolyte-to-sulfur ratio plays a significant role in the reactions that occur on the cathode surface and the shuttle mechanism of polysulfide because of its effect on the polysulfide concentration on the cathode surface [14], [16], [45]. At very low E/S ratios, the discharge capacity and cycling performance of the cells are poor; an increase in the electrolyte viscosity due to the rising polysulfide concentration results in lower ionic conductivity and poor reaction kinetics. Moreover, low E/S ratios may lead to the deficiency of the electrolyte in the cell due to Li metal consuming the electrolyte via unwanted reactions. An increase in the electrolyte amount impacts the voltage, cycle life and capacity of the cell favorably by improving sulfur utilization and reaction kinetics. However, a further increase in the E/S ratio adversely affects capacity retention since it may accelerate the polysulfide shuttle mechanism. High electrolytes amount also diminishes energy [4], [43–48].

1.1. Aim and Scope of the Work

There is excellent attention on Li-S batteries among researchers and companies as alternative energy storage systems due to their perfect features such as high theoretical specific energy, high energy density, eco-friendliness, and low cost compared to commercial batteries. However, there are crucial challenges in these batteries, which have not been commercialized yet. These challenges include the polysulfide shuttle mechanism, the morphological changes in the anode, and the insulating nature of S and Li_2S. Therefore, there are various approaches in the literature to overcome these problems [41], [48]. One of these approaches is electrolyte design. As Q. Jin stated, an electrolyte is like the blood of the batteries [49] because it enables ions to transport between electrodes. As seen from this metaphor, electrolytes play a vital role in battery performance by affecting ionic transportation, the polysulfide shuttle mechanism, and cycling characteristics. The electrolyte-to-sulfur ratio is one of the crucial electrolyte design parameters because it significantly impacts battery performance. Reaction and precipitation/dissolution kinetics, thus, the sulfur utilization improves greatly at higher E/S ratios, resulting in higher discharge capacities and cycling performance. On the other hand, to achieve high energy density at the pack level, which is critical for commercializing these batteries, the electrolyte-to-sulfur ratio should be minimized within the cell. Therefore, the bottleneck of achieving high-performance Li-S batteries is to attain reasonable capacities and cycling performance at low E/S ratios, which may be possible using electrolyte systems differing from the conventional one.

Although the electrolyte amount is crucial for the performance of the cell, there is limited research on the impact of the E/S ratio on performance of the battery, specifically for alternative electrolyte systems [50]. Some of these studies are discussed in Chapter 2, “Literature Review” section of the thesis. As is clearly seen from this section, the impact of the E/S ratio on the performance of the Li-S battery is tremendous, and a better understanding of this critical connection is required. In addition, for investigating the impact of the E/S ratio on performance of the cell, generally, 1M LiTFSI in DOL: DME electrolyte, which is the most common electrolyte, is used in the literature. However, as discussed above, the discharge behavior of a Li-S cell at different electrolyte systems, which may be promising at lower E/S ratios, should be better comprehended.

Understanding the effect of the electrolyte-to-sulfur ratio on battery performance might enable researchers to shed light on overcoming the challenges seen in Li-S batteries. In this regard, the aim of this study is to understand the influence of the E/S ratio on the the Li-S battery performance with different electrolyte systems through experimental characterization and electrochemical modeling. The impact of the E/S ratio on the voltage curve, discharge capacity, cycle life, capacity retention, and cell resistance of Li-S cells is examined experimentally using galvanostatic cycling and electrochemical impedance spectroscopy (EIS) methods. Two electrochemical models, zero-dimensional neglecting mass transport and one-dimensional considering concentration variance, are also proposed to discuss the influence of the E/S ratio on the discharge profile. Therefore, this study is believed to be light supporting the literature.

For this purpose, more details regarding the experimental work, such as the chemicals used, the electrolyte amounts tested, cell assembly, and electrochemical tests, are given in Chapter 3, “Experimental Work.” Two types of electrochemical models are developed in this study: zero-dimensional and one-dimensional electrochemical models. The next part of this thesis, Chapter 4, contains information about these models in detail, such as assumptions, reactions, and equations used in these models. Then, the results, together with the discussions of the experimental study, are given in the first part of Chapter 5. The second part of Chapter 5 includes discussions on the results of the zero-dimensional and the one-dimensional models. The last part of this thesis presents the conclusions of the study.

2. LITERATURE REVIEW

The objective of this thesis is to explore the impact of the electrolyte-to-sulfur ratio on the performance of Li-S batteries not only through experimental characterization but also mechanistically by developing electrochemical models. Thus, first, a literature review of experimental studies on the effect of electrolyte amount on battery performance is given. Then, electrochemical models developed to understand the discharge pattern and performance of the Li-S batteries in the literature are discussed in this section of the thesis.

2.1. Experimental Studies on the Effect of the Electrolyte-to-Sulfur Ratio on Li-S Battery Performance

Eunho Cha et al. [51] investigated the impact of three different E/S ratios (6, 8, and 10 mL/g) on a three-dimensional carbon nanotube cathode without a binder. According to the cycling performance results, the capacity retention of the cell with a higher E/S ratio is more stable than others; the capacity of the cell containing the lowest E/S ratio decreases continuously with cycling. They concluded that the discharge capacity diminishes along with the decrease in the E/S ratio.

Chao Shen et al. [52] studied the effect of different E/S ratios on performance of the battery by using Li_2S_4 as an active material instead of elemental sulfur to prevent the possible limitation of the solubility of elemental sulfur. It is seen that there is a sharp decrease in the capacities of high and low-voltage plateaus at low E/S ratios. In contrast to the conventional Li-S cell, Li_2S_4 utilization is high even at low E/S ratios.

Instead of using high E/S ratios, Frank Y. Fan and Yet-Ming Chiang [53] studied the influence of low electrolyte amount on performance. They postulated that there is a significant impact of the electrolyte-to-sulfur ratio on electrolyte properties and battery performance, including ionic conductivity and current density. They concluded that low E/S ratios reach high polysulfide concentrations in Li-S batteries. Lower capacity is seen for an E/S ratio of 2.4 mL/g, compared to 4.2 and 7.9 mL/g, which have the same capacity.

Shuru Chen et al. [54] who used dimethyl sulfide (DMDS) as a co-solvent to improve the alternative electrochemical pathway previously, investigated the impact of low E/S ratios containing organosulfides on the capacity of the batteries. In contrast to the cell that has a high E/S ratio, the cells containing a low E/S ratio have low capacity. However, the cell prepared with DMDS shows a more stable specific capacity (almost 1000 mAh g^{-1}) even at a low E/S ratio of 5 mL/g. Also, the capacity of the cell produced with DMDS is two-fold higher than the cell containing DOL: DME for not only high E/S ratios but also low E/S ratios.

H.M. Bilal and D. Eroglu [55] studied the relationship between the E/S ratio and performance of the Li-S batteries for four different electrolyte amounts (35, 20, 13, and 10 mL/g). The E/S ratio of 20 mL/g shows the highest initial discharge capacity, but the best capacity retention is seen for 13 mL/g. Also, they concluded that an increase in the E/S ratio raises the cell capacity and voltage by boosting cathode kinetics, but a further rise in the electrolyte amount has an adverse effect on capacity retention by accelerating the shuttle mechanism leading to corrosion on the anode surface. Briefly, they analyzed that the best battery performance is seen for the E/S ratio of 13 mL/g.

Y. Zhao et al. investigated the interfacial processes in Li-S batteries under low electrolyte conditions, and they concluded that the reason for having low specific energy in a low E/S ratio is the obstruction of the kinetics taking place during the cycling [56].

A. Kilic and D. Eroglu studied the influence of the design parameters, including the electrolyte to sulfur ratio, on cell resistance and performance of the batteries. They investigated the influence of two different E/S ratios on capacity at a constant carbon-to-sulfur ratio, C/S, of 1 and constant sulfur loading. The result of this investigation shows that an E/S ratio of 6 mL/g leads to an initial capacity of 485 mAh/g, which declines sharply with cycling. As for the E/S ratio of 19 mL/g, the cell starts cycling with almost 1292 mAh/g, which decreases to nearly 800 mAh/g after cycling. It was concluded that the best performance is seen at higher E/S ratios, mainly due to much lower cell resistances, and the capacity fade is faster in cells with low E/S ratios [57].

Q. Jin et al. studied Li-S battery performance at various E/S ratios (1, 2, 3, 4, 6, and 10 µL/mg) at different C-rates (C/125, C/40, C/20, and C/10). In their study, they used 1M LiTFSI in DOL: DME (1:1 vol%). They did not report any significant change in the capacity of the cell for low E/S ratios at low C-rates, C/125 and C/40; reported capacities are around 1200-1300 mAh/g at this condition. On the other hand, at higher C-rates, C/20 and C/10, the capacity of the cells with low E/S ratios, especially 1 µL/mg, decreases tremendously, and voltage plateaus are not clear. They concluded that in lean electrolyte conditions, the dissolution of the LiPSs adversely affects the ionic conductivity and wettability of the electrolyte, resulting in a decrease in the high-voltage plateau capacity. Also, they asserted that one of the main causes of the failure of lithium-sulfur cells is the degradation of the electrolyte in the case of lean electrolyte [49].

Another study was carried out by V.S. Kolosnitsyn et al. to understand the causes of the effect of the E/S ratio (1, 1.5, 2, 3, and 4 µL/mg) on the performance of the Li-S batteries. In this study, they used two types of lithium salts, CF_3SO_3Li and $LiClO_4$, in sulfolane, which differs from the common electrolyte used in the literature. The capacity of the cell diminishes along with the diminishing the E/S ratio for both electrolyte systems; the E/S ratio affects the battery capacity to the same degree for both electrolyte systems. In addition, they found that the minimum E/S ratio needed for acceptable sulfur utilization while cycling is a function of the constitution of the solvate complexes of LiPSs produced during cycling. Furthermore, they proposed that the increase in the E/S ratio increases cycle life and depth of sulfur reduction. As for the $LiClO_4$ in the sulfolane electrolyte system, they concluded that while the capacity of the cell is affected by the component of the electrolyte, cycle life is not affected [58].

T. Zerrin et al. investigated the influence of the E/S ratio on the capacity fade and used the most popular electrolyte (1M LiTFSI in DOL: DME (1:1 vol%) with 1wt % $LiNO_3$). Moreover, they also explored the impact of resting time before cycling on the performance of the battery. The study was divided into two groups. In group 1, the resting time of all cells is 12 hours, whilst the resting time of all cells is 6 hours in group 2. Also, before cycling tests, all batteries in both groups are cycled at C/50 for a few cycles for the conditioning. They concluded that the reason for the capacity decay at low electrolyte amount is the decrease in the electrolyte with cycling. Meanwhile, the capacity decay seen in the cells with

high E/S ratios may result from the accelerated polysulfide shuttle mechanism. The highest capacity is procured with the highest electrolyte amount in the first cycle (nearly 1100 mAh/g), while the lowest capacity in the first cycle is seen in the cell with the lowest E/S ratio in both groups. However, the capacity retention of the battery with the highest electrolyte-to-sulfur ratio is smaller than others; the capacity of the batteries with the E/S ratio of 30 μL/mg decreases to nearly 500 mAh/g at the end of the 5th cycle. In addition, they conclude that there is no significant difference between the Coulombic efficiency of the two highest electrolyte-to-sulfur ratios in the two groups, while the difference is seen in the two lowest E/S ratios. They thought that the reason for these differences is inadequate electrolyte wetting and an increase in the LiPSs concentration resulting in an increase in viscosity, impacting the Coulombic efficiency [50]. Table 2.1 summarizes the previous experimental studies on the impact of the E/S ratio on the performance of the Li-S cells.

2.2. Electrochemical Modeling of Li-S Batteries

K. Kumaresan et al. proposed a one-dimensional electrochemical model, which is the origin of almost all previous models, to predict the initial discharge profile of a Li-S batteries. They developed a highly complex model including six electrochemical reactions and five precipitation/dissolution reactions. Due to being a one-dimensional model, the mass flux of the species is taken into consideration, but the shuttle effect is ignored in this model. The change in concentration of the species, the porosity of the separator and electrodes, and the volume fraction of the precipitated species as a function of space and time are considered in the calculation of the voltage profile at a given current density with this detailed model [59].

T. Zhang et al. developed a 0-D electrochemical model by modifying Kumaresan et al.'s model in order to understand the change in the resistance during discharge and the initial discharge behavior of the Li-S cell at a given C-rate. For this purpose, they used six electrochemical reactions and one precipitation reaction in their model. In this model, mass transport and the shuttle mechanism are not taken into account. However, they included the voltage drop due to the electrolyte resistance, which is a function of the species concentration in their model. Then, they conclude that the concentrations of the S^{2-} and Li^{+} increase at the higher discharge current. As a result of this, electrolyte resistance increases as well [60].

The aim of the study by M. Ghaznavi and P. Chen was to conduct a sensitivity analysis on the model by Kumaresan et al. At first, they investigated the impact of the discharge current and electronic conductivity of the cathode. They concluded that the behavior of the discharge profile changes with the variation of the discharge current, especially at high discharge currents. Also, there is no impact of the change in conductivity on the capacity. However, under the highest discharge current conditions, the alteration in the capacity is seen with the increase in the conductivity [61].

In the second part of their study, they investigated the effect of the precipitation rate constants and sulfur content on predicted discharge behavior. They concluded that these rate constants have a noteworthy impact on discharge patterns. Furthermore, they claimed that the optimum sulfur content could be obtained by this model [62]. In the last part of their study, the effect of the exchange current densities as the electrochemical reaction kinetic parameters and diffusion coefficients as the transport property were examined. They found that among the exchange current densities, the performance of the cell is affected tremendously by the exchange current densities of the reduction of S and S_2^{2-}, and decreasing these exchange current densities lead to capacity loss. In addition, the capacity is not influenced by the change in diffusion coefficients at first, but after some point, the capacity is affected adversely [63].

In order to predict the impact of the carbon-to-sulfur ratio and electrolyte-to-sulfur ratio, which are crucial design parameters, on the performance of Li-S batteries, N. Erisen et al. developed a one-dimensional concentration-independent electrochemical model that predicts the cell voltage at 60% depth of discharge corresponding to the second plateau voltage at a given current density. For simplification, they assumed a single electrochemical reaction for each plateau. They concluded that the cell voltage increases with the amount of carbon till the carbon-to-sulfur ratio (C/S) of 1 because the active surface area increases, improving the cathode kinetics. As for the E/S ratio, the model is successful in the prediction of the improvement of the cathode kinetics, along with an increase in the E/S ratio, only when the exchange current density is changed [14].

N. Erisen and D. Eroglu also proposed a one-dimensional and concentration-dependent electrochemical model that projects the entire voltage profile at a given C-rate,

by modifying Kumaresan et al.'s model. In this model, they simplified the reaction scheme by considering dissolution/precipitation and two electrochemical reactions. B. Abdulkadiroglu et al. improved this model by defining the electrochemically active area in the model differently to predict the effect of the design parameters on the discharge behavior of the cell [64]. Two electrochemical and precipitation/dissolution reactions are combined, and the active area is determined as both the the weight fraction of carbon and porosity in this model. As a result, the model can capture the effect of the design parameters successfully at a discharge rate of 1C [64].

Table 2.1 The summary of the experimental studies in the literature for the effect of the E/S ratio on the capacity of the Li-S batteries.

E/S Ratio (ml/g)	Types of Solvent	Types of Salt	Conc. of Salt	Presence of $LiNO_3$	Carbon Type	Binder	Sulfur Loading (mg/cm^2)	C-Rate	Types of Separators	Cell Voltage Range	Discharge Capacity (mAh/g)	Ref. No.
10	DOL: DME (1:1 vol%)	LiTFSI	1M	0.25M	CNT	not mentioned	~4	0.1 C	Celgard	1.7-2.8 V	1300	[51]
8											1130	
6											1000	
17.5	DOL: DME (1:1 vol%)	LiTFSI	0.5M	0.5M	CNT	not mentioned	not mentioned	not mentioned	Celgard	1.8-2.5 V	1366	[52]
7.0											650	
4.4											371	
7.9	DOL: DME (1:1 vol%)	LiTFSI	0.5M	0.15M	Super Carbon	CMC	~2	0.25	Porous polymer separator	1.7-2.6 V	947	[53]
4.2											947	
2.4											103	
5	DOL: DME (1:1 vol%)	LiTFSI	1M	0.1M	Ketjenblack	PVDF	~4	0.1C	not mentioned	1.6-2.6 V	503	[54]
10											743	
5	DMDS: DOL: DME (2:1:1 vol%)										989	
10											1366 at 25. cycle	
35	DOL: DME (1:1 vol%)	LiTFSI	1M	0.1M	Carbon Black	PVDF	avg. 0.75	C/5	Celgard	1.5-3 V	809	[55]
20											1073	
13											1104	
6											1034	
10.3	DOL: DME (1:1 vol%)	LiTFSI $LiNO_3$	0.2M LiTFSI 1.5wt % of $LiNO_3$	✓	Ketjenblack	PVP PDAT	~6	not mentioned	Celgard	1.7-2.8 V	>1000	[56]
4.4											>1000	
2.4											<200	

Table 2.1 The summary of the experimental studies in the literature for the effect of the E/S ratio on the capacity of the Li-S batteries (cont.).

E/S Ratio (ml/g)	Types of Solvent	Types of Salt	Conc. of Salt	Presence of $LiNO_3$	Carbon Type	Binder	Sulfur Loading (mg/cm^2)	C-Rate	Types of Separators	Cell Voltage Range	Discharge Capacity (mAh/g)	Ref. No.
19	DOL: DME (1:1 vol%)	LiTFSI	1M	0.1M	Carbon Black	PVP	0.7-0.9	0.1C	Celgard	1.5-3.0 V	1292	[57]
6											485	
10	DOL: DME (1:1 vol%)	LiTFSI	1M	-	Ketjenblack	LA133	6.5	C/125	Celgard	1.0-2.5 V	1230	[49]
6											1222	
4											1283	
3											1289	
1											1274	
10	DOL: DME (1:1 vol%)	LiTFSI	1M	-	Ketjenblack	LA133	6.5	C/40	Celgard	1.0-2.5 V	1217	
6											1230	
4											1253	
3											1240	
2											1264	
1											1236	
10	DOL: DME (1:1 vol%)	LiTFSI	1M	-	Ketjenblack	LA133	6.5	C/20	Celgard	1.0-2.5 V	1139	
6											1221	
4											1212	
3											1188	
2											1105	
1											213	
6	DOL: DME (1:1 vol%)	LiTFSI	1M	-	Ketjenblack	LA133	6.5	C/10	Celgard	1.0-2.5 V	1181	
4											1267	
3											279	
2											169	
1											52	

Table 2.1 The summary of the experimental studies in the literature for the effect of the E/S ratio on the capacity of the Li-S batteries (cont.).

E/S Ratio (ml/g)	Types of Solvent	Types of Salt	Conc. of Salt	Presence of $LiNO_3$	Carbon Type	Binder	Sulfur Loading (mg/cm^2)	C-Rate	Types of Separators	Cell Voltage Range	Discharge Capacity (mAh/g)	Ref. No.
4	Sulfolane	CF_3SO_3Li	1M	-	Ketjenblack	PEO	~2	not mentioned	Celgard	1.5-2.8V	1322	[58]
3											1259	
2											1176	
1.5											1038	
1											543	
4	Sulfolane	$LiClO_4$	1M	-	Ketjenblack	PEO	~2	not mentioned	Celgard	1.5-2.8V	1268	
3											1125	
2											1039	
1.5											965	
1											591	
30	DOL: DME (1:1 vol%)	LiTFSI	1M	1 wt%	Acetylene Black	PAA	~2	C/10	not mentioned	1.7-2.8V	445	[50] Group1
20											569	
10											599	
5											633 at 5. cycle	
30	DOL: DME (1:1 vol%)	LiTFSI	1M	1 wt%	Acetylene Black	PAA	~2	C/10	not mentioned	1.7-2.8V	500	[50] Group2
20											593	
10											643	
5											635 at 5. cycle	

3. EXPERIMENTAL WORK

3.1. Chemicals

The chemicals used in the study are given in detail in Table 3.1.

Table 3.1. The chemicals used in the study.

Area of Usage	Chemicals	Abbreviation	Function	Source
Cathode	Carbon Black	Super C65	Conductive	MTI
Cathode	Elemental Sulfur	S	Active material	Sigma Aldrich
Cathode	Polyvinylidene difluoride	PVDF	Binder	MTI
Cathode	N-methyl-2-pyrolidone	NMP	Solvent	MTI
Cathode	Aluminum Foil	Al Foil	Current Collector	MTI
Anode	Lithium Metal Foil	Li Foil	Active material	MTI
Anode	Copper Foil	Cu Foil	Current Collector	MTI
Separator	Polymer Based Separator	–	Separator	Celgard
Electrolyte	1,3-Dioxolane	DOL	Solvent	Sigma Aldrich
Electrolyte	1,2-Dimethoxyethane	DME	Solvent	Sigma Aldrich
Electrolyte	Sulfolane	SL	Solvent	Sigma Aldrich
Electrolyte	Triethylene glycol dimethyl ether	G3	Solvent	Sigma Aldrich
Electrolyte	Lithium bis(trifluoromethanesulfonyl)imide	LiTFSI	Salt	Sigma Aldrich
Electrolyte	Lithium trifluoromethanesulfonate	LiTF	Salt	Sigma Aldrich
Electrolyte	Lithium perchlorate	$LiClO_4$	Salt	Sigma Aldrich
Electrolyte	Lithium nitrate	$LiNO_3$	Additive Salt	Sigma Aldrich

3.2. Cell Preparation

Lithium-sulfur batteries are composed mainly of a lithium metal anode, a separator, an organic electrolyte, and a cathode composed of sulfur and carbon. Except for the cathode and the electrolyte, the other materials of the cell are used directly. The preparation of the cathode and the electrolytes are given in the next sections, respectively.

3.2.1. Preparation of the Cathode

Cathodes used during the study are prepared by arranging the carbon/sulfur/binder weight ratio as 30/60/10 corresponding to a carbon-to-sulfur ratio of 0.5. Before mixing all powder materials, 90 mg of carbon black, and 180 mg of sulfur are weighed and put into the mortar and then pestled for 5 minutes to make the mixture more homogenous. The binder is not added in this step, in order to avoid any weight loss due to its sticky structure. Then, 30 mg PVDF, binder, is added into the carbon-sulfur mixture and mixed slowly. N-methyl-2-pyrrolidone, NMP, is added into the solid mixture till obtaining a uniform mixture with a honey texture with a solid mixture: NMP ratio of almost 1:7 wt: wt. After mixing all components of the cathode, to get a homogeneous slurry, it is mixed by a magnetic stirrer all night. After this step, it is heated to 50 ℃ for two hours while mixing, and then it is mixed in ultrasonic titration for two hours to achieve homogeneous mixing and get rid of the bubbles. Next, the slurry is cast onto the Aluminum foil and glided with a doctor blade, setting the thickness to 350 μm to obtain a sulfur loading of 1.1-1.3 mg/cm^2. The cathode layer on the Al foil is dried in the air atmosphere for removing the NMP solvent. Finally, the cathode is cut through a puncher as 2.01 cm^2 disks and weighed to check their sulfur loadings.

Figure 3.1. Prepared cathode film with a C/S ratio of 0.5 and sulfur loading of 1.2 mg/cm^2.

3.2.2. Preparation of the Electrolyte

The objective of this study is to understand the influence of the E/S ratio on lithium-sulfur battery performance for different electrolyte systems. Therefore, in this study, several types of electrolytes are used. DOL: DME with 1M LiTFSI and 0.1 M $LiNO_3$ additive, which is the conventional electrolyte in Li-S batteries, is used as a reference electrolyte. Before the preparation of the electrolytes, sulfolane, and triglyme solvents are dried by the molecular sieves (0.4 nm, Sigma Aldrich), which are calcined to 350 ℃ for 7 hours, in order to adsorb any remaining water and all the electrolyte preparation process is carried in a glove box under Ar atmosphere. 1:1 volume ratio of DOL and DME, which are dried, are mixed in an erlenmeyer. Then, 0.069 g $LiNO_3$ and 2.871 g LiTFSI are dissolved in the 10 ml DOL: DME mixture to get the DOL: DME electrolyte with 1M LiTFSI and 0.1M $LiNO_3$. After then, this mixture is stirred in a magnetic stirrer for almost one hour. The other electrolytes, sulfolane with 1M LiTFSI, 1M LiTF, 1M $LiClO_4$, and 1M $LiClO_4$ with 0.1M $LiNO_3$ additive, and triglyme with 1M LiTFSI and 1M LiTF, are prepared by the same method. The amount of chemicals used in these electrolytes is given in detail in Table 3.2.

Table 3.2. The different type of electrolytes used in the study.

		Solvent	**Salt**	**Additive**
1	**Name**	DOL: DME	LiTFSI	$LiNO_3$
	Amount	10 ml	2.871 g	0.069 g
	Concentration	–	1M	0.1M
2	**Name**	Sulfolane, SL	LiTFSI	–
	Amount	10 ml	2.871 g	–
	Concentration	–	1M	–
3	**Name**	Sulfolane, SL	LiTF	–
	Amount	10 ml	1.560 g	–
	Concentration	–	1M	–
4	**Name**	Sulfolane, SL	$LiClO_4$	–
	Amount	10 ml	1.064 g	–
	Concentration	–	1M	–

Table 3.2. The different type of electrolytes used in the study (cont.).

		Solvent	Salt	Additive
5	**Name**	Sulfolane, SL	$LiClO_4$	$LiNO_3$
	Amount	10 ml	1.064 g	0.069 g
	Concentration	–	1M	0.1M
6	**Name**	Triglyme, G3	LiTFSI	–
	Amount	10 ml	2.871 g	–
	Concentration	–	1M	–
7	**Name**	Triglyme, G3	LiTF	–
	Amount	10 ml	1.560 g	–
	Concentration	–	1M	–

3.2.3. Coin Cell Assemble

All cells are assembled in the glovebox under an Ar atmosphere with oxygen and water levels under 0.5 ppm. For the assembly of coin cells (CR2032), firstly, one spring is put into the negative case, and one spacer is placed onto the spring. Then, copper foil and lithium foil (2.01 cm^2) are placed in order. Next, the half of the electrolyte amount calculated according to the desired value of the E/S ratio is dropped on the lithium anode by a micropipette. After the separator (3.1 cm^2) is placed, the other half of the electrolyte is dropped to the other side of the separator. And then, the sulfur cathode is placed. Before closing the cell with the positive case, another spacer is also placed. Finally, the battery is crimpled through the crimper and is ready for cycling. Batteries with different E/S ratios of 6, 9, 16, and 23 mL/g are prepared for different types of electrolytes by changing the electrolyte amount added to the cell while keeping other parameters such as sulfur loading and carbon-to-sulfur ratio constant. At least three replicates are tested for each case. The parameters of cells for each replicate are given in Table 3.3.

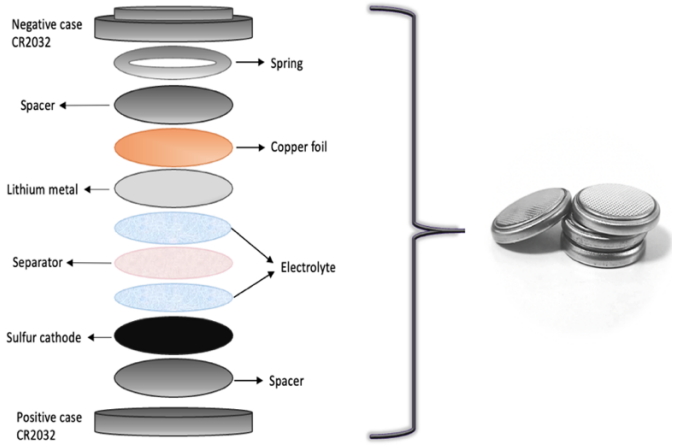

Figure 3.2. Schematic illustration of a Li-S coin cell.

Also, a sample calculation of the E/S ratio used for the replicates is given as

$$\text{Cathode mass} = \text{Total cathode mass} - \text{Al foil mass} = 12.1 - 8.14 = 3.96\text{mg}, \quad (3.1)$$

$$\text{Sulfur mass} = \text{Cathode mass} \times \text{sulfur weight \%} = 3.96 \times 0.6 = 2.376\ \text{mg}, \quad (3.2)$$

$$\text{S} - \text{Loading} = \frac{\text{Sulfur mass}}{\text{Cathode area}} = \frac{2.376}{2.01} = 1.18\frac{\text{mg}}{\text{cm}^2}, \quad (3.3)$$

$$\text{E/S ratio} = \frac{\text{Electrolyte volume}}{\text{Sulfur mass}} = \frac{54.65}{2.376} = 23, \quad (3.4)$$

$$\text{Current rate} = \frac{1675\ \text{mAh/gS}}{10\ \text{h}} \times \text{Sulfur mass},$$

$$= \frac{1675\ \text{mAh/gS}}{10\ \text{h}} \times 2.376\ \text{mg S} = 398\ \mu\text{A}. \quad (3.5)$$

Table 3.3. Parameters used in cell assemble.

Type of Electrolyte	E/S Ratio (µL/mg)	Volume of the Electrolyte (µL)	Sulfur Loading (mg/cm^2)	Total Cathode Mass (mg)	Cathode Mass (mg)	Current Density (µA)
1M LiTFSI 0.1M $LiNO_3$ in DOL: DME	23	54.6	1.18	12.1	3.96	398
		54.6	1.18	12.1	3.96	398
		51.9	1.12	11.9	3.76	3781
	16	36.1	1.12	11.9	3.76	378
		38.0	1.18	12.1	3.96	398
		38.0	1.18	12.1	3.96	396
	9	21.4	1.18	12.1	3.96	398
		21.4	1.18	12.1	3.96	398
		20.8	1.15	12.0	3.86	388
	6	15.3	1.27	12.4	4.26	428
		13.5	1.12	11.9	3.76	378
		14.3	1.18	12.1	3.96	398

Table 3.3. Parameters used in cell assemble (cont.).

Type of Electrolyte	E/S Ratio (µL/mg)	Volume of the Electrolyte (µL)	Sulfur Loading (mg/cm^2)	Total Cathode Mass (mg)	Cathode Mass (mg)	Current Density (µA)
1M LiTFSI in Triglyme	23	53.3	1.15	12.0	3.86	388
		57.4	1.24	12.3	4.16	418
		53.3	1.15	12.0	3.86	388
	16	39.0	1.21	12.2	4.06	408
		39.9	1.24	12.3	4.16	418
		39.9	1.24	12.3	4.16	418
	9	22.5	1.24	12.3	4.16	418
		21.9	1.21	12.2	4.06	408
		20.8	1.15	12.0	3.86	388
	6	13.5	1.12	11.9	3.76	378
		13.2	1.09	11.8	3.66	368
		14.6	1.21	12.2	4.06	406
1M LiTF in Triglyme	23	50.5	1.09	11.8	3.66	368
		50.5	1.09	11.8	3.66	368
		53.3	1.15	12.0	3.86	388
	16	40.9	1.27	12.4	4.26	428
		39.9	1.24	12.3	4.16	418
		35.1	1.09	11.8	3.66	368
	9	21.9	1.21	12.2	4.06	408
		22.5	1.24	12.3	4.16	418
		22.5	1.24	12.3	4.16	418
	6	13.9	1.15	12.0	3.86	388
		15.3	1.27	12.4	4.26	428
		13.5	1.12	11.9	3.76	378
1M LiTFSI in Sulfolane	23	50.5	1.09	11.8	3.66	368
		50.5	1.09	11.8	3.66	368
		53.3	1.15	12.0	3.86	388
	16	39.0	1.21	12.2	4.06	408
		37.1	1.15	12.0	3.86	388
		37.1	1.15	12.0	3.86	388
	9	20.3	1.12	11.9	3.76	378
		20.3	1.12	11.9	3.76	378
		20.8	1.15	12.0	3.86	388
	6	14.6	1.21	12.2	4.06	408
		14.6	1.21	12.2	4.06	408
		13.2	1.09	11.8	3.66	368

Table 3.3. Parameters used in cell assemble (cont.).

Type of Electrolyte	E/S Ratio (µL/mg)	Volume of the Electrolyte (µL)	Sulfur Loading (mg/cm^2)	Total Cathode Mass (mg)	Cathode Mass (mg)	Current Density (µA)
1M LiTF in Sulfolane	23	53.3	1.15	12.0	3.86	388
		50.5	1.09	11.8	3.66	368
		50.5	1.09	11.8	3.66	368
	16	36.1	1.12	11.9	3.76	378
		37.1	1.15	12.0	3.86	388
		39.0	1.21	12.2	4.06	408
	9	21.4	1.18	12.1	3.96	398
		22.5	1.24	12.3	4.16	418
		22.5	1.24	12.3	4.16	418
	6	13.5	1.12	11.9	3.76	378
		13.2	1.09	11.8	3.66	368
		15.3	1.27	12.4	4.26	428
1M $LiClO_4$ in Sulfolane	23	51.9	1.12	11.9	3.76	378
		51.9	1.12	11.9	3.76	378
		51.9	1.12	11.9	3.76	378
	16	37.1	1.15	12.0	3.86	388
		37.1	1.15	12.0	3.86	388
		36.1	1.12	11.9	3.76	378
	9	20.8	1.15	12.0	3.86	388
		21.9	1.21	12.2	4.06	408
		20.3	1.12	11.9	3.76	378
	6	13.5	1.12	11.9	3.76	378
		15.3	1.27	12.4	4.26	428
		13.9	1.15	12.0	3.86	388
1M $LiClO_4$ 0.1M $LiNO_3$ in Sulfolane	23	57.4	1.24	12.3	4.16	418
		54.6	1.18	12.1	3.96	398
		56.0	1.21	12.2	4.06	408
	16	40.9	1.27	12.4	4.26	428
		35.1	1.09	11.8	3.66	368
		39.0	1.21	12.2	4.06	408
	9	23.5	1.3	12.5	4.36	438
		19.2	1.06	11.7	3.56	358
		24.1	1.3	12.6	4.46	448
	6	15.7	1.3	12.5	4.36	438
		14.6	1.21	12.2	4.06	408
		15.0	1.24	12.3	4.16	418

3.3. Electrochemical Characterization Methods

3.3.1. Electrochemical Cycling Measurements of Coin Cells

Galvanostatic cycling is carried out at room temperature, and the Neware battery cycler is used for the investigation of the battery performance. Before cycling, each cell is kept resting for 16 hours at the open circuit in order to stabilize. After resting, each cell is cycled at 0.1 C-rate until the completion of 100 cycles. For the cells prepared with an electrolyte not containing $LiNO_3$, the lower and upper voltage are arranged to 1.5-2.8 V, whereas the voltage window is set between 1.7-3.0 V for the cells with an electrolyte containing $LiNO_3$ in order to prevent the decomposition of the additive.

3.3.2. Electrochemical Impedance Spectroscopy of Coin Cells

The electrochemical impedance spectroscopy (EIS) method is performed at room temperature, and a Biologic SP-300 potentiostat is used for the investigation of the effect of the electrolyte amount with different types of electrolyte systems on the resistance of the batteries. In this analysis, E/S ratios of 6 µL/mg and 9 µL/mg are used for all electrolytes because low electrolyte amounts are required for practical Li-S batteries, and lean electrolyte conditions are taken into account in this analysis. Two replicates are tested for each case. Before the discharge of the cells at 0.1 C-rate, each cell is rested for 16h. In addition, a 10 mHz-100 kHz frequency range is used during the EIS measurements, and each cell is rested again for 30 min for stabilization.

The spectra obtained from the EIS experiments are fitted by means of Bio-Logic Z-fit software. Figure 3.1 shows the proposed equivalent circuit and an example of the Z-fitting used in the EIS characterization. In this figure, R_1, R_2, and R_3 represent the resistance of the electrolyte, charge transfer resistance, and film resistance of Li_2S, respectively. Q_2 and Q_3 are capacitances, whereas W_1 is the Warburg diffusion resistance.

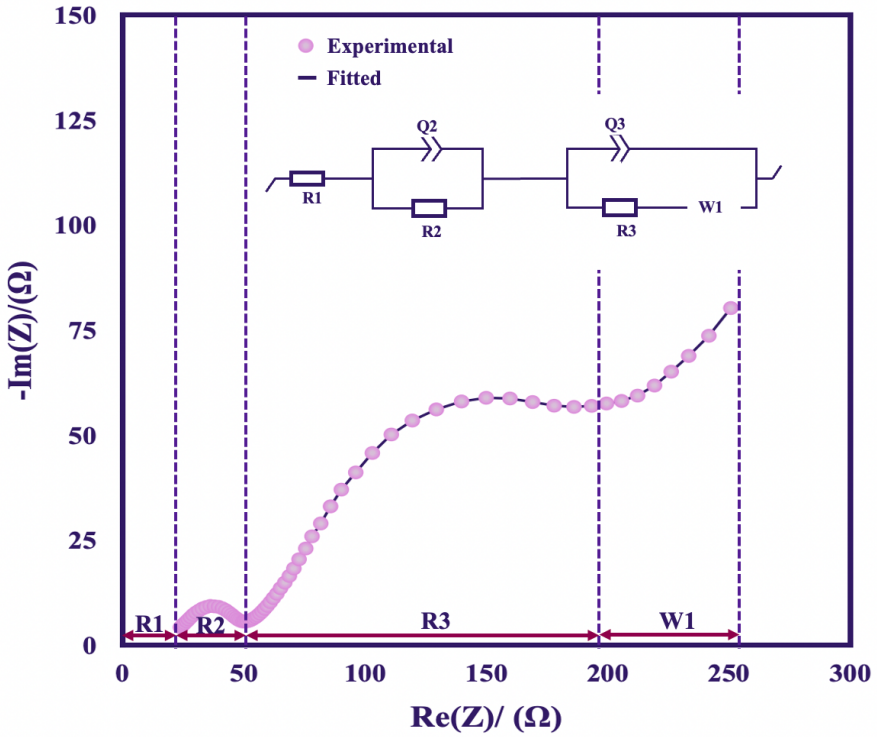

Figure 3.3. Recommended equivalent circuit and example of the Z-fitting.

4. MODEL DEVELOPMENT

In this part of the study, zero-dimensional and one-dimensional electrochemical models are developed to mechanistically investigate the effect of the electrolyte-to-sulfur, E/S, ratio on battery performance and capture the experimental trends observed in the previous part. In order to solve equations by using the block tridiagonal matrix algorithm that Newman and Thomas Alyea used in their study, Fortran Programming Language is used. Before running the models, all the equations used in the two models are linearized [66]. For the two models, only the cathode part of the cell is taken into account, and the anode/separator interphase is ignored. Therefore, the separator/cathode and cathode/current collector interphases are used to set the electrochemical model domain (Figure 4.1). All details, such as equations, model parameters, and initial and boundary conditions, are given in the next part.

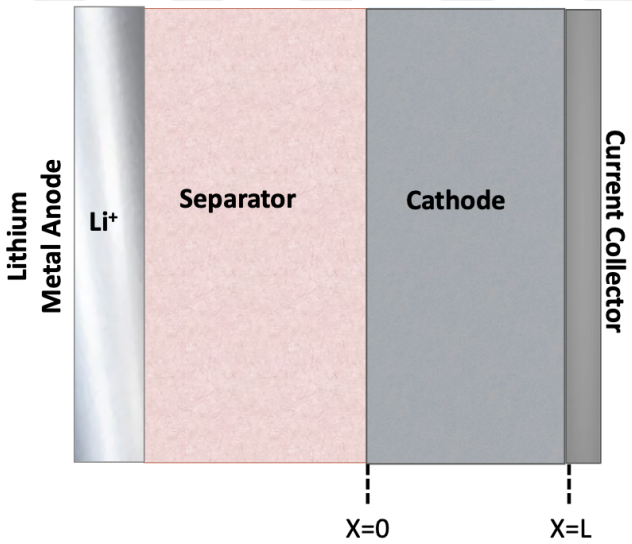

Figure 4.1. Schematic illustration of the electrochemical model domain.

4.1. Zero-Dimensional Electrochemical Model

A time-dependent, concentration-independent, zero-dimensional electrochemical model, which was based on Zhang et al. [60], was developed. Contrary to the Zhang et al. model, the dissolution reaction of S_8 was included in this model. By doing so, critical experimental parameters, such as the mass fraction of sulfur, sulfur loading, and C/S and

E/S ratios, can be defined in the model. Moreover, the electrochemically active area is modified by the use of a reference porosity and carbon mass fraction, and correspondingly the change of the electrochemically active area with the E/S ratio is considered. Therefore, a total of seven reactions, five electrochemical reactions and two precipitation/dissolution reactions of sulfur and lithium sulfide, were used in this model. These reactions are given as

$$0.5S_8^0 + e^- \longrightarrow 0.5\,S_8^{2-}, \tag{4.1}$$

$$3/2S_8^{2-} + e^- \longrightarrow 2\,S_6^{2-}, \tag{4.2}$$

$$S_6^{2-} + e^- \longrightarrow 3/2\,S_4^{2-}, \tag{4.3}$$

$$0.5S_4^{2-} + e^- \longrightarrow S_2^{2-}, \tag{4.4}$$

$$0.5S_2^{2-} + e^- \longrightarrow S^{2-}, \tag{4.5}$$

$$2Li^+ + S^{2-} \longrightarrow Li_2S, \tag{4.6}$$

$$S_{8(s)} \longrightarrow S_8^0. \tag{4.7}$$

In this way, a total of 22 variables are obtained for this model and these variables are $C_{Li^+}, C_{S_8^0}, C_{S_8^{2-}}, C_{S_6^{2-}}, C_{S_4^{2-}}, C_{S_2^{2-}}, C_{S^{2-}}, i_1, i_2, i_3, i_4, i_5, \eta_1, \eta_2, \eta_3, \eta_4, \eta_5, \varepsilon, \varepsilon_{Li_2S}, \varepsilon_{S_8^0}, V_{cell}, R_s$. $C_{Li^+}, C_{S_8^0}, C_{S_8^{2-}}, C_{S_6^{2-}}, C_{S_4^{2-}}, C_{S_2^{2-}}, C_{S^{2-}}$ represent the concentration of the species. i_1, i_2, i_3, i_4, i_5 and $\eta_1, \eta_2, \eta_3, \eta_4, \eta_5$ demonstrate the current density and overpotential of the electrochemical reactions, respectively. ε is porosity (or the electrolyte volume fraction), and ε_{Li_2S} and $\varepsilon_{S_8^0}$ represent the volume fractions of precipitates $Li_2S_{(s)}$ and $S_{8(s)}$, consecutively. Also, V_{cell} is the cell voltage, whereas R_S is the electrolyte resistance.

The following assumptions were made in the model:

- The cell operates isothermally at 298 K,
- Unlike the Zhang et al. model, S_8 dissolution reaction is taken into account in this model.
- Unlike the Zhang et al. model, carbon mass and electrolyte volume fractions are used in the definition of the electrochemically active area for the control of the electrolyte-to-sulfur ratio.
- Lithium and separator overpotentials are ignored due to the lack of considerable effect of these on the voltage of the battery.
- The polysulfide shuttle mechanism is not taken into consideration in the model.

- There is only Li_2S precipitation at the end of the discharge of the cell.
- The discharge and charge reactions in the cathode are symmetric. Therefore, the charge transfer coefficient is 0.5.

The material balance of the species, except Li^+, is defined by the Nernst-Plank equation. The general form of this equation is given as

$$\frac{\partial \varepsilon C_i}{\partial t} = -\Delta N_i + r_i - R_i \ . \tag{4.8}$$

However, the first term on the left side, representing the mass flux, is neglected due to the concentration independency of the zero-dimensional model. The production/consumption rate of $S_8^{2-}, S_6^{2-}, S_4^{2-}, S_2^{2-}$, species is only due to the electrochemical reactions; the equation used to estimate C_i changing with time for these species is given as

$$\frac{d(\varepsilon C_i)}{dt} = a_v \sum_{J=2}^{4} \frac{s_{i,j} i_j}{n_j F} \ . \tag{4.9}$$

In this equation, ε is cathode porosity, i_j is the current density of electrochemical reaction j, $s_{i,j}$ is the stoichiometric coefficient of the species i in reaction j (Table 4.1), n_j is the number of electrons transferred, which is one for this model, F is the Faraday's constant and ξ represents the fitting parameter that is 1.5. In order to account for the change of the cathode kinetics with the E/S ratio, the electrochemical active area is defined as a function of carbon weight fraction and a reference electrolyte volume fraction written as [64]

$$\frac{d(\varepsilon C_i)}{dt} = a_0 \omega_c \left(\frac{\varepsilon}{\varepsilon_{ref}}\right)^{\xi} \sum_{J=2}^{4} \frac{s_{i,j} i_j}{n_j F} \ . \tag{4.10}$$

Table 4.1. Stoichiometric coefficient of species.

Species, *i*	$S_{i,j}$				
	1	**2**	**3**	**4**	**5**
Li^+	0	0	0	0	0
S_8^0	-1/2	0	0	0	0
S_8^{2-}	1/2	-3/2	0	0	0

Table 4.1. Stoichiometric coefficient of species (cont.).

Species, i	$S_{i,j}$				
	1	**2**	**3**	**4**	**5**
S_6^{2-}	0	2	-1	0	0
S_4^{2-}	0	0	3/2	-1/2	0
S_2^{2-}	0	0	0	1	-1/2
S^{2-}	0	0	0	0	1
A^-	0	0	0	0	0

Here, a_0 is the active area parameter, ω_c is the carbon mass fraction in the cathode, ε_{ref} is reference porosity, and ξ is the empirical morphology parameter, which is taken as 1.5 in the model. The change of the concentration of the species S_8^0 and S^{2-} is also due to the dissolution/precipitation reactions, given as

$$\frac{d(\varepsilon C_i)}{dt} = a_0 \omega_c \left(\frac{\varepsilon}{\varepsilon_{ref}}\right)^{\xi} \frac{s_{i,j} i_j}{n_j F} - R_k \qquad j = 1 \text{ to } 5. \tag{4.11}$$

Herein, k is the solid species and R_k is the production/consumption rate of the solid species of S_8^0 and Li_2S due to the dissolution/precipitation reactions. R_k is defined as

$$R_k = k_k \varepsilon_k \left(\prod_i C_i^{\gamma_{i,k}} - K_{sp,k}\right), \tag{4.12}$$

where $K_{sp,k}$ is the solubility product of k in the electrolyte whereas k_k is the rate constant. ε_k is the volume fraction of the solid species [59].

Table 4.2. The mole numbers of ionic species, i in the precipitated species, k.

Subscript k	$\gamma_{i.k}$	
Subscript i	$Li_2S_{(s)}$	$S_{8(s)}$
Li^+	2	0
S_8^0	0	1
S^{2-}	1	0

For calculating the concentration of Li^+, the electroneutrality principle is applied and equation is given as

$$C_{Li^+} = C_{Li^+,0} + 2\sum_{i=2}^{8} C_{S_i^{2-}} . \tag{4.13}$$

In this equation, $C_{Li^+,0}$ is the initial concentration of the Li^+. The change of the cathode porosity with time is defined as

$$\frac{d\varepsilon}{dt} = -\sum_{k} \tilde{V}_k R_k . \tag{4.14}$$

Here R_k is the precipitation rate and $\tilde{V}_k$ is the partial molar volume of precipitated solid species. In addition, the volume fraction of the precipitate solid species k is defined as

$$\frac{d\varepsilon_k}{dt} = \tilde{V}_k R_k. \tag{4.15}$$

Also, the sum of the volume fractions of all materials is equal to 1, given as

$$\varepsilon s_8^0 + \varepsilon + \varepsilon_{Li_2S} + \varepsilon_{carbon} + \varepsilon_{binder} = 1. \tag{4.16}$$

The current densities are defined by the Butler-Volmer equation given as

$$i_j = 2i_j^0 \sinh\left(\frac{n_j F}{2RT}\eta_j\right). \tag{4.17}$$

In the equation, i_j^0 is the exchange current densities of reaction j, R is the ideal gas constant, η_j is the overpotential of reaction j and T is the temperature. In addition, the sum of the current densities of the electrochemical reactions are set to the applied current density written as

$$a_0\omega_c\left(\frac{\varepsilon}{\varepsilon_{ref}}\right)^{\xi}\sum_{j=1}^{5} i_j = \frac{I}{Al}. \tag{4.18}$$

Here, A and l represent the apparent geometric area and thickness of the cathode, respectively. For determining the overpotential of the cell, the Nernst equation, defining the reduction potential of reactions, is used. This equation is given as

$$E_j = E_j^0 - \frac{RT}{n_j F}\sum_{j} s_{i,j} \ln\left(\frac{C_i}{1\ \left(\frac{mol}{L}\right)}\right). \tag{4.19}$$

In this equation, E_j^0 is the standard reduction potential of the reaction j. The total electrolyte resistance is

$$R_s = \frac{l}{A\sigma}, \tag{4.20}$$

σ is the conductivity of the electrolyte and it is defined as

$$\varepsilon^{1.5}\left(\sigma_0 - b\left|C_{Li^+} - C_{Li^+,0}\right|\right). \tag{4.21}$$

Finally, cell voltage at a given current density is calculated by the following equation:

$$V_{cell} = \left(E_j + \eta_j\right) - \left(E_{Li^+} + \eta_{Li^+}\right) - IR_s. \tag{4.22}$$

Here, E_{Li^+} and η_{Li^+} are the reduction potential and overpotential of the lithium. η_{Li^+} is neglected because dissolution kinetics of Li^+ is assumed fast. IR_s is the potential drop.

4.1.1. Governing Equations

Governing equations used in the model for all variables are given below:

$$C_{Li^+} = C_{Li^+,0} + 2\left(C_{S_2^{2-}} + C_{S_4^{2-}} + C_{S_6^{2-}} + C_{S_8^{2-}}\right), \tag{4.23}$$

$$\frac{d\left(\varepsilon C_{S_8^0}\right)}{dt} = a_0\omega_c\left(\frac{\varepsilon}{\varepsilon_{ref}}\right)^{\xi}\left(\frac{-0.5i_1}{F}\right) - \left[k_{S_8^0}\varepsilon_{S_8^0}\left(C_{S_8^0} - K_{sp,S_{8(s)}}\right)\right], \tag{4.24}$$

$$\frac{d\left(\varepsilon C_{S_8^{2-}}\right)}{dt} = a_0\omega_c\left(\frac{\varepsilon}{\varepsilon_{ref}}\right)^{\xi}\left(\frac{0.5i_1 - {}^3\!/_2\, i_2}{F}\right), \tag{4.25}$$

$$\frac{d\left(\varepsilon C_{S_6^{2-}}\right)}{dt} = a_0\omega_c\left(\frac{\varepsilon}{\varepsilon_{ref}}\right)^{\xi}\left(\frac{2i_2 - i_3}{F}\right), \tag{4.26}$$

$$\frac{d\left(\varepsilon C_{S_4^{2-}}\right)}{dt} = a_0\omega_c\left(\frac{\varepsilon}{\varepsilon_{ref}}\right)^{\xi}\left(\frac{{}^3\!/_2\, i_3 - 0.5i_4}{F}\right), \tag{4.27}$$

$$\frac{d\left(\varepsilon C_{S_2^{2-}}\right)}{dt} = a_0\omega_c\left(\frac{\varepsilon}{\varepsilon_{ref}}\right)^{\xi}\left(\frac{i_4 - 0.5i_5}{F}\right), \tag{4.28}$$

$$\frac{d\left(\varepsilon C_{S^{2-}}\right)}{dt} = a_0\omega_c\left(\frac{\varepsilon}{\varepsilon_{ref}}\right)^{\xi}\frac{i_5}{F} - \left[k_{Li_2S}\,\varepsilon_{Li_2S}\left(C_{Li^+}{}^2\, C_{S^{2-}} - K_{sp,Li_2S}\right)\right], \tag{4.29}$$

$$\frac{I}{Al} = a_0\omega_c\left(\frac{\varepsilon}{\varepsilon_{ref}}\right)^{\xi}\left(i_1 + i_2 + i_3 + i_4 + i_5\right), \tag{4.30}$$

$$i_1 = 2i_1^0\, sin\, h\left(\frac{F\eta_1}{2RT}\right), \tag{4.31}$$

$$i_2 = 2i_2^0\, sin\, h\left(\frac{F\eta_2}{2RT}\right), \tag{4.32}$$

$$i_3 = 2i_3^0\, sin\, h\left(\frac{F\eta_3}{2RT}\right), \tag{4.33}$$

$$i_4 = 2i_4^0\, sin\, h\left(\frac{F\eta_4}{2RT}\right), \tag{4.34}$$

$$i_5 = 2i_5^0 \sin h\left(\frac{F\eta_5}{2RT}\right), \tag{4.35}$$

$$\eta_1 = V_{cell} + E_0 + IR_s - \left(E_1^0 - \frac{RT}{F} ln\left(\frac{C_{S_8^{2-}}}{C_{S_8^0}}\right)\right), \tag{4.36}$$

$$\eta_2 = V_{cell} + E_0 + IR_s - \left(E_2^0 - \frac{RT}{F} ln\left(\frac{(C_{S_6^{2-}})^2\ 1000^{3/2}}{(C_{S_8^{2-}})^{3/2}\ 1000^2}\right)\right), \tag{4.37}$$

$$\eta_3 = V_{cell} + E_0 + IR_s - \left(E_3^0 - \frac{RT}{F} ln\left(\frac{(C_{S_4^{2-}})^{3/2}\ 1000}{(C_{S_6^{2-}})\ 1000^{3/2}}\right)\right), \tag{4.38}$$

$$\eta_4 = V_{cell} + E_0 + IR_s - \left(E_4^0 - \frac{RT}{F} ln\left(\frac{(C_{S_2^{2-}})\ 1000^{0.5}}{(C_{S_4^{2-}})^{0.5}\ 1000}\right)\right), \tag{4.39}$$

$$\eta_5 = V_{cell} + E_0 + IR_s - \left(E_5^0 - \frac{RT}{F} ln\left(\frac{(C_{S^{2-}})\ 1000^{0.5}}{(C_{S_2^{2-}})^{0.5}\ 1000}\right)\right), \tag{4.40}$$

$$\frac{d\varepsilon}{dt} = -\Big(\tilde{V}_{Li_2S_{(s)}} \times k_{Li_2S}\ \varepsilon_{Li_2S}\big(C_{Li^+}{}^2\ C_{S^{2-}} - K_{sp,Li_2S}\big) + \tilde{V}_{S_{8(s)}} \times k_{S_8^0}\varepsilon_{S_8^0}\left(C_{S_8^0} - K_{sp,S_{8(s)}}\right)\Big), \tag{4.41}$$

$$\frac{d\varepsilon_{Li_2S}}{dt} = \tilde{V}_{Li_2S_{(s)}} \times k_{Li_2S}\ \varepsilon_{Li_2S}\big[\big(C_{Li^+}{}^2\ C_{S^{2-}}\big) - K_{sp,Li_2S}\big], \tag{4.42}$$

$$\varepsilon s_8^0 = 1 - \varepsilon - \varepsilon_{Li_2S} - \varepsilon_{carbon} - \varepsilon_{binder}, \tag{4.43}$$

$$R_s = \frac{I}{A\varepsilon^{1.5}\big(\tau_0 - b\big|C_{Li^+} - C_{Li^+,0}\big|\big)}. \tag{4.44}$$

4.1.2. Initial Conditions

It is assumed that only the first electrochemical reaction occurs initially. Therefore, the initial current densities and overpotentials of the reactions are derived according to this assumption. In addition, the concentrations of the species are equal to the reference concentrations. The initial conditions used in the model are given as

$$C_{Li^+} = C_{Li^+,ref}, \tag{4.45}$$

$$C_{S_8^0} = C_{S_8^0,ref}, \tag{4.46}$$

$$C_{S_8^{2-}} = C_{S_8^{2-},ref}, \tag{4.47}$$

$$C_{S_6^{2-}} = C_{S_6^{2-},ref}, \tag{4.48}$$

$$C_{S_4^{2-}} = C_{S_4^{2-},ref}, \tag{4.49}$$

$$C_{S_2^{2-}} = C_{S_2^{2-},ref}, \tag{4.50}$$

$$C_{S^{2-}} = C_{S^{2-},ref}, \tag{4.51}$$

$$i_1 = -\frac{I_{app}}{a_0 L}, \tag{4.52}$$

$$i_2 = 0, \tag{4.53}$$

$$i_3 = 0, \tag{4.54}$$

$$i_4 = 0, \tag{4.55}$$

$$i_5 = 0, \tag{4.56}$$

$$\eta_1 = \frac{2RT}{n_1 F} arc\ sinh\left(\frac{-i_1}{2i_{01,ref}}\right), \tag{4.57}$$

$$\eta_2 = 0, \tag{4.58}$$

$$\eta_3 = 0, \tag{4.59}$$

$$\eta_4 = 0, \tag{4.60}$$

$$\eta_5 = 0, \tag{4.61}$$

$$\varepsilon = \varepsilon_{initial}, \tag{4.62}$$

$$\varepsilon_{Li_2S} = \varepsilon_{Li_2S_{(s)},initial}, \tag{4.63}$$

$$\varepsilon_{S_8^0} = \varepsilon_{S_{8(s)},initial}, \tag{4.64}$$

$$V_{cell} = 2.5, \tag{4.65}$$

$$R_s = \frac{I_{app}}{A\ a_0 L}. \tag{4.66}$$

Moreover, the parameters used in the model are reported in Table 4.3.

Table 4.3. Parameters used in zero-dimensional model.

Parameters	**Units**	**0-D Model**
$\boldsymbol{C_{Li^+,ref}}$	$mol\ m^{-3}$	1100
$\boldsymbol{C_{S_8^0,ref}}$	$mol\ m^{-3}$	412.1
$\boldsymbol{C_{S_8^{2-},ref}}$	$mol\ m^{-3}$	100
$\boldsymbol{C_{S_6^{2-},ref}}$	$mol\ m^{-3}$	8.2
$\boldsymbol{C_{S_4^{2-},ref}}$	$mol\ m^{-3}$	5.6×10^{-3}

Table 4.3. Parameters used in zero-dimensional model (cont.).

Parameters	Units	0-D Model
$C_{S_2^{2-},ref}$	$mol\ m^{-3}$	8.0×10^{-6}
$C_{S^{2-},ref}$	$mol\ m^{-3}$	1.4×10^{-8}
E_1	V	2.35
E_2	V	2.33
E_3	V	2.24
E_4	V	2.06
E_5	V	2.01
T	K	298
R	$J\ K^{-1}mol^{-1}$	8.3145
F	$C\ mol^{-1}$	9.649×10^4
$i^0_{1,ref}$	$A\ m^{-2}$	1.972
$i^0_{2,ref}$	$A\ m^{-2}$	0.019
$i^0_{3,ref}$	$A\ m^{-2}$	0.019
$i^0_{4,ref}$	$A\ m^{-2}$	1.97×10^{-4}
$i^0_{5,ref}$	$A\ m^{-2}$	1.97×10^{-7}
k_{Li_2S}	$m^6 mol^2 s^{-1}$	6.875×10^{-4}
k_{S_8}	s^{-1}	1.0
K_{sp,Li_2S}	$m\ mol^3$	3.0×10^{-5}
K_{sp,S_8}	$m\ mol^3$	19.0
V_{Li_2S}	$mol^{-1}m^3$	2.768×10^{-5}
V_{S_8}	$mol^{-1}m^3$	2.354×10^{-4}
a_0	$m^2\ m^{-3}$	796,572

4.2. One-Dimensional Electrochemical Model

In addition to the zero-dimensional electrochemical model discussed above, a time- and concentration-dependent electrochemical model is developed based on Kumarasan et al. [59]. A total of seven reactions, five electrochemical reactions, and two precipitation/dissolution reactions, are used in this model like in the zero-dimensional model. The assumptions applied in the 0-D model are viable in this 1-D model as well. In addition to them, it is assumed that there is an unlimited lithium amount in the anode.
The model contains 20 variables given as $C_{Li^+}, C_{S_8^0}, C_{S_8^{2-}}, C_{S_6^{2-}}, C_{S_4^{2-}}, C_{S_2^{2-}}$, $C_{S^{2-}}, C_{A^-}, i_1, i_2, i_3, i_4, i_5, \theta_s, \theta_e, i_s, i_e, \varepsilon, \varepsilon_{Li_2S}, \varepsilon_{S_8^0}$.

Here, $C_{Li^+}, C_{S_8^0}, C_{S_8^{2-}}, C_{S_6^{2-}}, C_{S_4^{2-}}, C_{S_2^{2-}}$ *and* $C_{S^{2-}}$ represent the concentration of the species, and C_{A^-} is the anion of the lithium salt such as $TFSI^-$ in the LiTFSI used in the

electrolyte. Current densities of the reactions are i_1, i_2, i_3, i_4, i_5. In addition, i_s *and* i_e, represent the current densities of the solid and liquid phases while Φ_s *and* Φ_e are solid and liquid phase potentials. Next, $\varepsilon, \varepsilon_{Li_2S}$ *and* $\varepsilon_{S_8^0}$ are the volume fractions of the electrolyte, Li_2S and S_8, respectively.

The concentrations of the species are defined by the Nernst-Plank equation like in the 0-D model. In contrast to the 0-D model, the variation of the concentration of the species depends on not only time but also space in this model. Therefore, the mass flux term in the Nernst-Plank equation is taken into account in the 1-D model and this equation is given as

$$\frac{\partial \varepsilon \mathrm{C}_i}{\partial \mathrm{t}} = -\nabla \mathrm{N_i} + r_\mathrm{i} - R_\mathrm{i}. \tag{4.67}$$

In this equation, N_i is the flux of the species given as

$$\mathrm{N_i} = -\mathrm{D_i}\nabla \mathrm{C_i} + z_\mathrm{i}\frac{\mathrm{D}_i}{\mathrm{RT}}\mathrm{C}_i \mathrm{F}\nabla\Phi_e. \tag{4.68}$$

Here, $\mathrm{z_i}$ is the charge number, Φ_e is the liquid phase potential. Also, D_i represents the diffusion coefficient of the species *i,* and it is defined by the Bruggeman expression given as

$$\mathrm{D_i} = \mathrm{D_{i,0}}\varepsilon^b. \tag{4.69}$$

In this equation, $\mathrm{D_{i,0}}$ is the diffusion coefficient in the medium and b is the Bruggeman coefficient, which is taken as 1.5 in the model. The other terms in the Nernst-Plank equation are the same with the 0-D model. For the concentration of C_{A^-}, the electroneutrality principle is applied, written as

$$C_{A^-} = C_{Li^+} - 2\sum_{i=1}^{8} C_{S_i^{2-}}\ . \tag{4.70}$$

The current densities arising from the electrochemical reactions are defined by the Butler-Volmer Equation like in the 0-D model expressed as

$$i_j = i_{0,j\,ref}\left\{\prod_i\left(\frac{C_i}{C_{i,0\,ref}}\right)^{p_{i,j}} exp\left(\frac{\alpha_{a_j}F}{RT}\eta_j\right) - \prod_i\left(\frac{C_i}{C_{i,0\,ref}}\right)^{q_{i,j}} exp\left(\frac{-\alpha_{C_j}F}{RT}\eta_j\right)\right\}. \tag{4.71}$$

In here, $p_{i,j}$ and $q_{i,j}$ are stoichiometric coefficients of the anodic and cathodic species, respectively, and the overpotential, η_j is defined in terms of the liquid and solid phase potentials below

$$\eta_j = \Phi_s - \Phi_e - E_{j,ref}. \tag{4.72}$$

And the standard potential of the electrochemical reactions, E_j, is defined as in the 0-D model below

$$E_j = E_j^0 \; - \frac{RT}{n_j F} \sum_j s_{i,j} \; \ln\left(\frac{C_i}{1\left(\frac{mol}{L}\right)}\right). \tag{4.73}$$

The liquid phase current density is defined based on the porous electrode theory and is given as

$$i_e = F \sum_i z_i N_i \,. \tag{4.74}$$

On the other hand, the solid phase current density is defined according to the Ohm's Law:

$$i_s = -\sigma \frac{\partial \Phi_s}{\partial x} \;, \tag{4.75}$$

$$\nabla i_e = a_0 \omega_c \left(\frac{\varepsilon}{\varepsilon_{ref}}\right)^{\xi} \sum_j i_j \,. \tag{4.76}$$

Table 4.4. Transport, kinetics, and thermodynamics properties.

Species, *i*	z_i	$p_{i,j}$					$q_{i,j}$				
		1	**2**	**3**	**4**	**5**	**1**	**2**	**3**	**4**	**5**
Li^+	1	0	0	0	0	0	0	0	0	0	0
S_8^0	0	0	0	0	0	0	0.5	0	0	0	0
S_8^{2-}	-2	0.5	0	0	0	0	0	3/2	0	0	0
S_6^{2-}	-2	0	2	0	0	0	0	0	1	0	0
S_4^{2-}	-2	0	0	3/2	0	0	0	0	0	0.5	0
S_2^{2-}	-2	0	0	0	1	0	0	0	0	0	0.5
S^{2-}	-2	0	0	0	0	1	0	0	0	0	0
A^-	-1	0	0	0	0	0	0	0	0	0	0

Table 4.4. Transport, kinetics, and thermodynamics properties (cont.).

Species, *i*	$\alpha_{a,j}$	$\alpha_{c,j}$	n_j
Li^+	0.5	0.5	1
S_8^0	0.5	0.5	1
S_8^{2-}	0.5	0.5	1
S_6^{2-}	0.5	0.5	1
S_4^{2-}	0.5	0.5	1
S_2^{2-}	0.5	0.5	1
S^{2-}	0.5	0.5	1
A^-	0.5	0.5	1

In addition, the liquid phase current density is given in Equation (4.76), in which the electrochemical active area is defined as a function of carbon weight fraction and electrolyte volume fraction in this model as well [64]. And the sum of the charge of both phases must be zero as given below

$$\nabla i_s + \nabla i_e = 0. \tag{4.77}$$

Volume fraction of the electrolyte in the cathode, ε, volume fraction of Li_2S precipitated, ε_{Li_2S}, and volume fraction of $S_{8(s)}$, $\varepsilon_{S_8^0}$ are defined as in the 0-D model. Figure 4.1 shows the electrochemical model area used in the model. Finally, the cell voltage is calculated as

$$V_{cell} = \Phi_s(L) - \Phi_s(L). \tag{4.78}$$

Here, $\Phi_s(L)$ and $\Phi_s(L)$ are the solid-phase and the liquid-phase potential at x=L and x=0 respectively.

4.2.1. Governing Equations

The governing equations for the variables in the 1-D model are given as

$$\frac{\partial \varepsilon C_{Li^+}}{\partial t} = -\frac{\partial}{\partial x}\left[\left(-D_{Li^+,0} \times \varepsilon^b\right)\frac{\partial C_{Li^+}}{\partial x} - z_{Li^+}\frac{\left(D_{Li^+,0} \times \varepsilon^b\right)}{RT}F\, C_{Li^+}\,\frac{\partial \phi_e}{\partial x}\right] - \gamma_{Li^+,Li_2S} \times \left[k_{Li_2S} \times \varepsilon_{Li_2S} \times \left\{\left(C_{Li^+}{}^{\gamma_{Li^+,Li_2S}} \times C_{S^{2-}}{}^{\gamma_{S^{2-},Li_2S}}\right) - K_{sp,Li_2S}\right\}\right], \quad (4.79)$$

$$\frac{\partial \varepsilon C_{S_8^0}}{\partial t} = -\frac{\partial}{\partial x}\left[\left(-D_{S_8^0,0} \times \varepsilon^b\right)\frac{\partial C_{S_8^0}}{\partial x} - z_{S_8^0}\frac{\left(D_{S_8^0,0} \times \varepsilon^b\right)}{RT}F\, C_{S_8^0}\,\frac{\partial \phi_e}{\partial x}\right] + \left[-a_0 \times \left(\frac{\varepsilon}{\varepsilon_0}\right)^{\xi} \times \left(\frac{1/2\; i_1}{F}\right)\right] - \gamma_{S_8^0,S_{8(s)}} \times \left[k_{S_8^0} \times \varepsilon_{S_8^0} \times \left\{\left(C_{S_8^0}{}^{\gamma_{S_8^0,S_{8(s)}}} \times C_{S^{2-}}{}^{\gamma_{S^{2-},Li_2S}}\right) - K_{sp,Li_2S}\right\}\right], \quad (4.80)$$

$$\frac{\partial \varepsilon C_{S_8^{2-}}}{\partial t} = -\frac{\partial}{\partial x}\left[\left(-D_{S_8^{2-},0} \times \varepsilon^b\right)\frac{\partial C_{S_8^{2-}}}{\partial x} - z_{S_8^{2-}}\frac{\left(D_{S_8^{2-},0} \times \varepsilon^b\right)}{RT}F\, C_{S_8^{2-}}\,\frac{\partial \phi_e}{\partial x}\right] + \left[-a_0 \times \left(\frac{\varepsilon}{\varepsilon_0}\right)^{\xi} \times \left(\frac{1/2\; i_1 - 3/2\; i_2}{F}\right)\right], \quad (4.81)$$

$$\frac{\partial \varepsilon C_{S_6^{2-}}}{\partial t} = -\frac{\partial}{\partial x}\left[\left(-D_{S_6^{2-},0} \times \varepsilon^b\right)\frac{\partial C_{S_6^{2-}}}{\partial x} - z_{S_6^{2-}}\frac{\left(D_{S_6^{2-},0} \times \varepsilon^b\right)}{RT}F\, C_{S_6^{2-}}\,\frac{\partial \phi_e}{\partial x}\right] + \left[-a_0 \times \left(\frac{\varepsilon}{\varepsilon_0}\right)^{\xi} \times \left(\frac{2\, i_2 - i_3}{F}\right)\right], \quad (4.82)$$

$$\frac{\partial \varepsilon C_{S_4^{2-}}}{\partial t} = -\frac{\partial}{\partial x}\left[\left(-D_{S_4^{2-},0} \times \varepsilon^b\right)\frac{\partial C_{S_4^{2-}}}{\partial x} - z_{S_4^{2-}}\frac{\left(D_{S_4^{2-},0} \times \varepsilon^b\right)}{RT}F\, C_{S_4^{2-}}\,\frac{\partial \phi_e}{\partial x}\right] + \left[-a_0 \times \left(\frac{\varepsilon}{\varepsilon_0}\right)^{\xi} \times \left(\frac{3/2\, i_3 - 1/2\, i_4}{F}\right)\right], \quad (4.83)$$

$$\frac{\partial \varepsilon C_{S_2^{2-}}}{\partial t} = -\frac{\partial}{\partial x}\left[\left(-D_{S_2^{2-},0} \times \varepsilon^b\right)\frac{\partial C_{S_2^{2-}}}{\partial x} - z_{S_2^{2-}}\frac{\left(D_{S_2^{2-},0} \times \varepsilon^b\right)}{RT}F\, C_{S_2^{2-}}\,\frac{\partial \phi_e}{\partial x}\right] + \left[-a_0 \times \left(\frac{\varepsilon}{\varepsilon_0}\right)^{\xi} \times \left(\frac{i_4 - 1/2\, i_5}{F}\right)\right], \quad (4.84)$$

$$\frac{\partial \varepsilon C_{S^{2-}}}{\partial t} = -\frac{\partial}{\partial x}\left[\left(-D_{S^{2-},0} \times \varepsilon^b\right)\frac{\partial C_{S^{2-}}}{\partial x} - z_{S^{2-}}\frac{\left(D_{S^{2-},0} \times \varepsilon^b\right)}{RT}F\, C_{S^{2-}}\,\frac{\partial \phi_e}{\partial x}\right]$$

$$+\left[-a_0 \times \left(\frac{\varepsilon}{\varepsilon_0}\right)^{\xi} \times \left(\frac{i_5}{F}\right)\right] - \gamma_{S^{2-},Li_2S}$$

$$\times \left[k_{Li_2S} \times \varepsilon_{Li_2S} \times \left\{\left(C_{Li^+}{}^{\gamma_{Li^+,Li_2S}} \times C_{S^{2-}}{}^{\gamma_{S^{2-},Li_2S}}\right) - K_{sp,Li_2S}\right\}\right], \quad (4.85)$$

$$C_{A^-} = C_{Li^+} - 2C_{S_8^{2-}} - 2C_{S_6^{2-}} - 2C_{S_4^{2-}} - 2C_{S_2^{2-}} 2C_{S^{2-}}, \quad (4.86)$$

$$i_1 = i_{0,1\,ref}\left\{\begin{array}{l}\left(\frac{C_{S_8^0}}{C_{S_8^{2-},0\,ref}}\right)^{\frac{1}{2}} exp\left(\frac{\alpha_{a_1}F}{RT} \times \left(\phi_s - \phi_e - E_{1,ref}\right)\right) \\ -\left(\frac{C_{S_8^0}}{C_{S_8^{2-},0\,ref}}\right)^{\frac{1}{2}} exp\left(\frac{-\alpha_{C_1}F}{RT} \times \left(\phi_s - \phi_e - E_{1,ref}\right)\right)\end{array}\right\}, \quad (4.87)$$

$$i_2 = i_{0,2\,ref}\left\{\begin{array}{l}\left(\frac{C_{S_6^{2-}}}{C_{S_6^{2-},ref}}\right)^{2} exp\left(\frac{\alpha_{a_2}F}{RT}\left(\phi_s - \phi_e - E_{2,ref}\right)\right) \\ -\left(\frac{C_{S_8^{2-}}}{C_{S_8^{2-},ref}}\right)^{\frac{3}{2}} exp\left(\frac{-\alpha_{C_2}F}{RT}\left(\phi_s - \phi_e - E_{2,ref}\right)\right)\end{array}\right\}, \quad (4.88)$$

$$i_3 = i_{0,3\,ref}\left\{\begin{array}{l}\left(\frac{C_{S_4^{2-}}}{C_{S_4^{2-},ref}}\right)^{\frac{3}{2}} exp\left(\frac{\alpha_{a_3}F}{RT}\left(\phi_s - \phi_e - E_{3,ref}\right)\right) \\ -\left(\frac{C_{S_6^{2-}}}{C_{S_6^{2-},ref}}\right) exp\left(\frac{-\alpha_{C_3}F}{RT}\left(\phi_s - \phi_e - E_{3,ref}\right)\right)\end{array}\right\}, \quad (4.89)$$

$$i_4 = i_{0,4\,ref}\left\{\begin{array}{l}\left(\frac{C_{S_2^{2-}}}{C_{S_2^{2-},ref}}\right) exp\left(\frac{\alpha_{a_4}F}{RT}\left(\phi_s - \phi_e - E_{4,ref}\right)\right) \\ -\left(\frac{C_{S_4^{2-}}}{C_{S_4^{2-},ref}}\right)^{\frac{1}{2}} exp\left(\frac{-\alpha_{C_4}F}{RT}\left(\phi_s - \phi_e - E_{4,ref}\right)\right)\end{array}\right\}, \quad (4.90)$$

$$i_5 = i_{0,5\,ref}\left\{\begin{array}{l}\left(\frac{C_{S^{2-}}}{C_{S^{2-},ref}}\right) exp\left(\frac{\alpha_{a_5}F}{RT}\left(\phi_s - \phi_e - E_{5,ref}\right)\right) \\ -\left(\frac{C_{S_2^{2-}}}{C_{S_2^{2-},ref}}\right)^{\frac{1}{2}} exp\left(\frac{-\alpha_{C_5}F}{RT}\left(\phi_s - \phi_e - E_{5,ref}\right)\right)\end{array}\right\}, \quad (4.91)$$

$$i_s = -\sigma\frac{\partial\theta_s}{\partial x}, \quad (4.92)$$

$$i_e = F \times \left[\left\{ z_{Li^+} \times \left[\left(-D_{Li^+,0} \times \varepsilon^b\right) \frac{\partial C_{Li^+}}{\partial x} - z_{Li^+} \frac{\left(D_{Li^+,0} \times \varepsilon^b\right)}{RT} F\, C_{Li^+} \frac{\partial \phi_e}{\partial x} \right] \right\} \right.$$
$$+ \left\{ z_{S_8^0} \times \left[\left(-D_{S_8^0,0} \times \varepsilon^b\right) \frac{\partial C_{S_8^0}}{\partial x} - z_{S_8^0} \frac{\left(D_{S_8^0,0} \times \varepsilon^b\right)}{RT} F\, C_{S_8^0} \frac{\partial \phi_e}{\partial x} \right] \right\}$$
$$+ \left\{ z_{S_8^{2-}} \times \left[\left(-D_{S_8^{2-},0} \times \varepsilon^b\right) \frac{\partial C_{S_8^{2-}}}{\partial x} - z_{S_8^{2-}} \frac{\left(D_{S_8^{2-},0} \times \varepsilon^b\right)}{RT} F\, C_{S_8^{2-}} \frac{\partial \phi_e}{\partial x} \right] \right\}$$
$$+ \left\{ z_{S_6^{2-}} \times \left[\left(-D_{S_6^{2-},0} \times \varepsilon^b\right) \frac{\partial C_{S_6^{2-}}}{\partial x} - z_{S_6^{2-}} \frac{\left(D_{S_6^{2-},0} \times \varepsilon^b\right)}{RT} F\, C_{S_6^{2-}} \frac{\partial \phi_e}{\partial x} \right] \right\}$$
$$+ \left\{ z_{S_4^{2-}} \times \left[\left(-D_{S_4^{2-},0} \times \varepsilon^b\right) \frac{\partial C_{S_4^{2-}}}{\partial x} - z_{S_4^{2-}} \frac{\left(D_{S_4^{2-},0} \times \varepsilon^b\right)}{RT} F\, C_{S_4^{2-}} \frac{\partial \phi_e}{\partial x} \right] \right\}$$
$$+ \left\{ z_{S_2^{2-}} \times \left[\left(-D_{S_2^{2-},0} \times \varepsilon^b\right) \frac{\partial C_{S_2^{2-}}}{\partial x} - z_{S_2^{2-}} \frac{\left(D_{S_2^{2-},0} \times \varepsilon^b\right)}{RT} F\, C_{S_2^{2-}} \frac{\partial \phi_e}{\partial x} \right] \right\}$$
$$+ \left\{ z_{S^{2-}} \times \left[\left(-D_{S^{2-},0} \times \varepsilon^b\right) \frac{\partial C_{S^{2-}}}{\partial x} - z_{S^{2-}} \frac{\left(D_{S^{2-},0} \times \varepsilon^b\right)}{RT} F\, C_{S^{2-}} \frac{\partial \phi_e}{\partial x} \right] \right\}$$
$$\left. + \left\{ z_{A^-} \times \left[\left(-D_{A^-,0} \times \varepsilon^b\right) \frac{\partial C_{A^-}}{\partial x} - z_{A^-} \frac{\left(D_{A^-,0} \times \varepsilon^b\right)}{RT} F\, C_{A^-} \frac{\partial \phi_e}{\partial x} \right] \right\} \right], \quad (4.93)$$

$$I_{applied} = i_s + i_e, \quad (4.94)$$

$$\frac{\partial i_e}{\partial x} = a\omega_c \left(\frac{\varepsilon}{\varepsilon_{ref}} \right)^{\xi} (i_1 + i_2 + i_3 + i_4 + i_5), \quad (4.95)$$

$$\frac{\partial \varepsilon}{\partial t} = -\left\{ \tilde{V}_{Li_2S_{(s)}} \times k_{Li_2S} \times \varepsilon_{Li_2S} \times \left[\left(C_{Li^+}{}^{\gamma_{Li^+,Li_2S}} \times C_{S^{2-}}{}^{\gamma_{S^{2-},Li_2S}} \right) - K_{sp,Li_2S} \right] \right.$$
$$\left. + \tilde{V}_{S_{8(s)}} \times k_{S_8^0} \times \varepsilon_{S_8^0} \times \left[\left(C_{S_8^0}{}^{\gamma_{S_8^0,S_{8(s)}}} \right) - K_{sp,Li_2S} \right] \right\}, \quad (4.96)$$

$$\frac{\partial \varepsilon_{Li_2S_{(s)}}}{\partial t} = \tilde{V}_{Li_2S_{(s)}} \times k_{Li_2S} \times \varepsilon_{Li_2S} \times \left[\left(C_{Li^+}{}^{\gamma_{Li^+,Li_2S}} \times C_{S^{2-}}{}^{\gamma_{S^{2-},Li_2S}} \right) - K_{sp,Li_2S} \right], \quad (4.97)$$

$$\varepsilon s_8^0 = 1 - \varepsilon - \varepsilon_{Li_2S} - \varepsilon_{carbon} - \varepsilon_{binder}\,. \quad (4.98)$$

4.2.2. Initial Conditions

It is presumed that only the first reaction occurs at first in this model as well. Moreover, it is assumed that there are no concentration variations initially within the cell.

Therefore, the initial conditions are derived using the same approach used in the 0-D model. The initial conditions for the model are given as

$$C_{Li^+} = C_{Li^+,ref}, \tag{4.99}$$

$$C_{S_8^0} = C_{S_8^0,ref}, \tag{4.100}$$

$$C_{S_8^{2-}} = C_{S_8^{2-},ref}, \tag{4.101}$$

$$C_{S_6^{2-}} = C_{S_6^{2-},ref}, \tag{4.102}$$

$$C_{S_4^{2-}} = C_{S_4^{2-},ref}, \tag{4.103}$$

$$C_{S_2^{2-}} = C_{S_2^{2-},ref}, \tag{4.104}$$

$$C_{S^{2-}} = C_{S^{2-},ref}, \tag{4.105}$$

$$C_{A^-} = C_{A^-,ref}, \tag{4.106}$$

$$i_1 = -\frac{I_{app}}{a_0 L}, \tag{4.107}$$

$$i_2 = 0, \tag{4.108}$$

$$i_3 = 0, \tag{4.109}$$

$$i_4 = 0, \tag{4.110}$$

$$i_5 = 0, \tag{4.111}$$

$$\theta_s = \frac{-I_{app}}{2L\sigma} x^2, \tag{4.112}$$

$$\theta_e = \theta_s - \left(E_{1,ref} + \frac{RT}{-\alpha_C F} \ln\left(\frac{I_{app}}{a_0 L i_{0,1ref}} \right) \right), \tag{4.113}$$

$$i_s = I_{app} - i_e, \tag{4.114}$$

$$i_e = I_{app} \left(1 - \frac{x}{L}\right), \tag{4.115}$$

$$\varepsilon = \varepsilon_{initial}, \tag{4.116}$$

$$\varepsilon_{Li_2S} = \varepsilon_{Li_2S_{(s)},initial}, \tag{4.117}$$

$$\varepsilon_{s_8^0} = \varepsilon_{S_{8(s)},initial}. \tag{4.118}$$

4.2.3. Boundary Conditions

Boundary conditions for the separator- cathode interface, in other words, at x=0, given as

$$C_{Li^+} = C_{Li^+,ref}, \tag{4.119}$$

$$N_{S_8^0} = 0, \tag{4.120}$$

$$\mathrm{N}_{S_8^{2-}} = 0, \tag{4.121}$$

$$\mathrm{N}_{S_6^{2-}} = 0, \tag{4.122}$$

$$\mathrm{N}_{S_4^{2-}} = 0, \tag{4.123}$$

$$\mathrm{N}_{S_2^{2-}} = 0, \tag{4.124}$$

$$\mathrm{N}_{S^{2-}} = 0, \tag{4.125}$$

$$C_{A^-} = C_{Li^+} - 2C_{S_8^{2-}} - 2C_{S_6^{2-}} - 2C_{S_4^{2-}} - 2C_{S_2^{2-}} - 2C_{S^{2-}}, \tag{4.126}$$

$$\theta_s = 0, \tag{4.127}$$

$$i_s = 0, \tag{4.128}$$

$$i_e = I_{app}. \tag{4.129}$$

The boundary conditions for the cathode-current collector interface, in other words, at x=L, given as

$$\mathrm{N}_{Li^+} = 0, \tag{4.130}$$

$$\mathrm{N}_{S_8^0} = 0, \tag{4.131}$$

$$\mathrm{N}_{S_8^{2-}} = 0, \tag{4.132}$$

$$\mathrm{N}_{S_6^{2-}} = 0, \tag{4.133}$$

$$\mathrm{N}_{S_4^{2-}} = 0, \tag{4.134}$$

$$\mathrm{N}_{S_2^{2-}} = 0, \tag{4.135}$$

$$\mathrm{N}_{S^{2-}} = 0, \tag{4.136}$$

$$C_{A^-} = C_{Li^+} - 2C_{S_8^{2-}} - 2C_{S_6^{2-}} - 2C_{S_4^{2-}} - 2C_{S_2^{2-}} - 2C_{S^{2-}}, \tag{4.137}$$

$$i_s = I_{app,} \tag{4.138}$$

$$i_e = 0. \tag{4.139}$$

Table 4.5. Parameters used in the one-dimensional model.

Parameters	**Units**	**1-D Model**
$\boldsymbol{C_{Li^+,ref}}$	$mol\ m^{-3}$	1001.4
$\boldsymbol{C_{S_8^0,ref}}$	$mol\ m^{-3}$	19.0
$\boldsymbol{C_{S_8^{2-},ref}}$	$mol\ m^{-3}$	0.178

Table 4.5. Parameters used in the one-dimensional model (cont.).

Parameters	Units	1-D Model
$C_{S_6^{2-},ref}$	$mol\ m^{-3}$	0.324
$C_{S_4^{2-},ref}$	$mol\ m^{-3}$	0.02
$C_{S_2^{2-},ref}$	$mol\ m^{-3}$	5.229×10^{-7}
$C_{S^{2-},ref}$	$mol\ m^{-3}$	8.267×10^{-10}
$C_{A^-,ref}$	$mol\ m^{-3}$	1000
E_1	V	2.35
E_2	V	2.33
E_3	V	2.24
E_4	V	2.06
E_5	V	2.01
T	K	298
R	$J\ K^{-1}mol^{-1}$	8.3145
F	$C\ mol^{-1}$	9.649×10^4
$i^0_{1,ref}$	$A\ m^{-2}$	2.0
$i^0_{2,ref}$	$A\ m^{-2}$	1.5
$i^0_{3,ref}$	$A\ m^{-2}$	1.0
$i^0_{4,ref}$	$A\ m^{-2}$	0.6
$i^0_{5,ref}$	$A\ m^{-2}$	0.3
k_{Li_2S}	$m^6mol^2s^{-1}$	1.5×10^{-5}

Table 4.5. Parameters used in the one-dimensional model (cont.).

Parameters	Units	1-D Model
k_{S_8}	s^{-1}	3.0×10^{-4}
K_{sp,Li_2S}	$m\ mol^3$	1000
K_{sp,S_8}	$m\ mol^3$	386.0
V_{Li_2S}	$mol^{-1}m^3$	2.8×10^{-5}
V_{S_8}	$mol^{-1}m^3$	7.56×10^{-5}
D_{Li^+}	m^2s^{-1}	3.0×10^{-11}
$D_{S_8^0}$	m^2s^{-1}	3.0×10^{-10}
$D_{S_8^{2-}}$	m^2s^{-1}	1.8×10^{-10}
$D_{S_6^{2-}}$	m^2s^{-1}	1.8×10^{-10}
$D_{S_4^{2-}}$	m^2s^{-1}	3.0×10^{-11}
$D_{S_2^{2-}}$	m^2s^{-1}	3.0×10^{-11}
$D_{S^{2-}}$	m^2s^{-1}	3.0×10^{-11}
D_{A^-}	m^2s^{-1}	1.2×10^{-10}
a_0	$m^2\ m^{-3}$	796,572

Table 4.5 presents the model parameters, whereas Table 4.6 shows the parameters used for the calculation of the E/S ratio as a design parameter. These values seen in the table are used in both the zero-dimensional and the one-dimensional electrochemical models developed in this study.

Table 4.6. Parameters used for the E/S ratio calculation in both models.

E/S Ratio (mL gS-1)	**3**	**6**	**9**	**13**	**16**	**20**	**23**
C/S Ratio	0.5	0.5	0.5	0.5	0.5	0.5	0.5
ω_c **C:S:B (wt:wt:wt)**	0.6:0.3:0.1	0.6:0.3:0.1	0.6:0.3:0.1	0.6:0.3:0.1	0.6:0.3:0.1	0.6:0.3:0.1	0.6:0.3:0.1
ρ_S **(g/cm^3)**	2.07	2.07	2.07	2.07	2.07	2.07	2.07
ρ_C **(g/cm^3)**	1.8	1.8	1.8	1.8	1.8	1.8	1.8
ρ_{Binder} **(g/cm^3)**	1.77	1.77	1.77	1.77	1.77	1.77	1.77
$\rho_{Electrolyte}$ **(g/cm^3)**	1.2	1.2	1.2	1.2	1.2	1.2	1.2
$\rho_{Cathode}$ **(g/cm^3)**	0.4327	0.2433	0.1692	0.1203	0.0989	0.0799	0.0699
ε	0.778	0.875	0.913	0.938	0.949	0.959	0.964
$\varepsilon_{S_{8(s)},initial}$	0.125	0.071	0.049	0.035	0.029	0.023	0.020
ε_{Carbon}	0.072	0.041	0.028	0.020	0.016	0.013	0.012
$\varepsilon_{binder,initial}$	0.023	0.013	0.009	0.006	0.005	0.004	0.003
$\varepsilon_{Li_2S_{(s)},initial}$	1×10^{-4}	1×10^{-4}	1×10^{-4}	1×10^{-4}	1×10^{-4}	1×10^{-4}	1×10^{-4}
ε_{ref}	0.99	0.99	0.99	0.99	0.99	0.99	0.99
E/S Ratio (mL gS-1)	3	6	9	13	16	20	23
Sulfur Loading (mgS cm^{-2})	1.2	1.2	1.2	1.2	1.2	1.2	1.2
L**, µm**	46	82	118	166	202	250	287
$I_{applied}$ $A\,m^{-2}$	2.01	2.01	2.01	2.01	2.01	2.01	2.01

While changing the E/S ratio in both models, the applied current densities and carbon-to-sulfur ratios are kept constant. A sample calculation of the E/S ratio and the other design parameters are given as

$$\varepsilon + \varepsilon_{Li_2S} + \varepsilon_{S_{8(s),initial}} + \varepsilon_{carbon} + \varepsilon_{binder} = 1, \tag{4.140}$$

$$\omega_C + \omega_s + \omega_B = 1, \tag{4.141}$$

$$\frac{1-\varepsilon}{{\omega_S}/{\rho_S} + {\omega_C}/{\rho_C} + {\omega_{binder}}/{\rho_{binder}}} = \rho_{Cathode}, \tag{4.142}$$

$$\frac{\omega_S}{\rho_S} \times \rho_{Cathode} = \varepsilon_{S_{8(s)}}, \tag{4.143}$$

$$\text{E/S Ratio} = \frac{\varepsilon_{initial}}{\varepsilon_{S_{8(s),initial}} \times \rho_S} = \frac{0.7780}{0.12554 \times 2.07} = 3. \tag{4.144}$$

4.3. Linearization and Simulation Procedure

In order to solve equations by block tridiagonal matrix algorithm, which Newman and Thomas Alyea used, in FORTRAN programming language, all equations are linearized by using the Taylor series [66].

$$\sum_k a_{i,k}(x)\frac{d^2C_k}{dx^2} + b_{i,k}(x)\frac{dC_k}{dx} + d_{i,k}(x)C_k = g_i(x), \tag{4.145}$$

$$\sum_k p_{i,k}(x)\frac{dC_k}{dx} + e_{i,k}(x)C_k = f_i. \tag{4.146}$$

General formula used in the linearization of the governing equations and boundary conditions are given Equation 4.145 and Equation 4.146, respectively. $a_{i,k}(x)$, $b_{i,k}(x)$, $d_{i,k}(x)$, $g_i(x)$, $p_{i,k}(x)$, $e_{i,k}(x)$ and $f_i(x)$ coefficients are obtained for each equation and then used in the subroutines generated by Newman and Thomas. The example of the linearization is given for Equation 4.85 in Appendix A.

5. RESULTS AND DISCUSSION

5.1. Experimental Characterization of the Effect of the Electrolyte-to-Sulfur Ratio on Battery Performance for Different Electrolyte Systems

In this part of the thesis, the results of the impact of the electrolyte-to-sulfur ratio on the lithium-sulfur battery performance are reported. Firstly, the results of the experimental studies on the effect of the E/S ratio on the cell performance, such as cycling performance and discharge profiles, and resistance of batteries for different electrolyte systems, are given. Then, the predictions of two electrochemical models - zero-dimensional and one-dimensional electrochemical models- for the influence of the E/S ratio on battery performance for various types of electrolyte systems are discussed.

5.1.1. Electrochemical Characterization of the Lithium-Sulfur Batteries by Galvanostatic Cycling

As a design parameter, the electrolyte-to-sulfur ratio plays a significant role in the performance of Li-S batteries because it affects the polysulfide shuttle mechanism, ionic conductivity, and wettability, and all these impacts the battery performance [48]. Therefore, the Li-S battery performance is experimentally characterized for four different E/S ratios with seven types of electrolyte systems.

Figure 5.1 shows the change in discharge capacity along with the cycle number for 1M LiTFSI and 0.1 $LiNO_3$ in DOL: DME electrolyte, which is the most commonly used electrolyte in Li-S cells, at varied E/S ratios. Even though the E/S ratio of 6 µL/mg shows the highest capacity, especially till the 70^{th} cycle, the capacity retention is the worst among others. Therefore, as is seen in the figure, the E/S ratio of 9 µL/mg shows the best capacity retention and high discharge capacity. Except for the E/S ratio of 6 µL/mg, the capacity fade increases with increasing E/S ratio because higher electrolyte amounts enhance the polysulfide shuttle mechanism in the cell.

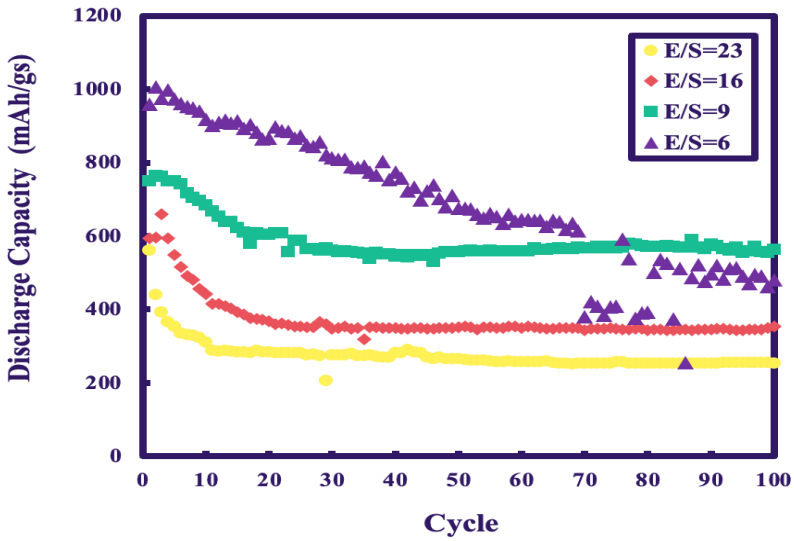

Figure 5.1. Variation of discharge capacity with the number of cycles for 1M LiTFSI and 0.1M $LiNO_3$ in DOL: DME (1:1 vol %) electrolyte at a constant C-rate of 0.1C and sulfur loading of 1.2 mg/cm^2.

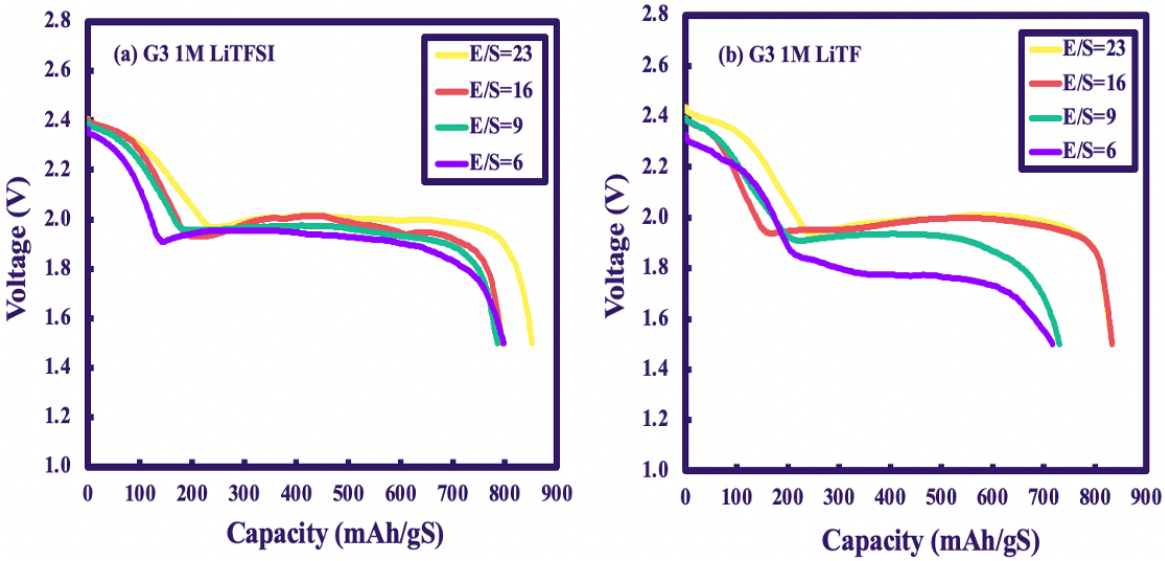

Figure 5.2. Impact of the E/S ratio on the initial discharge profile of Li-S batteries for (a) 1M LiTFSI and (b) 1M LiTF in triglyme electrolytes.

Figure 5.2 depicts the effect of the electrolyte amount on the first discharge profile of the Li-S batteries with 1M LiTFSI and 1M LiTF in triglyme electrolytes. Even though higher E/S ratios give rise to higher first discharge capacities and cell voltages, in general, there is no remarkable change in the capacity of cells with changing E/S ratio for both

electrolyte systems, especially for triglyme with 1M LiTFSI electrolyte (Figure 5.2a). In Figure 5.2b, the first discharge capacities of cells with E/S ratios of 23 and 16 µL/mg are highly similar, while there is a slight difference between the cells with E/S ratios of 9 and 6 µL/mg. Overall, the first discharge profiles of the cells for both electrolytes do not change significantly along with the change in the electrolyte amount.

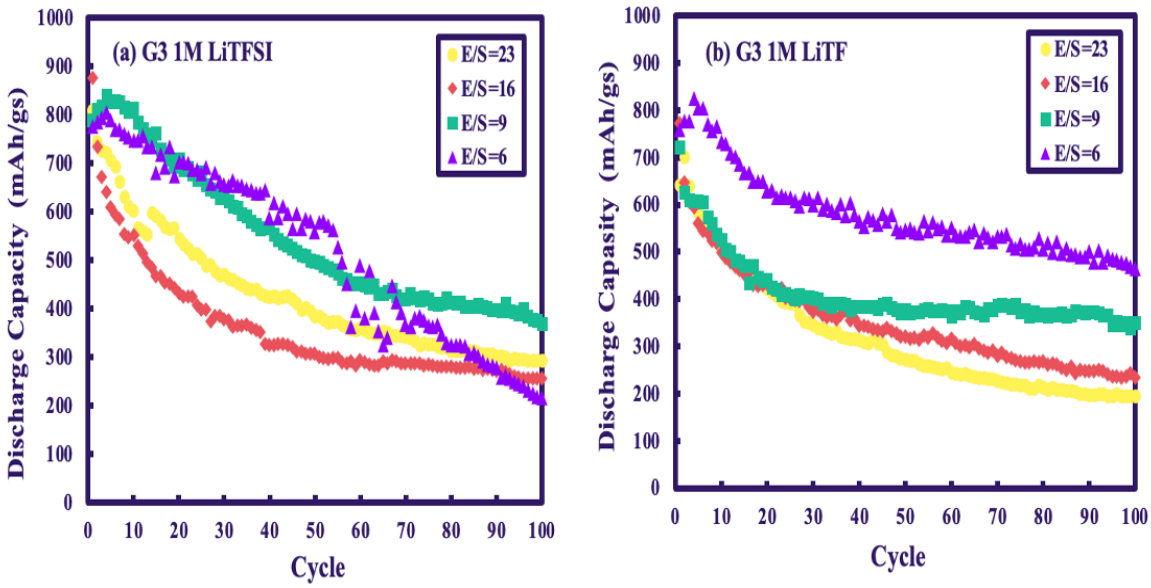

Figure 5.3. Change of the discharge capacity with the number of cycles for (a) 1M LiTFSI and (b) 1M LiTF in triglyme electrolyte at a constant C-rate of 0.1C and sulfur loading of 1.2 mg/cm^2.

Figure 5.3. illustrates the cycling performance of two triglyme-based electrolytes with LiTFSI or LiTF salts for four E/S ratios, 23, 16, 9, and 6 µL/mg. In Figure 5.3a, a rapid decline in the discharge capacities is seen for the two highest E/S ratios, 23 and 16 µL/mg, in the first 50 cycles. While cells with E/S ratios of 9 and 6 µL/mg have almost the same trend till the 50th cycle, the cycling performance for the lowest E/S ratio of 6 µL/mg gets poorer after the 50th cycle, and the capacity fade of the lowest E/S ratio becomes the highest. It is seen in Figure 5.3b that the cycling performance of the cells with E/S ratios of 23, 16, and 9 µL/mg is very similar until the 30th cycle. However, after this cycle, the impact of the E/S ratio on the cycling performance becomes clearer; the capacity for the cell with an E/S ratio of 9 µL/mg is almost constant, while the capacity for the cells with E/S ratios of 23 and 16 µL/mg continues to decrease slowly. Interestingly, the best cycling performance is seen for the lowest E/S ratio of 6 µL/mg for 1M LiTF in G3 electrolyte system, which suggests

that LiTF may be a better alternative compared to LiTFSI, which is the most common type of salt used in Li-S batteries, in G3-based electrolytes.

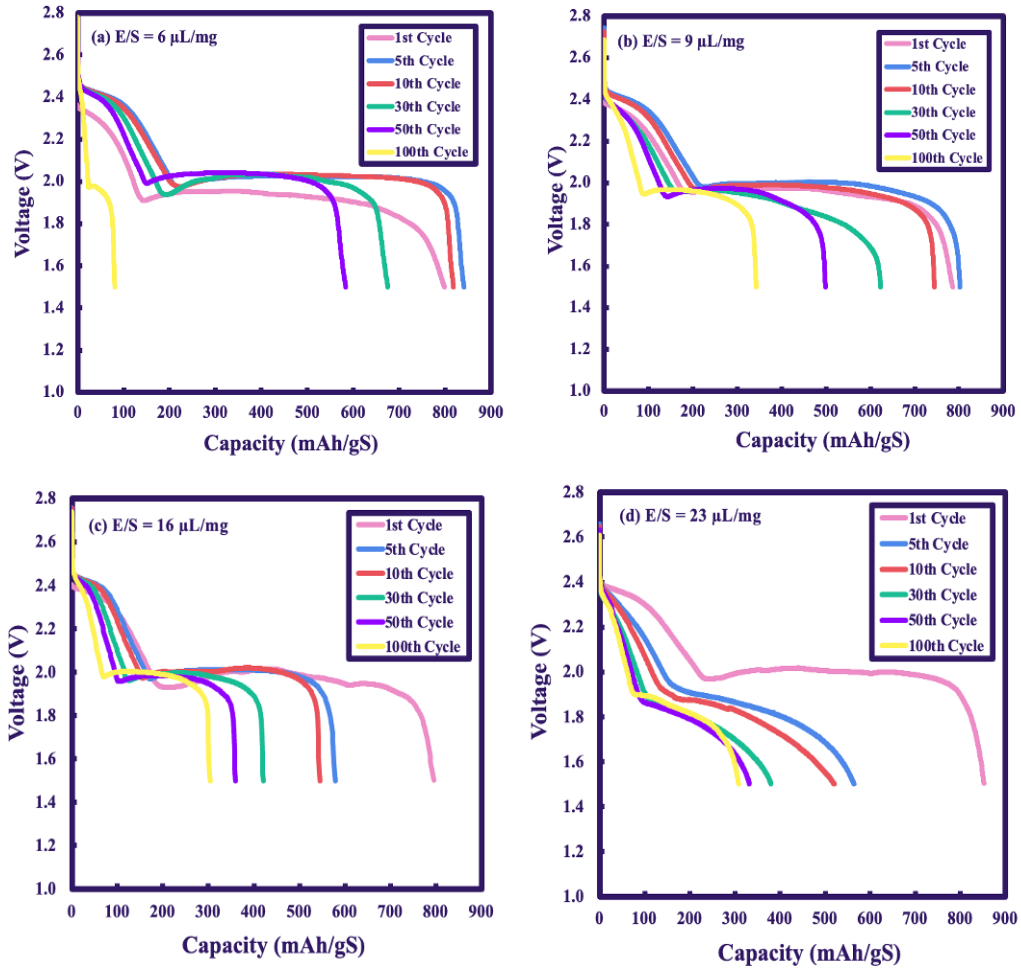

Figure 5.4. Discharge profiles of the Li-S cells with E/S ratios of (a) 6 µL/mg, (b) 9 µL/mg, (c) 16 µL/mg, and (d) 23 µL/mg for 1M LiTFSI in Triglyme.

Figure 5.4 illustrates the discharge profiles of the Li-S batteries for four different E/S ratios with electrolytes based on 1M LiTFSI in G3 at different cycles. In nearly all E/S ratios (Figure 5.4b, 5.4c, and 5.4d), except 6 µL/mg, the decrease in the capacity from the 1st cycle to the 100th is at nearly the same degree. As for the E/S ratio of 6 µL/mg (Figure 5.4a), a considerable decrease is seen between the 100th and the 1st cycle. In general, a decreasing trend in discharge capacity is seen for all E/S ratios while getting cycled because polysulfide concentration increases in the electrolyte after a while. This makes the electrolyte more viscous, leading to poor wettability and ionic conductivity. All of this gives rise to capacity fade [48]. Nevertheless, in the lowest E/S ratios of 9 and 6 µL/mg, after the first cycle, the

capacity increases at the 5th, and 5th, and 10th cycles, respectively. In addition, the first plateau of the discharge profile is not as clear as the others in the E/S ratio of 23 µL/mg (Figure 5.4d), except for the 1st cycle. Overall, it can be said that the E/S ratio of 9 µL/mg has the best capacity retention and cycling performance for 1M LiTFSI in G3-based electrolytes, among other electrolyte amounts.

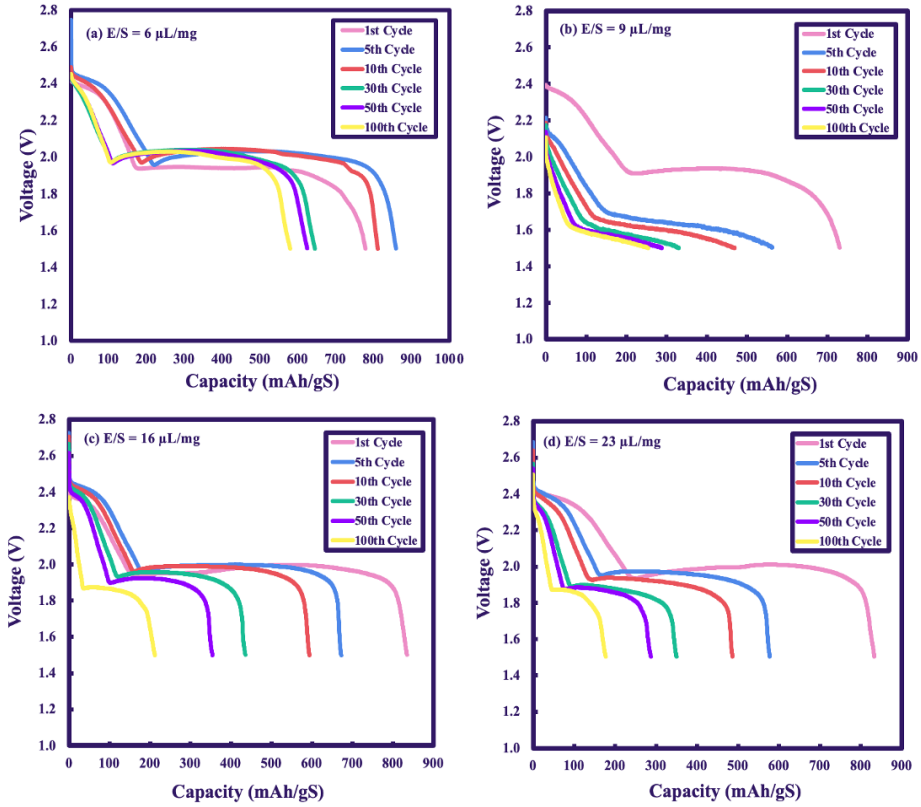

Figure 5.5. Discharge profiles of the Li-S cells with E/S ratios of (a) 6 µL/mg, (b) 9 µL/mg, (c) 16 µL/mg, and (d) 23 µL/mg for 1M LiTF in Triglyme.

Discharge profiles of the Li-S batteries with an electrolyte composed of 1M LiTF in G3 for different electrolyte amounts are depicted in Figure 5.5. There is a considerable decline in the capacity in all E/S ratios. E/S ratios of 16 and 23 µL/mg have approximately the same decline in capacity at the end of the cycles (Figure 5.5c and Figure 5.5d, respectively). In the two lowest E/S ratios of 6 and 9 µL/mg, capacity retention is better than the highest E/S ratios. However, the discharge profiles of the E/S ratios of 6 and 9 µL/mg are not as typical as others. The first and second plateaus are not very clear at an E/S ratio of 9 µL/mg, whereas the behavior of the E/S ratio of 6 µL/mg differs from others. At the

beginning of the cycling, the capacity increases, then it decreases after the 5th cycle. Also, besides the decline in capacity with cycling, the potential diminishes after the first cycle as well. When all E/S ratios are compared, the best capacity retention is observed for the E/S ratio of 6 µL/mg.

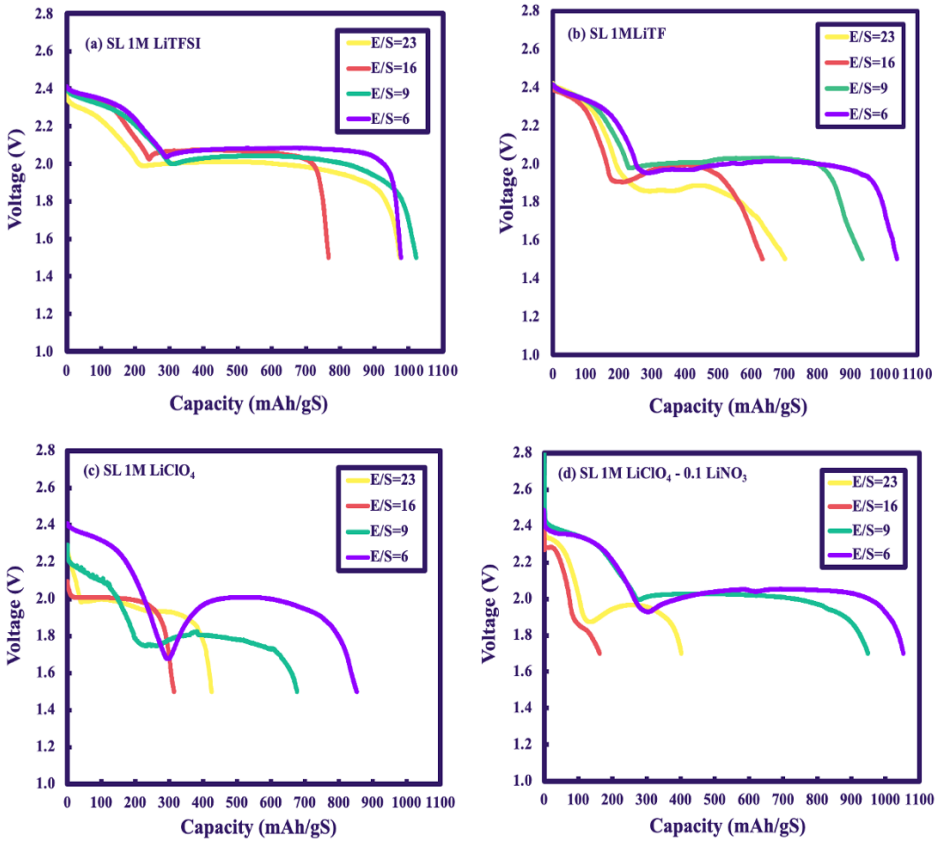

Figure 5.6. Effect of the E/S ratio on the initial discharge profile of Li-S batteries with (a) 1M LiTFSI, (b) 1M LiTF, (c) 1M $LiClO_4$, and (d) 1M $LiClO_4$ and 0.1M $LiNO_3$ in Sulfolane electrolytes.

Figure 5.6 demonstrates the change in the first discharge profile of Li-S batteries with four different types of salt in sulfolane-based electrolyte systems such as 1M LiTFSI, 1M LiTF, 1M $LiClO_4$, and 1M $LiClO_4$ and 0.1M $LiNO_3$ in sulfolane according to the E/S ratio. It is clearly seen that the salt type used in sulfolane-based electrolytes determines how the E/S ratio influences the capacity vitally because of having different chemical compounds and properties. In general, the same trend is obtained for the change in capacity while changing electrolyte amount. In Figure 5.6a and Figure 5.6b, capacity is not affected significantly by the alteration of the E/S ratio compared to the $LiClO_4$-based electrolyte. The

E/S ratio of 6 µL/mg has the highest capacity in 1M $LiClO_4$, and 1M $LiClO_4$ and 0.1M $LiNO_3$ in Sulfolane-based electrolyte systems (Figure 5.6c and Figure 5.6d). The change in the E/S ratio of both electrolytes affects the first discharge in the same way. However, the initial discharge capacity of the E/S ratio of 6 µL/mg in Figure 5.6d is higher than the E/S ratio of 6 µL/mg of 0.1M $LiNO_3$ in sulfolane.

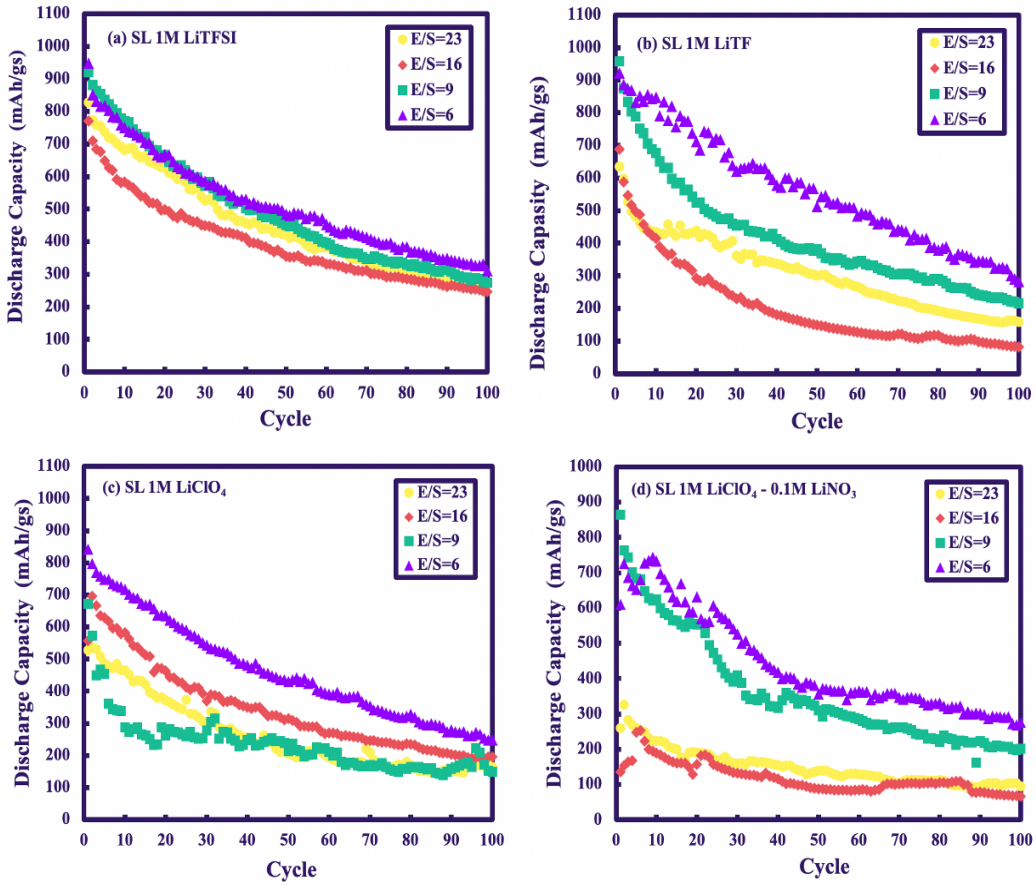

Figure 5.7. Change of the discharge capacity with the number of cycles for (a) 1M LiTFSI, (b) 1M LiTF, (c) 1M $LiClO_4$, and (d) 1M $LiClO_4$ and $LiNO_3$ in Sulfolane, SL electrolyte at a constant C-rate of 0.1C and sulfur loading of 1.2 mg/cm^2.

Figure 5.7 shows the cycling performance of the Li-S batteries with 1M LiTFSI, 1M LiTF, 1M $LiClO_4$, and 1M $LiClO_4$ and $LiNO_3$ in Sulfolane, SL-based electrolytes for various E/S ratios. 1M LiTFSI solution in SL (Figure 5.7a) is not much affected by the change of the electrolyte amount, but the E/S ratio of 6 µL/mg has better retention of the capacity and cycling performance among other types of electrolytes. In Figure 5.7b, the highest capacity is seen in the E/S ratio of 6µL/mg, but the capacity retention of this cell is not better than the

others. As for the 1M $LiClO_4$ in SL electrolyte systems, the lowest E/S ratio has the highest capacity (Figure 5.7c and Figure 5.7d). In addition, for the electrolyte containing 1M $LiClO_4$ and $LiNO_3$, the two lowest E/S amounts, 9 and 6 µL/mg, have a higher capacity than the two highest E/S ratios, 23 and 16 µL/mg, but as for capacity retention, the opposite trend is seen.

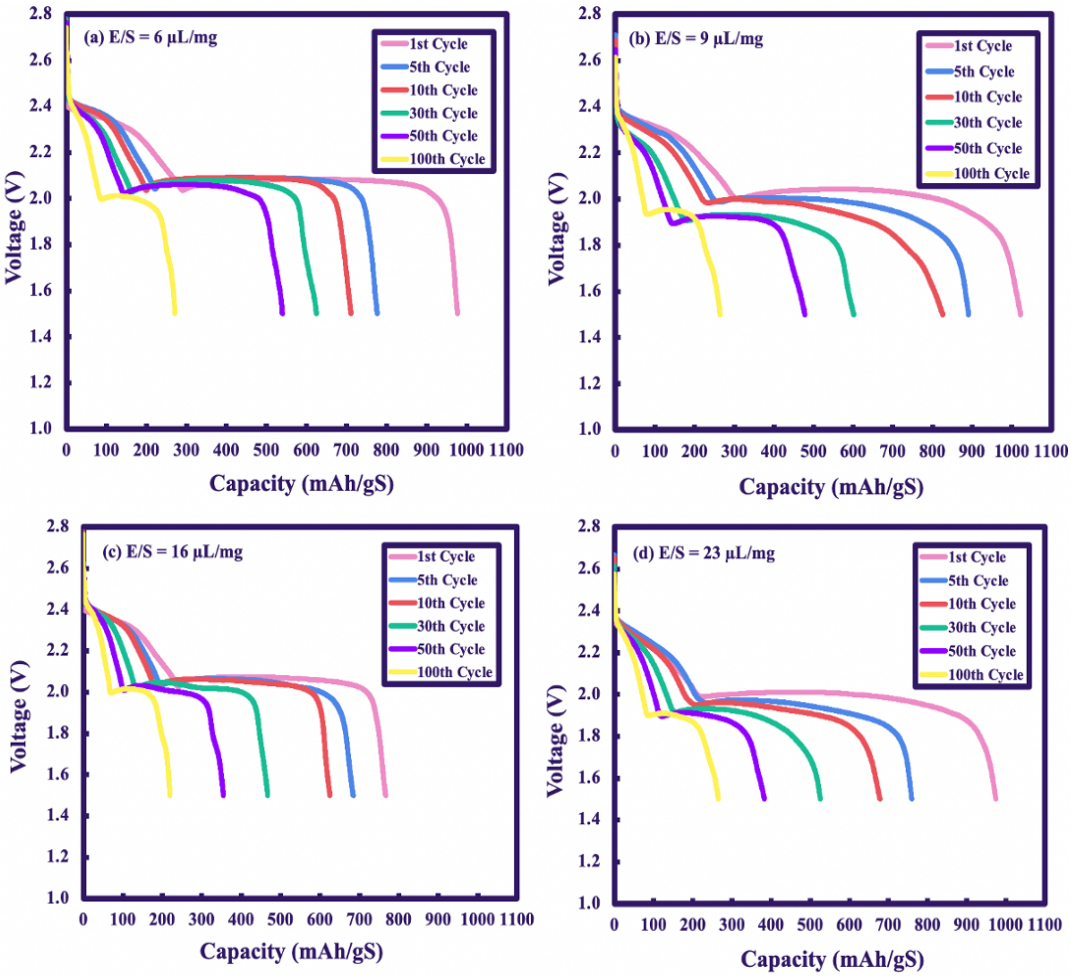

Figure 5.8. Discharge profiles of the Li-S cells with E/S ratios of (a) 6 µL/mg, (b) 9 µL/mg, (c) 16 µL/mg, and (d) 23 µL/mg for 1M LiTFSI in Sulfolane electrolyte.

Figure 5.8 shows the discharge profiles of Li-S batteries containing 1M LiTFSI in sulfolane with various E/S ratios at various cycles. It is seen that there is a considerable decline in the capacity of all E/S ratios during cycling. In addition, two plateaus of the discharge profile of all electrolyte amounts are clear. Also, in almost all E/S ratios, the capacity fade is similar, but the capacity fade for the E/S ratio of 16 µL/mg is minimally more than the other E/S ratios (Figure5.8c).

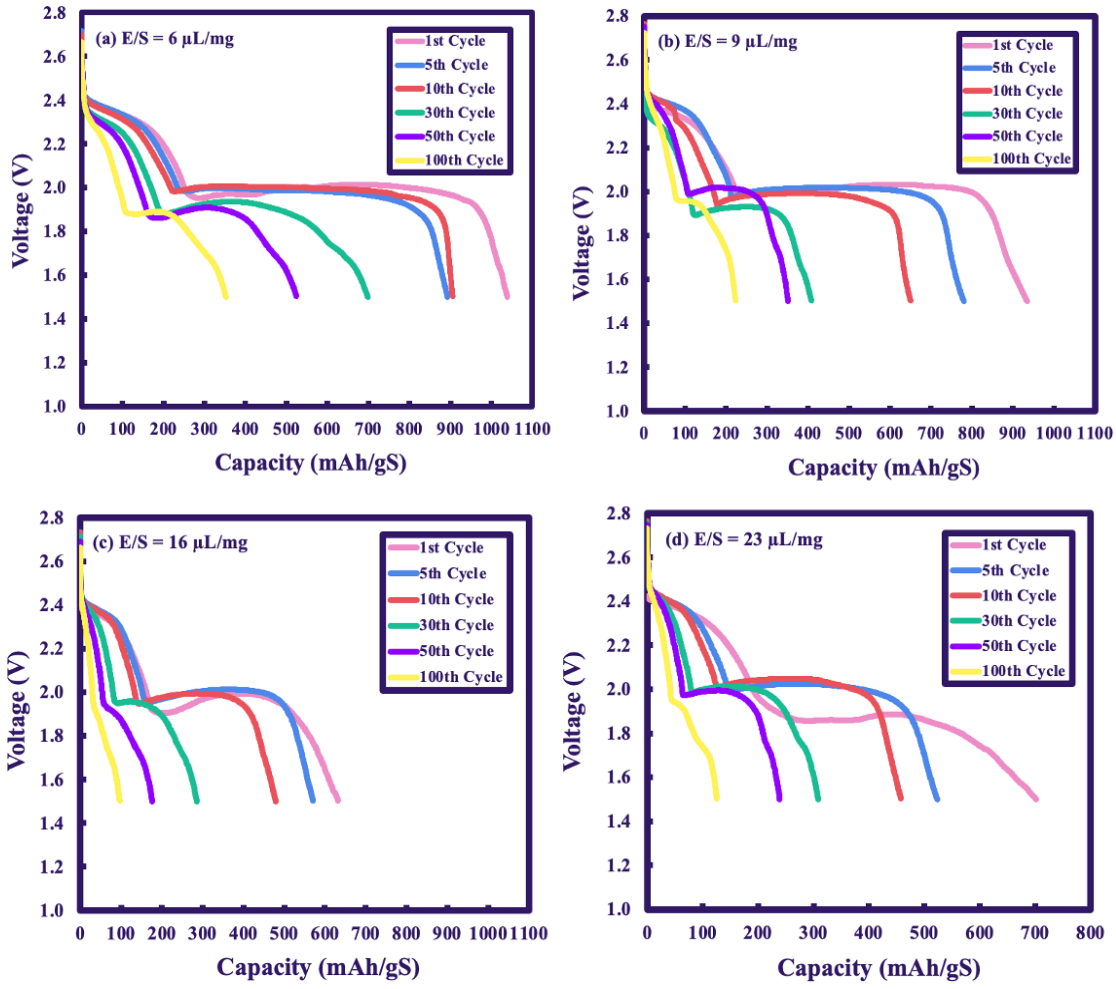

Figure 5.9. Discharge profiles of the Li-S cells with E/S ratios of (a) 6 µL/mg, (b) 9 µL/mg, (c) 16 µL/mg and (d) 23 µL/mg for 1M LiTF in Sulfolane electrolyte.

In Figure 5.9, the discharge profiles of Li-S cells with 1M LiTF in SL for E/S ratios of 23, 16, 9, and 6 µL/mg at various cycles are observed. In general, when compared to electrolytes comprising LiTFSI (Figure 5.8), the discharge profiles are not typical and apparent as in the cells with LiTFSI for the E/S ratio of 16 and 23 µL/mg (Figure 5.9c and 5.9d). Also, a noteworthy capacity fade is detected in all electrolyte amounts. Interestingly, while the capacity mitigates along with cycling in E/S ratios of 23, 16, and 9 µL/mg (Figure 5.9b, 5.9c, and 5.9d), at the beginning of the cycling of E/S ratio of 6 µL/mg, the capacity of this cell shows a different behavior. In other words, the capacity of E/S ratio of 6 µL/mg at the 10^{th} cycle is higher than the fifth cycle. Briefly, the E/S ratio of 6 µL/mg shows a different trend while cycling compared to the other E/S amounts.

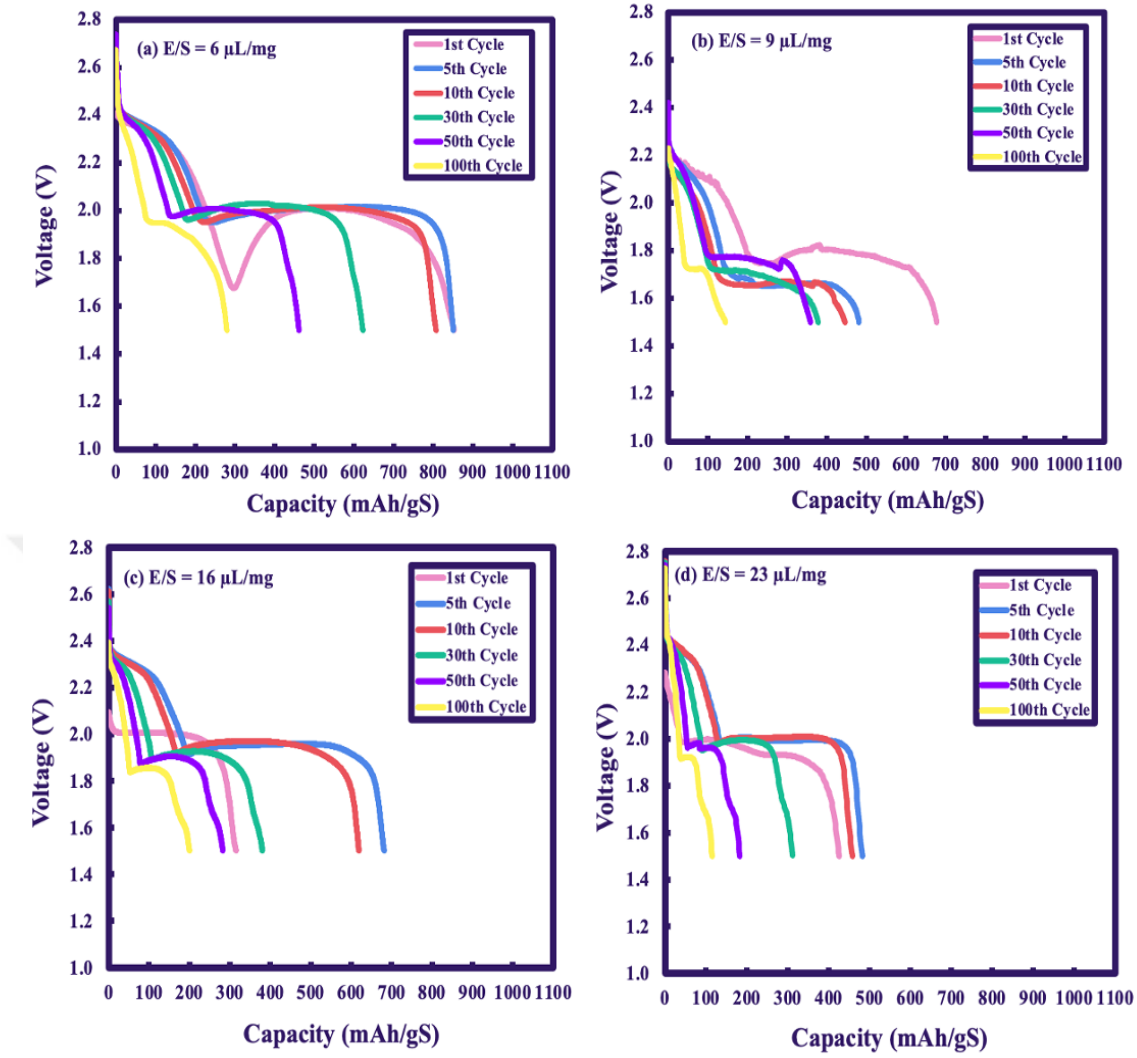

Figure 5.10. Discharge profiles of the Li-S cells with E/S ratios of (a) 6 µL/mg, (b) 9 µL/mg, (c) 16 µL/mg, and (d) 23 µL/mg for 1M $LiClO_4$ in Sulfolane electrolyte.

The discharge profiles of the lithium sulfur batteries with 1M $LiClO_4$ in Sulfolane at different E/S ratios are illustrated in Figure 5.10. Significant capacity fade is seen in all electrolyte amounts. E/S ratios of 6 and 9 µL/mg have the same trend of decline in capacity during cycling (Figure 5.10a and Figure 5.10b). While getting cycled, capacity decreases continuously in these E/S ratios. However, the capacity of the E/S ratios of 16 and 23 µL/mg increases at the beginning of cycling for a while and then starts to decline (Figure 5.10c and Figure 5.10d). In addition, the discharge profile is unclear for all cycles in the E/S ratio of 9 µL/mg. In general, the E/S ratio of 6 µL/mg has better capacity retention and discharge profile among other E/S ratios in this electrolyte system.

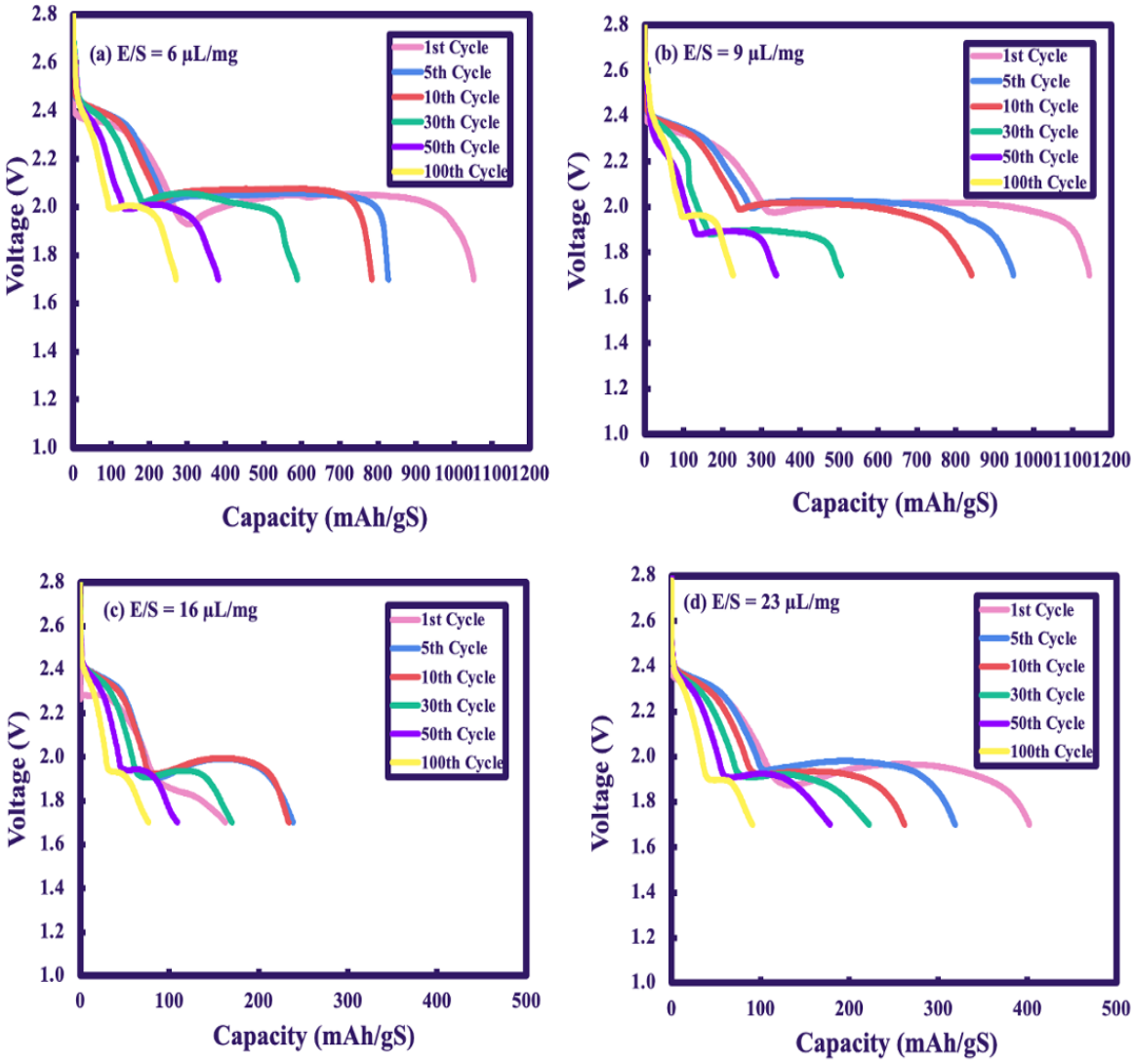

Figure 5.11. Discharge profiles of the Li-S cells with E/S ratios of (a) 6 µL/mg, (b) 9 µL/mg, (c) 16 µL/mg, and (d) 23 µL/mg for 1M $LiClO_4$ and $LiNO_3$ in Sulfolane electrolyte.

Figure 5.11 demonstrates the discharge profile of Li-S batteries with 1M $LiClO_4$ and $LiNO_3$ in sulfolane electrolyte for various electrolyte amounts during cycling. The capacity of the cell with E/S ratios of 6, 9, and 23 µL/mg shows a downward trend along with cycling. However, at first, the capacity of the E/S ratio of 16 µL/mg increases and then decreases (Figure 5.11c). Also, the discharge profile is the same in the 5^{th} and 20^{th} cycles. Overall, the discharge profile is better in the E/S ratio of 6 and 9 µL/mg.

5.1.2. Electrochemical Characterization of the Lithium-Sulfur Batteries by Electrochemical Impedance Spectroscopy (EIS)

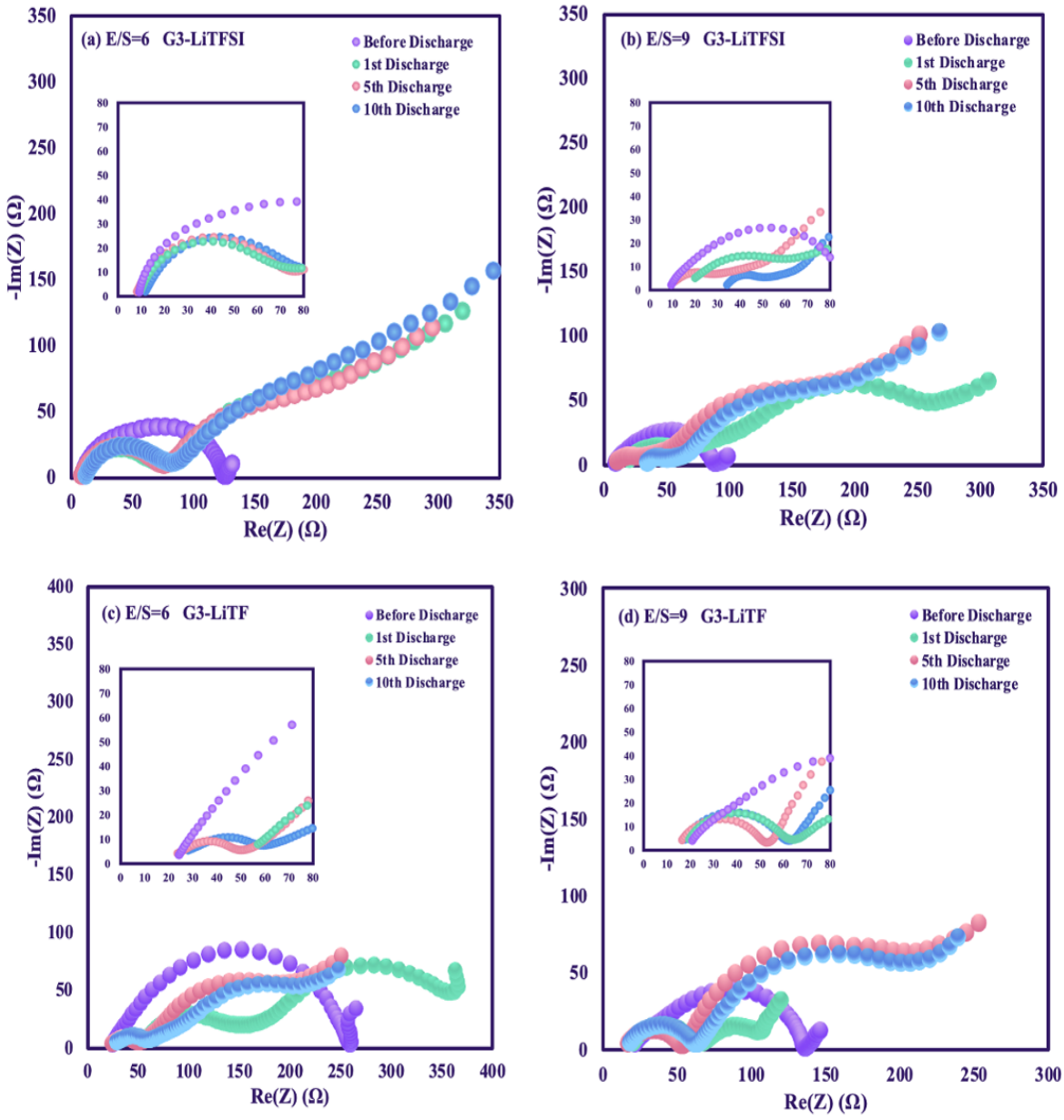

Figure 5.12. The electrochemical impedance spectrums of the Li-S cells with E/S ratios of (a) 6 µL/mg and (b) 9 µL/mg for 1M LiTFSI in Triglyme (G3), and E/S ratios of (c) 6 µL/mg and (d) 9 µL/mg for 1M LiTF in Triglyme (G3).

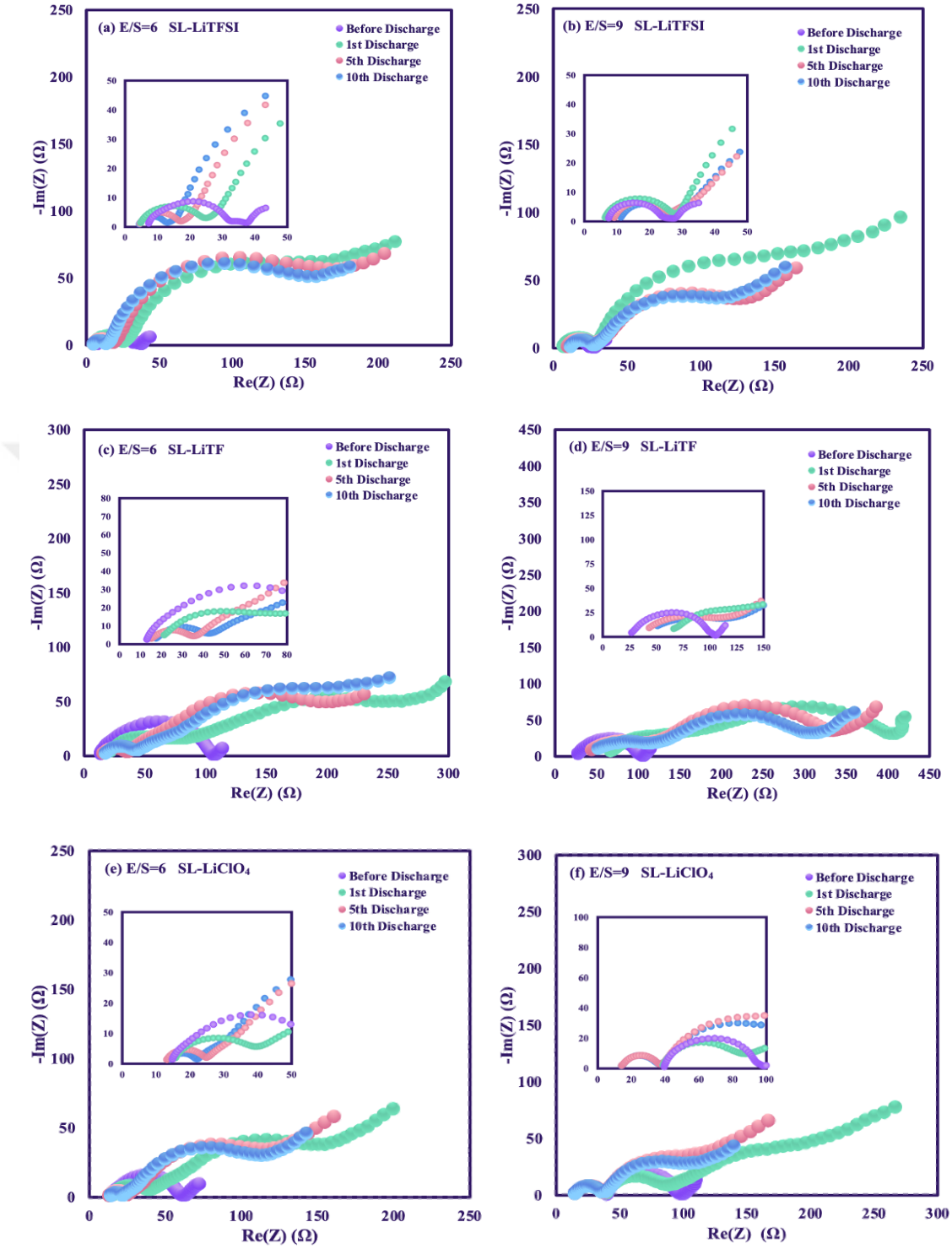

Figure 5.13. The electrochemical impedance spectrums of the Li-S cells with E/S ratios of (a) 6 µL/mg and (b) 9 µL/mg for 1M LiTFSI in Sulfolane (SL), E/S ratios of (c) 6 µL/mg and (d) 9 µL/mg for 1M LiTF in Sulfolane (SL), and E/S ratios of (e) 6 µL/mg and (f) 9 µL/mg for 1M $LiClO_4$ in Sulfolane (SL).

Figure 5.12 and Figure 5.13 show the electrochemical impedance spectroscopy results of cells prepared with 1M LiTFSI in triglyme (G3), 1 M LiTF in triglyme (G3), 1M LiTFSI in sulfolane (SL), 1M LiTF in sulfolane (SL), and 1M $LiClO_4$ in Sulfolane (SL) for E/S ratios of 6 µL/mg and 9 µL/mg for different cycles. Two semicircles and one linear line representing the Warburg diffusion resistance are clearly seen in the results.

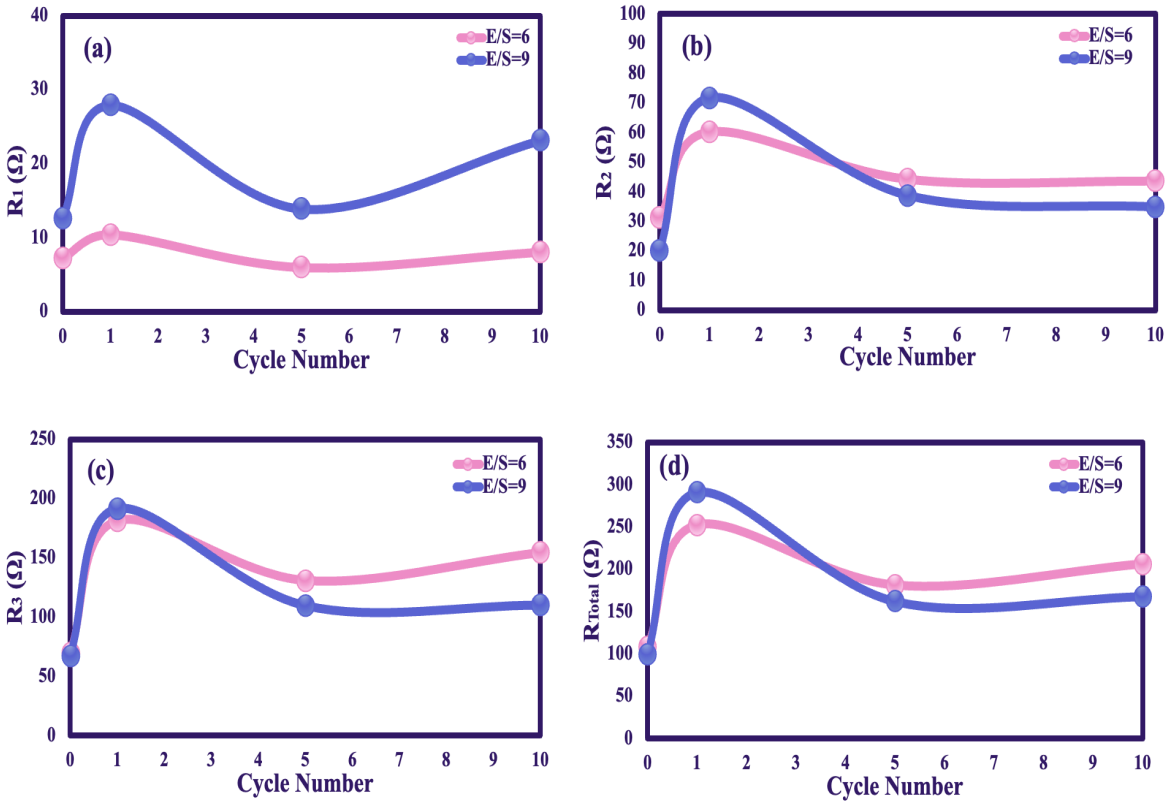

Figure 5.14. Change in (a) R_1, electrolyte resistance, (b) R_2, charge transfer resistance, (c) R_3, Li_2S film resistance, and (d) R_{Total}, total resistance of cells with LiTFSI in triglyme (G3) at E/S ratios of 6 µL/mg and 9 µL/mg.

Figure 5.14 illustrates the alteration of the cell resistances at two different E/S ratios for LiTFSI in triglyme electrolyte. In both E/S ratios, the same trends are seen for all resistances. At the beginning of the cycling, resistances increase sharply. Then, each resistance decreases gradually before increasing slightly again. In addition to having the same trends, almost the same values of the resistances in both E/S ratios are obtained. Except for R_1, the electrolyte resistance the E/S ratio of 9 µL/mg shows a higher resistance than the E/S ratio of 6 µL/mg (Figure 5.14c).

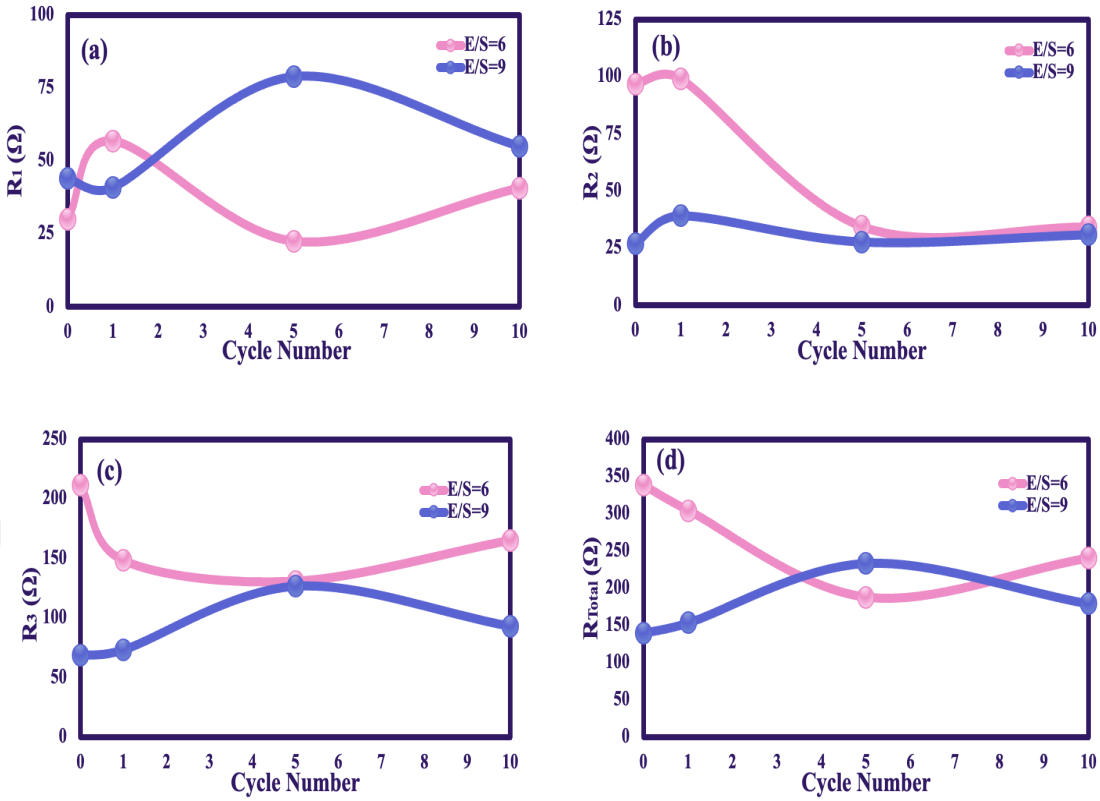

Figure 5.15. Change in (a) R_1, electrolyte resistance, (b) R_2, charge transfer resistance, (c) R_3, Li_2S film resistance, and (d) R_{Total}, total resistance of cells with LiTF in triglyme (G3) at E/S ratio of 6 µL/mg and 9 µL/mg.

Figure 5.15 shows the change in resistances of the LiTF in triglyme electrolyte for two electrolyte amounts. Interestingly, contrasting trends are observed for both E/S ratios for all resistances. While the resistance of E/S ratio of 6 µL/mg increases, resistance of the E/S ratio of 9 µL/mg diminishes. On the other hand, the values for the charge transfer resistance, R_2, at both E/S ratios are almost the same after the fifth cycle (Figure 5.15-b).

Figure 5.16 depicts the variation of the resistance of the cells with LiTFSI in Sulfolane electrolyte at two E/S ratios. Even though a different trend is seen in charge transfer resistances of the two E/S ratios at the beginning of cycling (Figure 5.16-b), in general, all resistances have the same trend with similar values. R_1 and R_2 at an E/S ratio of 9 µL/mg are higher than at an E/S ratio of 6 µL/mg while R_3 and R_{Total} present opposite trends.

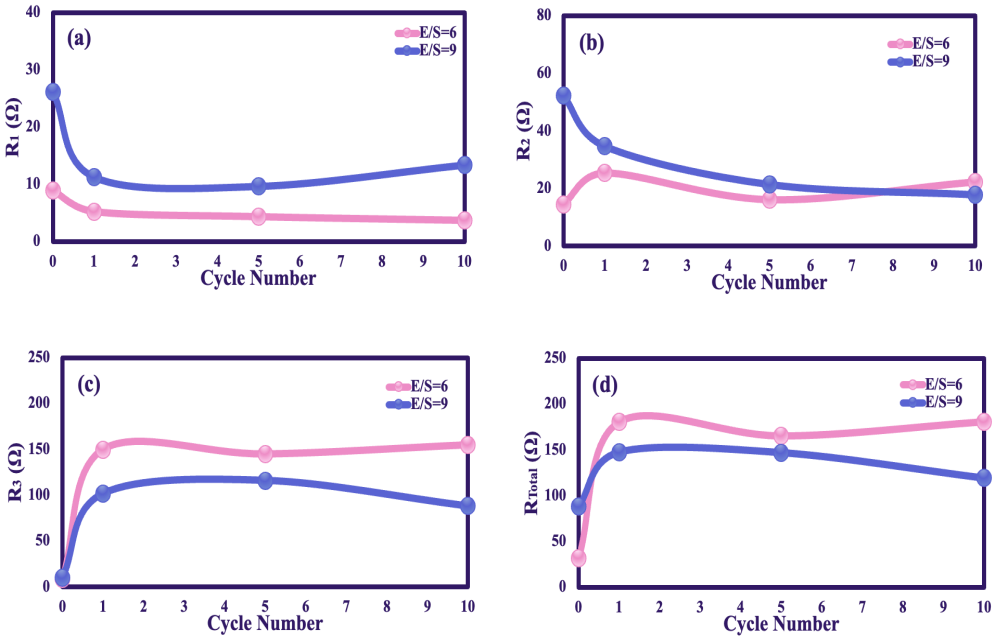

Figure 5.16. Change in (a) R_1, electrolyte resistance, (b) R_2, charge transfer resistance, (c) R_3, Li_2S film resistance, and (d) R_{Total}, total resistance of cells with LiTFSI in sulfolane (SL) at E/S ratio of 6 µL/mg and 9 µL/mg.

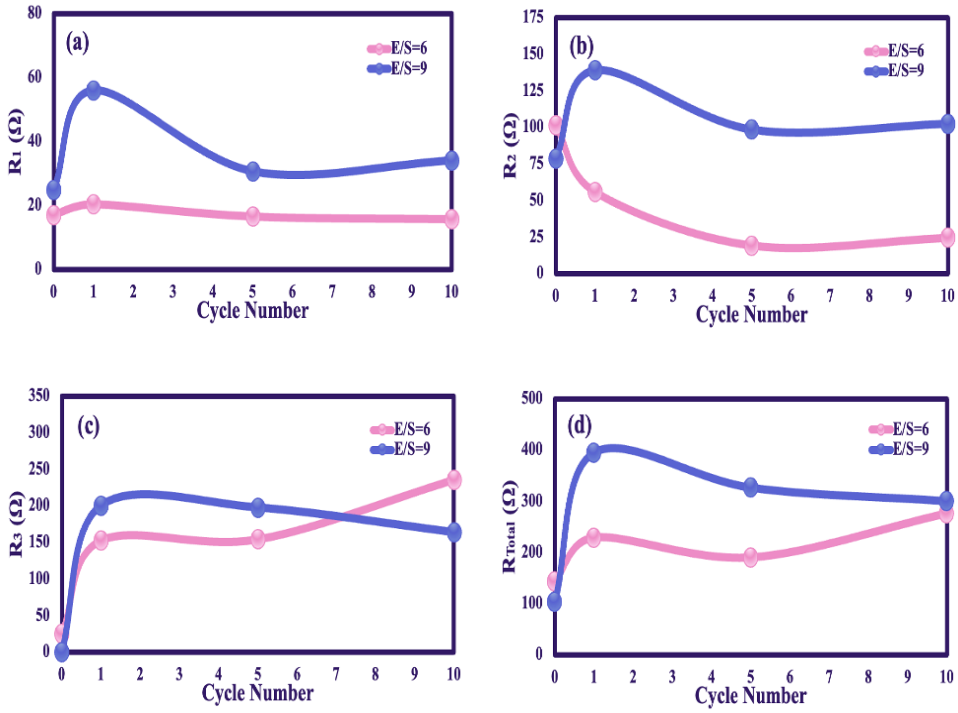

Figure 5.17. Change in (a) R_1, electrolyte resistance, (b) R_2, charge transfer resistance, (c) R_3, Li_2S film resistance, and (d) R_{Total}, total resistance of cells with LiTF in sulfolane (SL) at E/S ratio of 6 µL/mg and 9 µL/mg.

Figure 5.17 shows the alteration of the resistance of the cell with LiTF in sulfolane at E/S ratios of 6 µL/mg and 9 µL/mg. In general, an E/S ratio of 9 µL/mg gives the highest value in all resistances. Even though resistances of the cells with the two E/S ratios are similar before the discharge, the gap between them increases, especially for R_2 with cycling.

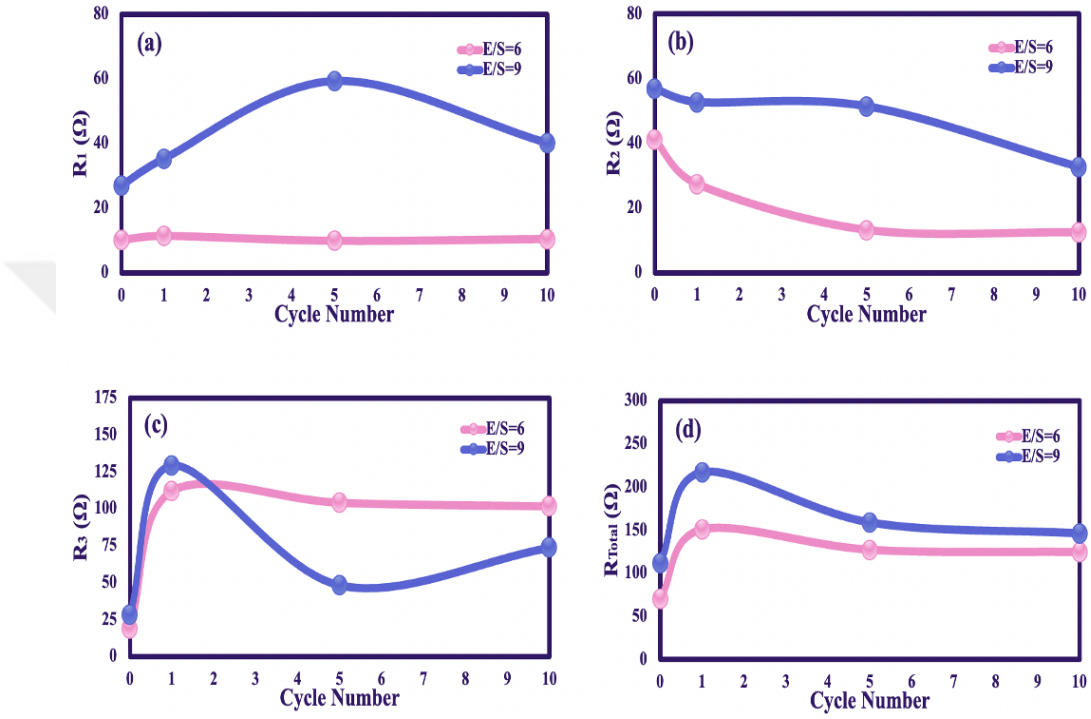

Figure 5.18. Change in (a) R_1, electrolyte resistance, (b) R_2, charge transfer resistance, (c) R_3, Li_2S film resistance, and (d) R_{Total}, total resistance of cells with $LiClO_4$ in sulfolane (SL) at E/S ratio of 6 µL/mg and 9 µL/mg.

Figure 5.18 illustrates the variation of the resistance of cells with $LiClO_4$ in sulfolane (SL) at E/S ratios of 6 µL/mg and 9 µL/mg. Except the film resistance, R_3, resistances at the E/S ratio of 9 µL/mg is higher than the E/S ratio of 6 µL/mg. An obvious change is seen in the E/S ratio of 9 µL/mg while there is not a significant change in the resistance at the E/S ratio of 6 µL/mg after the first cycle; especially R_1 remains almost stable during the discharge (Figure 5.18-a).

In summary, the best capacity and capacity retention are seen for Li-S cells with the 1M LiTF in triglyme and 1M LiTFSI in sulfolane electrolytes at the E/S ratio of 6 µL/mg. It is seen from this result, achieving high capacity and capacity retention in lean electrolyte

conditions may be possible with alternative electrolyte systems. In addition, different trends of discharge capacity are observed with the change in the E/S ratio on different electrolyte systems.

Table 5.1. Average EIS results of the different E/S ratios with various electrolyte system.

Type of Electrolyte	Cycle Number	R_1		R_2		R_3		R_{Total}	
		E/S=6 µL/mg	E/S=9 µL/mg	E/S=6 µL/mg	E/S=9 µL/mg	E/S=6 µL/mg	E/S=9 µL/mg	E/S=6 µL/mg	E/S=9 µL/mg
G3-LiTFSI	**0**	7.17	12.61	31.52	20.29	69.95	67.19	108.66	100.09
	1	10.43	27.85	60.23	71.66	181.7	191.4	252.36	290.91
	5	6	13.91	44.31	38.79	131.15	109.58	181.46	162.28
	10	8.08	23.12	43.69	34.93	154.7	110	206.47	168.04
G3-LiTF	**0**	29.97	44.11	96.71	27.04	211.35	68.89	338.03	140.04
	1	56.9	40.84	99.14	39.27	148.25	73.455	304.29	153.56
	5	22.42	78.86	34.53	27.71	130.9	126.65	187.85	233.22
	10	40.77	54.97	34.37	30.93	165.2	93.24	240.34	179.14
SL-LiTFSI	**0**	8.96	236.1	14.49	52.22	8.53	10.29	31.99	88.64
	1	5.26	11.25	25.41	34.69	149.8	101.75	180.47	147.69
	5	4.37	9.64	16.17	21.48	144.85	116.02	165.39	147.14
	10	3.72	13.37	22.35	17.94	154.8	88.18	180.87	119.48
SL-LiTF	**0**	17.1	24.9	101.33	78.72	24.83	0.228	143.26	103.85
	1	20.34	55.98	55.79	139	152.55	200.2	228.67	395.18
	5	16.58	30.72	19.2	98.51	154.1	197.5	189.88	326.73
	10	15.75	34.11	24.47	102.5	235.63	163.9	275.84	300.51
SL-$LiClO_4$	**0**	10.28	27.05	41.28	56.93	19.16	28.09	70.72	112.07
	1	11.54	35.38	27.48	52.83	111.9	129.1	150.93	217.31
	5	10.03	59.34	13.29	51.52	104.1	48.35	127.43	159.2
	10	10.58	40.22	12.57	32.76	101.65	73.67	124.79	146.65

Table 5.1. Average EIS results of the different E/S ratios with various electrolyte system (cont.).

Type of Electrolyte	Cycle Number	Q_2 x10^{-5}, (F s $^{(a-1)}$)		Q_3 x10^{-5}, (F s $^{(a-1)}$)	
		E/S=6 µL/mg	E/S=9 µL/mg	E/S=6 µL/mg	E/S=9 µL/mg
G3-LiTFSI	0	1.12	2.06	2.84	4.69
	1	8.76	37.91	408.4	393.35
	5	7.18	34.66	671.65	815.5
	10	7.10	32.97	785.15	841.05
G3-LiTF	0	3.39	2.57	1.37	1.06
	1	3.19	1.88	184.2	549.15
	5	6.73	1.29	558	580.75
	10	6.82	1.78	820.85	700
SL-LiTFSI	0	1313.83	1.002	413.44	901.4
	1	5.36	1.618	447.4	496.75
	5	9.16	1.88	413.8	558.65
	10	39.81	2.14	400.25	753.4
SL-LiTF	0	1.804	1.88	47523.5	3418000
	1	8.28	12.68	273	77.49
	5	4.913	6.702	526.05	65.95
	10	15.67	8.95	769.5	70.75
SL-$LiClO_4$	0	13901.34	1.77	8171.04	16697.25
	1	2.42	1.92	489.5	290.05
	5	2.13	9.79	533.05	511.25
	10	311.19	3.57	309.27	552.3

5.2. Model Predictions for the Effect of the E/S Ratio on the Performance of Li-S Batteries for Different Electrolyte Systems

In this section of the thesis, the results of the zero-dimensional concentration-independent and one-dimensional concentration-dependent electrochemical models are given, respectively. In addition, so as to understand the impact of the E/S ratio for electrolytes with different chemical compounds and properties, the influence of the E/S ratio on the initial discharge profile at various values of design parameters is investigated for both models.

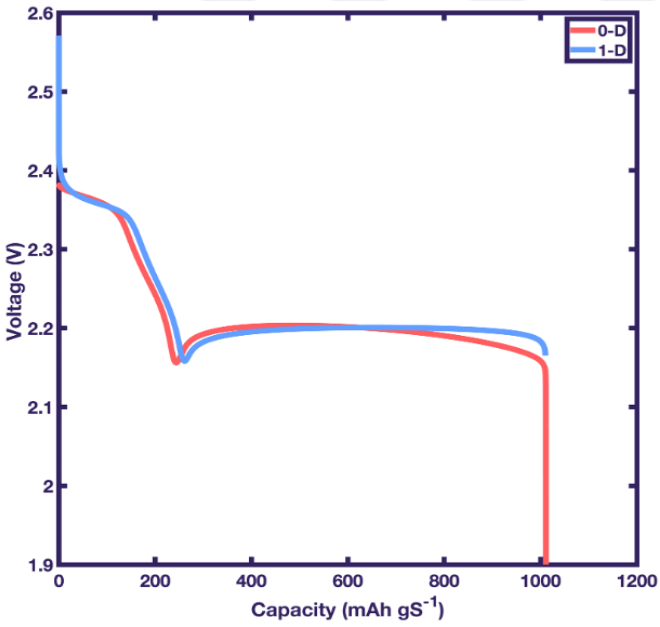

Figure 5.19. The discharge profiles of 0-D and 1-D electrochemical models at constant sulfur loading, C-rate, and E/S ratio.

Figure 5.19 illustrates the predicted discharge profiles of 0-D and 1-D electrochemical models. It is seen from the graph both models predict the discharge curve successfully and has the same pattern. Also, both plateaus, high and low plateaus, are seen obviously in both models. The high plateau is just below 2.4V, while the low plateau is near 2.2V.

5.2.1. 0-D Concentration-Independent Electrochemical Model Predictions for the Effect of the E/S Ratio on the Battery Performance

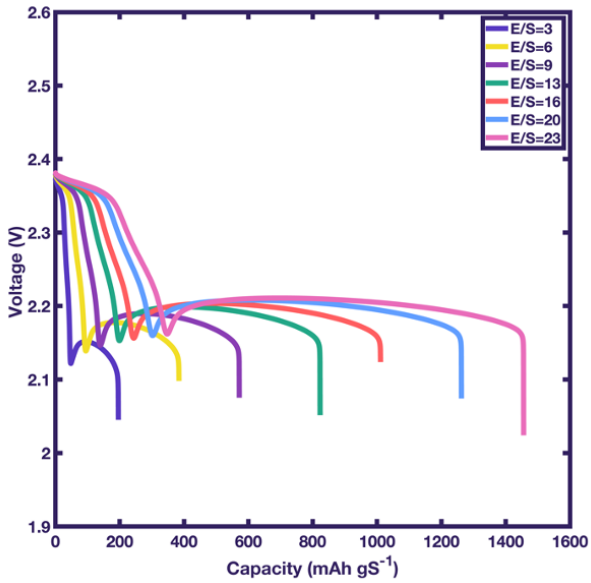

Figure 5.20. Prediction of the impact of the E/S ratio on the discharge profile of Li-S batteries for the 0-D model.

Figure 5.20 represents the change in the discharge capacity for different amounts of electrolytes at 0.1 C and a sulfur loading of 1.1-1.3 mg/cm^2. The alteration of the discharge capacity with the change in the E/S ratio is seen clearly. Therefore, it may be discussed that the predicted discharge profiles capture the expected trend adequately. There is a significant difference between the capacities at different E/S ratios, and an increase in the E/S ratio raises the discharge capacity and voltage plateaus. Overall, it is seen that the 0-D model is sensible to the alteration in the E/S ratio.

Physicochemical properties of the electrolyte, including donor number, dielectric constant, and acceptor number, impact the redox chemistry of Li-S batteries. These properties are associated with the solubility and precipitation/dissolution of the species resulting from electrochemical reactions [65].

The reduction and solubility of polysulfides are strongly affected by the donor number of the electrolyte. An electrolyte with a high donor number is required for the dissolution of lithium due to the strong Lewis acidity of Li^+. In addition, a high donor number

has the capability to coordinate the Li^+ cation, facilitating the efficient dissolution of lithium. On the other hand, it may result in a reaction between dissolved polysulfides and lithium metal anode, leading to low coulombic efficiency and short cycle life. For this reason, an electrolyte with a low donor number is needed to enhance the durability of the battery and hinder polysulfide dissolution [46], [66–68]. Furthermore, donor number plays a significant role in the morphology of the Li_2S that causes the passivation of the cathode surface because of its insulating nature. Thus, a high donor number leads to the 3D morphology of Li_2S, restraining the passivation of the cathode surface. As for the acceptor number, a high acceptor number increases the reduction of the S_8^- [65], [69,70]. Therefore, in order to understand how sensitive the 0-D model is against the E/S ratio for different electrolyte systems, the effect of the E/S ratio on the change in the discharge profile is investigated by varying selected model parameters, which are expected to depend on the electrolyte type and properties such as donor number, dielectric constant, and acceptor number.

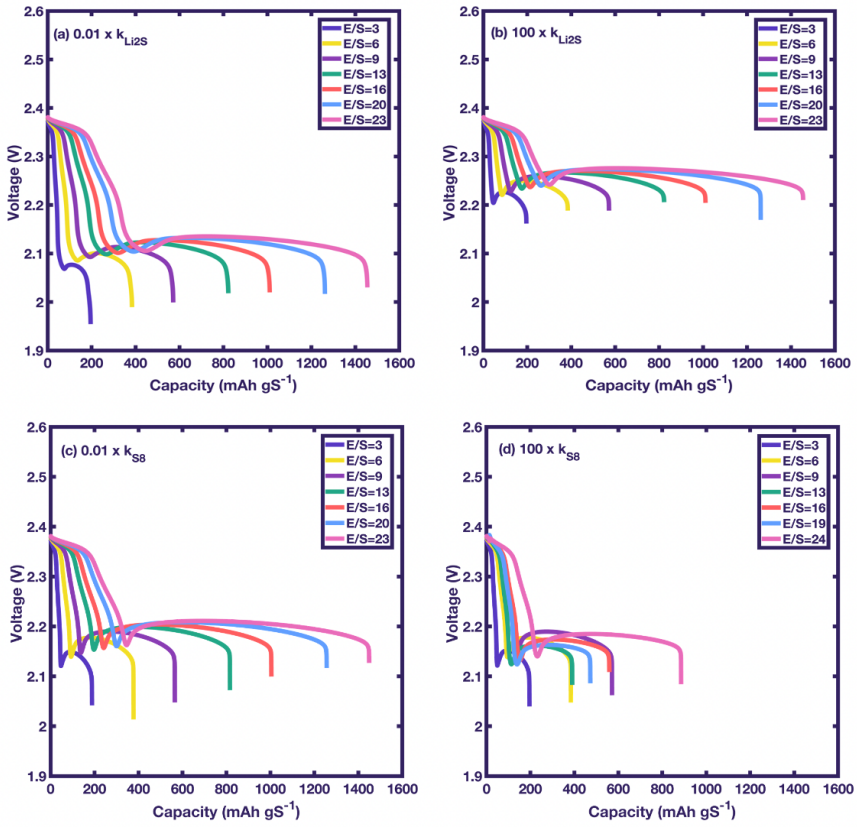

Figure 5.21. Effect of the E/S ratio on predicted discharge profiles of the Li-S batteries for 0-D model at (a) 0.01 k_{Li2S}, (b) 100 k_{Li2S}, (c) 0.01k_{S8}, and (d)100 k_{S8}.

Firstly, since the electrolyte system controls the precipitation kinetics in the cell, the precipitation rate constants in the model, k_{Li2S} and k_{S8}, are expected to vary with varying electrolyte properties. The Figure 5.21 shows the change in the discharge profiles with E/S ratio for 0.01 k_{Li2S}, 100 k_{Li2S}, 0.01 k_{S8}, and 100 k_{S8}. It is seen clearly that the reliance of the capacity on the electrolyte-to-sulfur ratio is not affected at 0.01 k_{Li2S}, 100 $k_{Li2S,}$ and 0.01$k_{S8,}$ but the voltage plateaus are impacted by the alteration of the values of the parameters. For example, in Figure 5.21a and Figure 5.21b, the second voltage plateau is adversely affected by the decline in the k_{Li2S}. Surprisingly, when k_{S8} increases, the discharge profile shows a different trend with the increase in the E/S ratio, as seen in Figure 5.21d. In addition, the discharge capacity of the cell declines when the value of k_{S8} increases. Overall, it is understood from these graphs that k_{S8} is a critical model parameter, and the impact of electrolyte properties on battery performance can be controlled via this parameter.

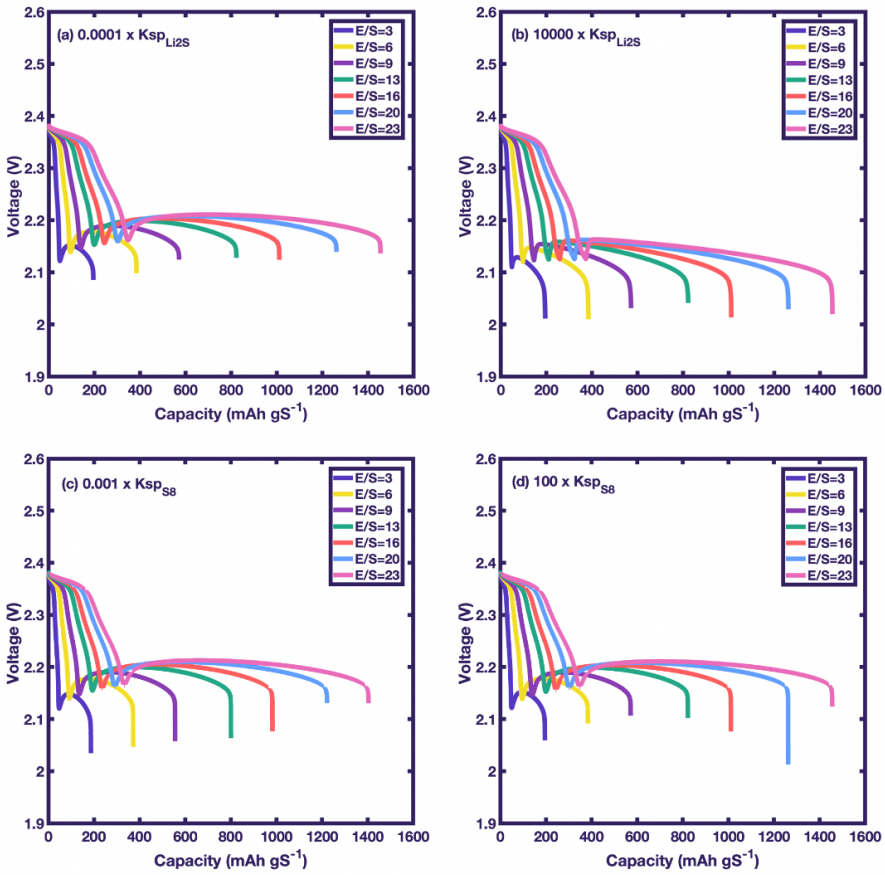

Figure 5.22. Effect of the E/S ratio on predicted discharge profiles of the Li-S batteries for 0-D model at (a) 0.0001Ksp_{Li2S}, (b) 10000 Ksp_{Li2S}, (c) 0.001Ksp_{S8}, and (d)100 Ksp_{S8}.

The variation of the discharge profiles with the E/S ratio for various values of the solubility products of Li_2S (Ksp_{Li2S}) and S_8 (Ksp_{S8}) is seen in Figure 5.22. There is no significant change in the discharge profiles and voltage plateaus with the alteration of both parameters for all E/S ratios. Furthermore, the trend of the change of the profiles with the E/S ratio is not affected by the change in the Ksp_{Li2S} and Ksp_{S8}. Overall, the discharge profiles of Li-S batteries for the 0-D model are sensible to the E/S ratio, but they are affected similarly for different Ksp_{Li2S} and Ksp_{S8} values.

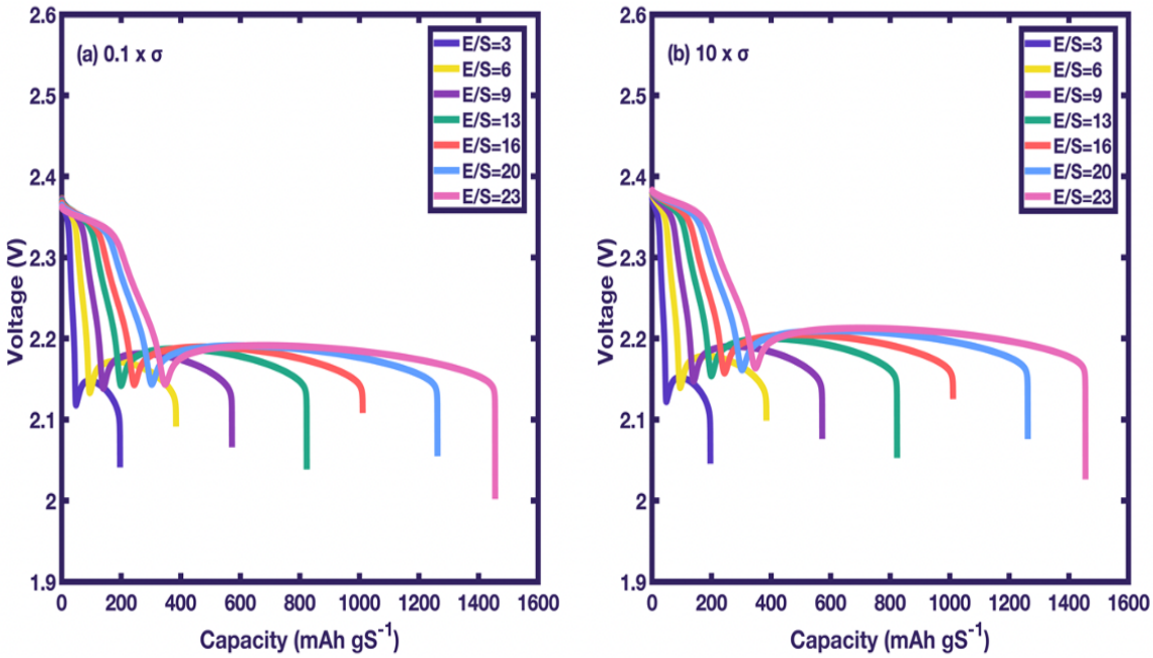

Figure 5.23. Effect of the E/S ratio on predicted discharge profiles of the Li-S batteries for 0-D model at (a) 0.1 σ and (b) 10 σ.

In Figure 5.23, it can be seen how the projected discharge profile is affected by the E/S ratios at different values of electrolyte conductivity, such as 0.1 σ and 10 σ. As is seen in Figure 5.22, here, the discharge capacity and voltage plateau are impacted in the same way by the alteration of the E/S ratio for both quantities of the electrolyte conductivity.

5.2.2. 1-D Concentration-Independent Electrochemical Model Predictions for the Effect of the E/S Ratio on the Battery Performance

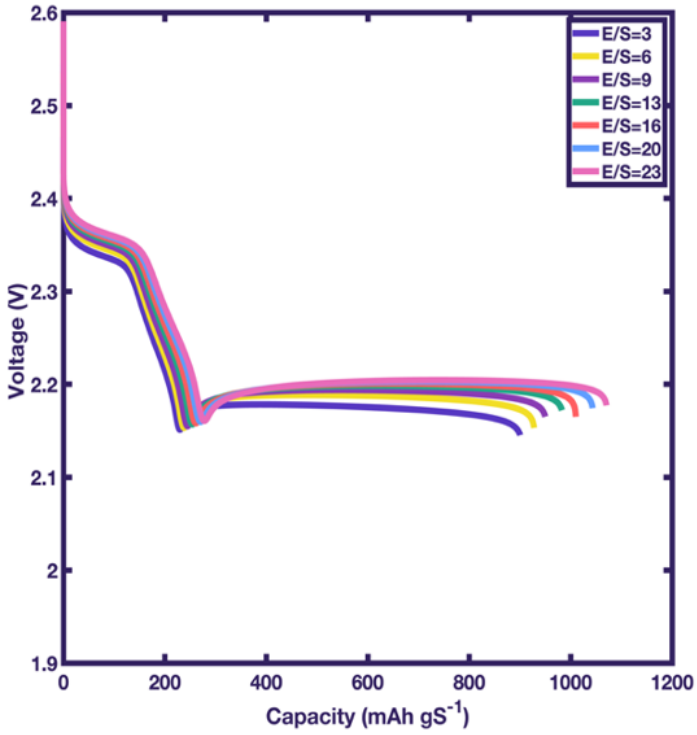

Figure 5.24. Prediction of the impact of the E/S ratio on the discharge profile of Li-S batteries for the 1-D model.

A 1-D concentration-dependent electrochemical model is also improved for the investigation of the impact of the E/S ratio on the initial discharge profile of Li-S batteries. So, the discharge profiles of Li-S cells with different E/S ratios at 0.1C and a sulfur loading of 1.1-1.3 mg/cm^2, the same as the 0-D model, are illustrated in Figure 5.24. As expected, both the discharge capacity and the voltage plateaus diminish with decreasing E/S ratio. Even though the characteristic trend is predicted for all E/S ratios, the change in the discharge profiles and capacities of the cells with the E/S ratio is subtle. In this case, it can be said that this model is less sensitive in capturing the expected trend.

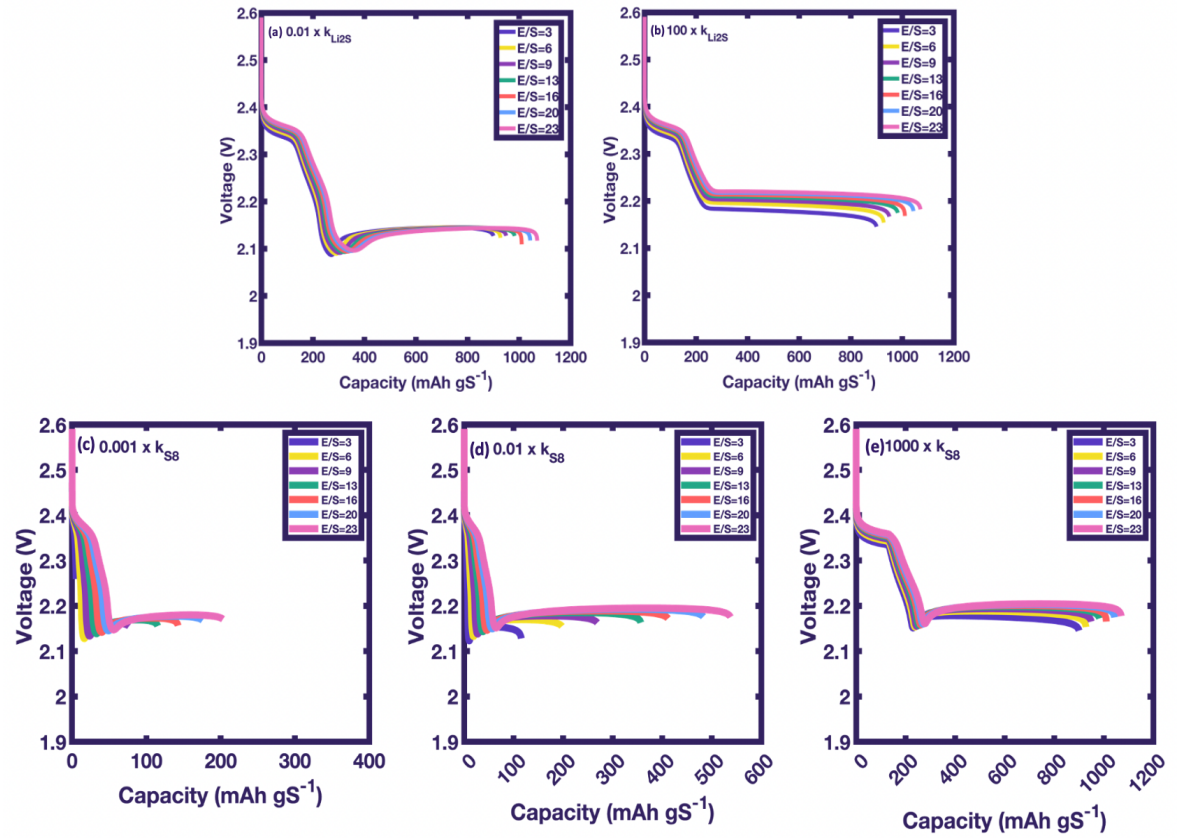

Figure 5.25. Effect of the E/S ratio on predicted discharge profiles of the Li-S batteries for the 1-D model at (a) 0.01k_{Li2S}, (b) 100 k_{Li2S}, (c) 0.001 k_{S8}, (d) 0.01 k_{S8} and e)1000 k_{S8}.

In Figure 5.25, the influence of the electrolyte amount on the predicted discharge profile is seen for different values of the precipitation rate constants of Li_2S (k_{Li2S}) and S_8 (k_{S8}). For different values of k_{Li2S}, the discharge capacities are slightly affected by the change in the E/S ratio. The second plateau is affected also by the alteration of the k_{Li2S}. However, interestingly, for different values of k_{S8}, especially for 0.01 and 0.001 k_{S8}, the 1-D model becomes better in predicting the change of discharge profiles with the E/S ratio (Figure 5.25c and Figure 5.25d). In Figure 5.25d, the impact of the E/S ratio on the discharge profile can be projected clearly. In general, the precipitation rate constant of k_{S8} has a considerable effect on the calculated discharge profile of the Li-S batteries and thus, it may be used to control the impact of the electrolyte type on the effect of the E/S ratio on performance of the cell. In addition, the 1-D model is more responsive to the influence of the E/S ratio on the discharge profile for lower k_{S8} values.

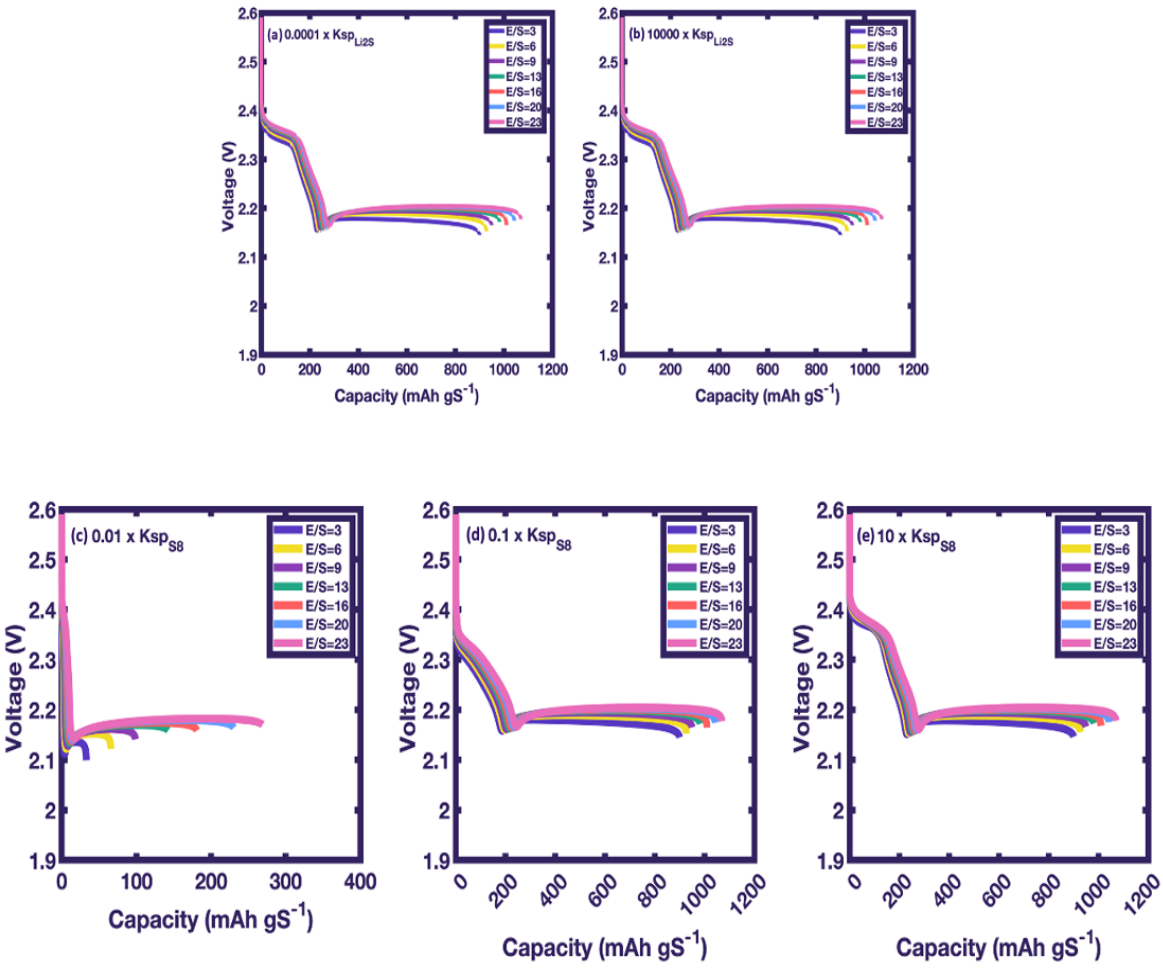

Figure 5.26. Effect of the E/S ratio on predicted discharge profiles of the Li-S batteries for the 1-D model at (a) 0.0001 Ksp_{Li2S}, (b) 10000 Ksp_{Li2S}, (c) 0.01 Ksp_{S8}, (d) 0.1 Ksp_{S8} and (e)10 Ksp_{S8}.

At various solubility products of Li_2S (Ksp_{Li2S}) and S_8 (Ksp_{S8}), the prediction of the discharge profiles as a function of the E/S ratio is illustrated in Figure 5.26. The dependence of the discharge profiles against the E/S ratio is similar to the precipitation rate. There is not any noteworthy change in both capacity and voltage of plateaus for these parameters, except for 0.01 Ksp_{S8}. It can be observed in Figure 5.26c that the predicted discharge profile becomes highly sensitive to the E/S ratio for low Ksp_{S8} values (0.01 Ksp_{S8}). Moreover, the impact of electrolyte properties on battery performance can be predicted using the 1-D model via this model parameter.

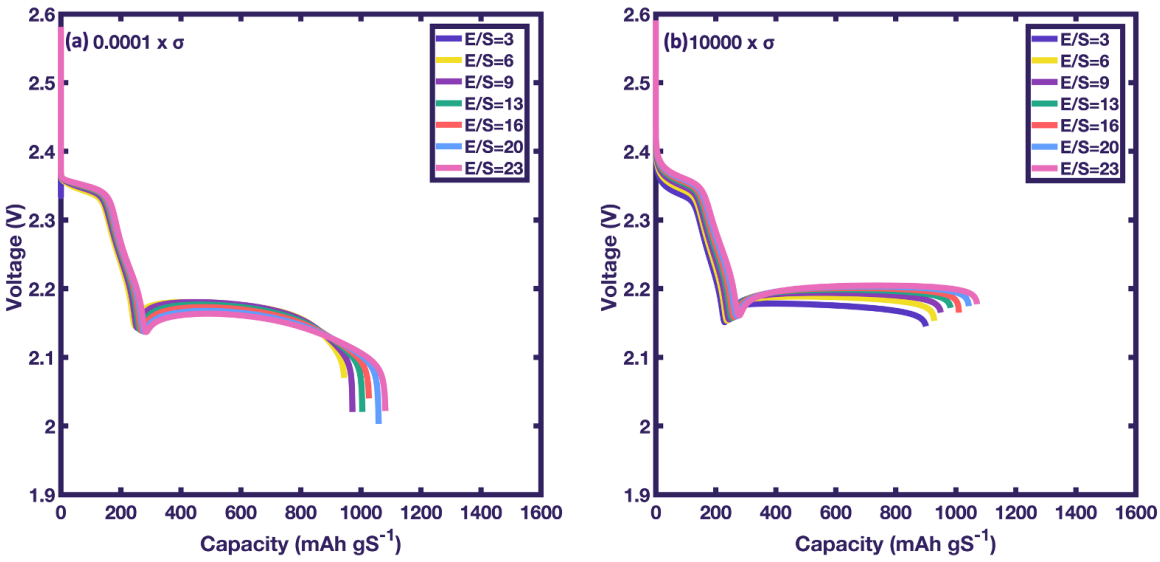

Figure 5.27. Effect of the E/S ratio on predicted discharge profiles of the Li-S batteries for the 1-D model at (a) 0.0001 σ and (b) 10000 σ.

As shown in Figure 5.27, for different electrical conductivity of the cathode in the model, the influence of the E/S ratio on the discharge profiles is predicted to be similar; there is a slight change both in capacity and voltage plateaus with the alteration of the E/S ratios in both values.

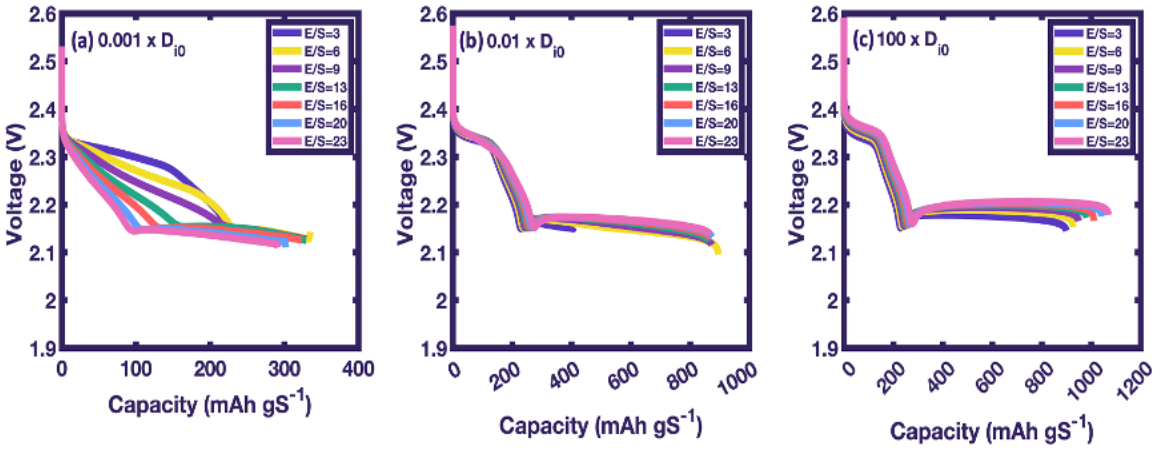

Figure 5.28. Effect of the E/S ratio on predicted discharge profiles of the Li-S batteries for the 1-D model at (a) 0.001 D_{i0}, (b) 0.01 D_{i0}, and (c)100 D_{i0}.

Finally, the impact of the E/S ratio for different diffusion coefficients, D_{i0}, on the battery performance is investigated for the 1-D model in Figure 5.28. In Figures 5.28b and

5.28c, the discharge profile is not significantly affected by the E/S ratio except for the E/S ratio of 3 in Figure 5.28. Even though there is no enormous change in the predicted profiles in 0.01 D_{i0} and 100 D_{i0}, the capacity of the cell diminishes significantly with further decreasing D_{i0}, especially for 0.001 D_{i0}. In addition to the capacity, the discharge profile is not very distinct, as in Figures 5.28b and 5.28c.

In summary, 0-D and 1-D electrochemical models are developed to predict the effect of the E/S ratio with various electrolytes in this part of the study. It is seen from the results that both models can predict the impact of the E/S ratio as expected; while the E/S ratio increases, the capacity of the battery increases as well. However, this change in capacity is more obvious in the 0-D model when compared with the 1-D model. In addition, the effect of the E/S ratio can be observed through the precipitation rate constant of S_8, $k_{S8,}$ and the diffusion coefficient of species by using these models.

6. CONCLUSIONS

This study investigated the impact of the electrolyte-to-sulfur ratio on the performance of lithium-sulfur batteries with various electrolyte systems by conducting experimental characterization and developing electrochemical models.

First, experimental characterization of the electrochemical performance of Li-S batteries as a function of the E/S ratio was conducted using galvanostatic cycling. Seven types of electrolytes were used in this study: 1M LiTFSI in DOL: DME (1:1 v:v %), sulfolane and triglyme, 1M LiTF in sulfolane and triglyme, 1M $LiClO_4$ in sulfolane and 1M $LiClO_4$ with 0.1M $LiNO_3$ in sulfolane. In order to investigate the influence of the electrolyte-to-sulfur ratio on Li-S battery performance for these electrolytes, coin cells (CR2032) were assembled with E/S ratios of 6, 9, 16, and 23 µL/mg and a sulfur loading of 1.1- 1.3 mg/cm^2. All cells rested for 16h before the galvanostatic cycling at 0.1 C. Experimental study results indicate that there is no significant impact of the E/S ratio on the first discharge capacity of cells with triglyme-based electrolytes. A decrease in the capacity of all cells is seen with cycling. Among the triglyme-based electrolytes, 1M LiTF in triglyme electrolyte system shows the best capacity and capacity retention at the E/S ratio of 6 µL/mg. As for the sulfolane-based electrolytes, the capacity and capacity retention are not affected significantly by the E/S ratio for 1M LiTFSI in sulfolane electrolyte system. On the other hand, cycling performance depends on the E/S ratio in the other sulfolane-based electrolytes, especially in 1M $LiClO_4$ with 0.1M $LiNO_3$ in sulfolane. Even though the capacities of cells with this electrolyte at E/S ratios of 23 and 16 µL/mg decrease slightly during cycling, their capacity is the lowest among the sulfolane-based electrolytes. In addition, the best performance is seen in the lowest E/S ratio, 6 µL/mg, in all sulfolane-based electrolytes; the best performance is seen for 1M LiTFSI in sulfolane electrolyte system when comparing the results for the lowest E/S ratio with each other.

To sum up, the impact of the E/S ratio on the discharge capacity and cycling performance of Li-S batteries greatly differs in different electrolyte systems. As previously discussed, Li-S battery electrolytes should be designed to perform well in lean electrolyte conditions to achieve high-performance specifications at the system level. Consequently,

our findings show that 1M LiTF in triglyme and 1M LiTFSI in sulfolane electrolyte systems are promising as they achieved superior performance at the lowest E/S ratio of 6 μL/mg.

Following the experimental study, a zero-dimensional model neglecting the mass transfer and a one-dimensional model considering the spatial species concentration variation was developed to forecastthe discharge behavior of the Li-S batteries as a function of the E/S ratio. Both models can capture the typical discharge curve of a Li-S cell, showing that including mass transfer may not be necessary for capturing the characteristic features of the voltage profile. It is seen from the results that the 0-D model is highly susceptible to the E/S ratio; the capacity declines significantly with decreasing E/S ratio, as expected from experimental trends. On the other hand, the 1-D model predictions are less responsive to the E/S ratio; even though the right trend is predicted, the decrease in the capacity with decreasing E/S ratio is slighter. In order to model the impact of the E/S ratio on the discharge profile of Li-S for different electrolyte systems, selected model parameters were changed systematically. The effect of the E/S ratio on the predicted discharge profiles is the same for different model parameters relying on electrolyte properties, except for the precipitation rate constant, k_{S8}. At the different values of k_{S8}, both 0-D and 1-D models predict different trends for the dependence of discharge profiles on the E/S ratio. Consequently, these models can capture the effect of the E/S ratio on the discharge behavior for various electrolyte systems implicitly through the variation of the aforementioned model parameter.

To sum up, for the different electrolyte systems, the E/S ratio influences the performance of the Li-S batteries in different ways and degrees because the electrolyte properties affect the reactions and mechanisms occurring inside the batteries. It is concluded that besides the E/S ratio, the electrolyte type has also a crucial impact on battery performance. In addition, among the models developed for predicting the effect of the E/S ratio, the 0-D model is more sensitive to the E/S ratio than the 1-D model. Also, along with the E/S ratio, the discharge profile does not respond to most of the selected model parameters, which should be affected by the electrolyte properties. Nevertheless, the influence of the E/S ratio on the discharge profile for different electrolyte systems can be captured via varying k_{S8}. Therefore, both the 0-D and 1-D models can be used for the prediction of the effect of the E/S ratio for different electrolyte systems.

For future work, at first, the experimental study can be integrated with the 0-D and 1-D models. In addition, both models can be expanded by including the separator in the electrochemical model area and modeling the charge of batteries to investigate the cycling performance of Li-S batteries deeply. Furthermore, the effect of the E/S ratio with the best type of electrolyte on cell performance can be investigated with the various types of cathodes, carbon-to-sulfur ratio, or sulfur loading.

REFERENCES

1. Nitta N., F. Wu, J. T. Lee, and G. Yushin, “Li-ion Battery Materials: Present and Future”, *Materials Today*, Vol. 18, No. 5, pp. 252–264, 2015.

2. Lu L., X. Han, J. Li, J. Hua, and M. Ouyang, “A Review on the Key Issues for Lithium-Ion Battery Management in Electric Vehicles”, *Journal of Power Sources*, Vol. 226, pp. 272–288, 2013.

3. Armand M., and J. M. Tarascon, “Building Better Batteries”, *Nature Journal,* Vol. 451, pp. 652–657, 2008.

4. Liu B., R. Fang, D. Xie, W. Zhang, H. Huang, Y. Xia, X. Wang, X. Xia, and J. Tu, “Revisiting Scientific Issues for Industrial Applications of Lithium–Sulfur Batteries”, *Energy and Environmental Materials*, Vol. 1, No. 4, pp. 196–208, 2018.

5. Ji X., and L. F. Nazar, “Advances in Li-S Batteries”, *Journal of Material Chemistry*, Vol. 20, No. 44, pp. 9821–9826, 2010.

6. Feng S., Z. H. Fu, X. Chen, and Q. Zhang, “A Review on Theoretical Models for Lithium–Sulfur Battery Cathodes”, *InfoMat*, Vol. 4, No. 3, 2022.

7. Yang S., Z. Zhang, J. Lin, L. Zhang, L. Wang, S. Chen, C. Zhang, and X. Liu, “Recent Progress in Quasi/All-Solid-State Electrolytes for Lithium–Sulfur Batteries”, *Frontiers in Energy Research*, Vol. 10, 2022.

8. Yoon S., Y. H. Lee, K. H. Shin, S. B. Cho, and W. J. Chung, “Binary Sulfone/Ether-Based Electrolytes for Rechargeable Lithium-Sulfur Batteries”, *Electrochimica Acta*, Vol. 145, pp. 170–176, 2014.

9. He L., S. Shao, C. Zong, B. Hong, M. Wang, and Y. Lai, “Electrode Interface Engineering in Lithium-Sulfur Batteries Enabled by a Trifluoroacetamide-Based Electrolyte”, *ACS Applied Materials Interfaces*, Vol. 14, No. 28, pp. 31814–31823, 2022.

10. Zhang Y.Z., S. Liu, G. C. Li, G. R. Li, and X. P. Gao, “Sulfur/Polyacrylonitrile/Carbon Multi-composites as Cathode Materials for Lithium/Sulfur Battery in the Concentrated Electrolyte”, *Journal of Materials Chemistry*, Vol. 2, No. 13, pp. 4652–4659, 2014.

11. Liao J., and Z. Ye, “Nontrivial Effects of ‘Trivial’ Parameters on the Performance of Lithium–Sulfur Batteries”, *Batteries*, Vol. 4, No. 2, 2018.

12. Kolosnitsyn V. S., and E. V. Karaseva, “Lithium-sulfur Batteries: Problems and Solutions”, *Russian Journal of Electrochemistry*, Vol. 44, No. 5, pp. 506–509, 2008.

13. Fan F. Y., M. S. Pan, K. C. Lau, R. S. Assary, W. H. Woodford, L. A. Curtiss, W. C. Carter, and Y. M. Chiang, “Solvent Effects on Polysulfide Redox Kinetics and Ionic Conductivity in Lithium-Sulfur Batteries”, *Journal of Electrochemical Society*, Vol. 163, No. 14, pp. A3111–A3116, 2016.

14. Erisen N., N. B. Emerce, S. C. Erensoy, and D. Eroglu, “Modeling the Effect of Key Cathode Design Parameters on the Electrochemical Performance of a Lithium-Sulfur Battery”, *International Journal of Energy Research*, Vol. 42, No. 8, pp. 2631–2642, 2018.

15. Gao Y., Q. Guo, Q. Zhang, Y. Cui, and Z. Zheng, “Fibrous Materials for Flexible Li–S Battery”, *Advanced Energy Materials*, Vol. 11, No. 15, 2021.

16. Eroglu D., K. R. Zavadil, and K. G. Gallagher, “Critical Link Between Materials Chemistry and Cell-Level Design for High Energy Density and Low Cost Lithium-Sulfur Transportation Battery”, *Journal of Electrochemical Society*, Vol. 162, No. 6, pp. A982–A990, 2015.

17. Mačák M., P. Vyroubal, T. Kazda, and K. Jaššo, “Numerical Investigation of Lithium-Sulfur Batteries by Cyclic Voltammetry”, *Journal of Energy Storage*, Vol. 27, 2020.

18. Rehman S., M. Pope, S. Tao, and E. McCalla, “Evaluating the Effectiveness of in Situ Characterization Techniques in Overcoming Mechanistic Limitations in Lithium-Sulfur Batteries”, *Energy and Environmental Science*, Vol. 15, No. 4, pp. 1423–1460, 2022.

19. Cha E., M. Patel, S. Bhoyate, V. Prasad, and W. Choi, “Nanoengineering to Achieve High Efficiency Practical Lithium-Sulfur Batteries”, *Nanoscale Horizons*, Vol. 5, No. 5, pp. 808–831, 2020.

20. Li Y., and S. Guo, “Material Design and Structure Optimization for Rechargeable Lithium-Sulfur Batteries”, *Matter*, Vol. 4, No. 4, pp. 1142–1188, 2021.

21. Song M. K., E. J. Cairns, and Y. Zhang, “Lithium/Sulfur Batteries with High Specific Energy: Old Challenges and New Opportunities”, *Nanoscale*, Vol. 5, No. 6, pp. 2186–2204, 2013.

22. Zhang S. S., “Liquid Electrolyte Lithium/Sulfur Battery: Fundamental Chemistry, Problems, and Solutions”, *Journal of Power Sources*, Vol. 231. pp. 153–162, 2013.

23. Li G., S. Wang, Y. Zhang, M. Li, Z. Chen, and J. Lu, “Revisiting the Role of Polysulfides in Lithium–Sulfur Batteries”, *Advanced Materials*, Vol. 30, No. 22, 2018.

24. Ren W., W. Ma, S. Zhang, and B. Tang, “Recent Advances in Shuttle Effect Inhibition for Lithium Sulfur Batteris”, *Energy Storage Materials*, Vol. 23, pp. 707–732, 2019.

25. Ma L., H. L. Zhuang, S. Wei, K. E. Hendrickson, M. S. Kim, G. Cohn, R. G. Hennig, and L. A. Archer, “Enhanced Li-S Batteries Using Amine-Functionalized Carbon Nanotubes in the Cathode”, *ACS Nano*, Vol. 10, No. 1, pp. 1050–1059, 2016.

26. X. Yang, X. Li, K. Adair, H. Zhang, and X. Sun, “Structural Design of Lithium–Sulfur Batteries: From Fundamental Research to Practical Application”, *Electrochemical Energy Reviews*, Vol. 1, No. 3, pp. 239–293, 2018.

27. Donato G. D., T. Ates, H. Adenusi, A. Varzi, M. A. Navarra, and S. Passerini, “Electrolyte Measures to Prevent Polysulfide Shuttle in Lithium-Sulfur Batteries”, *Batteries and Supercaps*, Vol. 5, No. 7, 2022.

28. Fotouhi A., D. J. Auger, L. O’Neill, T. Cleaver, and S. Walus, “Lithium-Sulfur Battery Technology Readiness and Applications - A Review”, *Energies*, Vol. 10, No. 12, 2017.

29. Xu R., J. Lu, and K. Amine, “Progress in Mechanistic Understanding and Characterization Techniques of Li-S Batteries”, *Advanced Energy Materials*, Vol. 5, No. 16, 2015.

30. Dörfler S., H. Althues, P. Härtel, T. Abendroth, B. Schumm, and S. Kaskel, “Challenges and Key Parameters of Lithium-Sulfur Batteries on Pouch Cell Level”, *Joule*, Vol. 4, No. 3, pp. 539–554, 2020.

31. Xu H., J. Hao, Y. Chen, H. You, X. Liu, and H. Yang, “High Performance of Sulfur/Carbon Cathode Synthesized via a Facile Green Microwave Approach”, *Energy and Fuels*, Vol. 35, No. 3, pp. 2750–2757, 2021.

32. Kim H. M., H. H. Sun, I. Belharouak, A. Manthiram, and Y. K. Sun, “An Alternative Approach to Enhance the Performance of High Sulfur-Loading Electrodes for Li-S Batteries”, *ACS Energy Letteres*, Vol. 1, No. 1, pp. 136–141,2016.

33. Jeong S., D. Bresser, D. Buchholz, M. Winter, and S. Passerini, “Carbon Coated Lithium Sulfide Particles for Lithium Battery Cathodes”, *Journal of Power Sources*, Vol. 235, pp. 220–225, 2013.

34. Zu C., Y. S. Su, Y. Fu, and A. Manthiram, "Improved Lithium-Sulfur Cells with a Treated Carbon Paper Interlayer", *Physical Chemistry Chemical Physics*, Vol. 15, No. 7, pp. 2291–2297, 2013.

35. Li M., W. Wahyudi, P. Kumar, F. Wu, X. Yang, H. Li, L. J. Li, and J. Ming, "Scalable Approach to Construct Free-Standing and Flexible Carbon Networks for Lithium-Sulfur Battery", *ACS Applied Materials and Interfaces*, Vol. 9, No. 9, pp. 8047–8054, 2017.

36. Li M., Y. Wan, J. Huang, A. H. Assen, C. Hsiung, H. Jiang, Y. Han, M. Eddaoudi, Z. Lai, J. Ming, and L. Li, "Metal-Organic Framework-Based Separators for Enhancing Li-S Battery Stability: Mechanism of Mitigating Polysulfide Diffusion", *ACS Energy Letter*, Vol. 2, No. 10, pp. 2362–2367, 2017.

37. Yao Y. X., X. Zhang, B. Li, C. Yan, P. Chen, J. Huang, and Q. Zhang, "A Compact Inorganic Layer for Robust Anode Protection in Lithium-Sulfur Batteries", *InfoMat*, Vol. 2, No. 2, pp. 379–388, 2020.

38. Chen J., W. A. Henderson, H. Pan, B. R. Perdeu, R. Cao, J. Z. Hu, C. Wan, K. S. Han, K. T. Mueller, J. Zhang, Y. Shao, and J. Liu, "Improving Lithium-Sulfur Battery Performance under Lean Electrolyte through Nanoscale Confinement in Soft Swellable Gels", *Nano Letter*, Vol. 17, No. 5, pp. 3061–3067, 2017.

39. Ming J., M. Li, P. Kumar, and L. J. Li, "Multilayer Approach for Advanced Hybrid Lithium Battery", *ACS Nano*, Vol. 10, No. 6, pp. 6037–6044, 2016.

40. Zhu Q., C. Ye, and D. Mao, "Solid-State Electrolytes for Lithium–Sulfur Batteries: Challenges, Progress, and Strategies", *Nanomaterials*, Vol. 12, No. 20, 2022.

41. Liu G., Q. Sun, Q. Li, J. Zhang, and J. Ming, "Electrolyte Issues in Lithium-Sulfur Batteries: Development, Prospect, and Challenges", *Energy and Fuels*, Vol. 35, No. 13. American Chemical Society, pp. 10405–10427, 2021.

42. Azimi N., W. Weng, C. Takoudis, and Z. Zhang, “Improved Performance of Lithium-Sulfur Battery with Fluorinated Electrolyte”, *Electrochemical Communication*, Vol. 37, pp. 96–99, 2013.

43. Adams B. D., E. V. Carino, J. G. Connel, K. S. Han, R. Cao, J. Chen, J. Zhen, Q. Li, K. T. Mueller, W. A. Henderson, and J. Zhang, “Long Term Stability of Li-S Batteries Using High Concentration Lithium Nitrate Electrolytes”, *Nano Energy*, Vol. 40, pp. 607–617, 2017.

44. Zhang S. S., “A New Finding on the Role of $LiNO_3$ in Lithium-Sulfur Battery”, *Journal of Power Sources*, Vol. 322, pp. 99–105, 2016.

45. Karaseva E. V., E. V. Kuzmina, D. V. Kolosnitsyn, N. V. Shakirova, L. V. Sheina, and V. S. Kolosnitsyn, “The Mechanism of Effect of Support Salt Concentration in Electrolyte on Performance of Lithium-Sulfur Cells”, *Electrochimica Acta*, Vol. 296, pp. 1102–1114, 2019.

46. Liu Y., Y. Elias, J. Meng, D. Aurbach, R. Zou, D. Xia, and Q. Pang, “Electrolyte Solutions Design for Lithium-Sulfur Batteries”, *Joule*, Vol. 5, No. 9, pp. 2323–2364, 2021.

47. Emerce N. B., and D. Eroglu, “Effect of Electrolyte-to-Sulfur Ratio in the Cell on the Li-S Battery Performance”, *Journal of The Electrochemical Society*, Vol. 166, No. 8, pp. A1490–A1500, 2019.

48. Zhao M., B. Q. Li, H. J. Peng, H. Yuan, J. Y. Wei, and J. Q. Huang, “Lithium–Sulfur Batteries under Lean Electrolyte Conditions: Challenges and Opportunities”, *Angewandte Chemie - International Edition*, Vol. 59, No. 31, pp. 12636–12652, 2020.

49. Jin Q., X. Qi, F. Yang, R. Jiang, Y. Xie, L. Qie, and Y. Huang, “The Failure Mechanism of Lithium-Sulfur Batteries under Lean-Ether-Electrolyte Conditions”, *Energy Storage Materials*, Vol. 38, pp. 255–261, 2021.

50. Zerrin T., R. Shang, B. Dong, E. C. Aguilar, J. Malvin, M. Ozkan, and C. S. Ozkan, "An overlooked parameter in Li-S batteries: The Impact of Electrolyte-to-Sulfur Ratio on Capacity Fading", *Nano Energy*, Vol. 104, 2022.

51. Cha E., M. D. Patel, T. Y. Choi, and W. Choi, "Lithium-Sulfur Batteries: The Effect of High Sulfur Loading on the Electrochemical Performance", *ECS Transactions*, Vol. 85, No. 13, pp. 295–302, 2018.

52. Shen C., J. Xie, M. Zhang, P. Andrei, J. P. Zheng, M. Hendrickson, and E. J. Plichta, "A Li-Li_2S_4 Battery with Improved Discharge Capacity and Cycle Life at Low Electrolyte/Sulfur Ratios", *Journal of Power Sources*, Vol. 414, pp. 412–419, 2019.

53. Fan F. Y., and Y.-M. Chiang, "Electrodeposition Kinetics in Li-S Batteries: Effects of Low Electrolyte/Sulfur Ratios and Deposition Surface Composition", *Journal of Electrochemical Society*, Vol. 164, No. 4, pp. A917–A922, 2017.

54. Chen S., Y. Gao, Z. Yu, M. L. Gordin, J. Song, and D. Wang, "High Capacity of Lithium-Sulfur Batteries at Low Electrolyte/Sulfur Ratio Enabled by an Organosulfide Containing Electrolyte", *Nano Energy*, Vol. 31, pp. 418–423, 2017.

55. Bilal H. M., and D. Eroglu, "Assessment of Li-S Battery Performance as a Function of Electrolyte-to-Sulfur Ratio", *Journal of The Electrochemical Society*, Vol. 168, No. 3, p. 030502, 2021.

56. Zhao Y., J. Zhang, and J. Guo, "Cathode-Electrolyte Interfacial Processes in Lithium‖Sulfur Batteries under Lean Electrolyte Conditions", *ACS Applied Materials Interfaces*, Vol. 13, No. 27, pp. 31749–31755, 2021.

57. Kilic A., and D. Eroglu, "Characterization of the Effect of Cell Design on Li−S Battery Resistance Using Electrochemical Impedance Spectroscopy", *ChemElectroChem*, Vol. 8, No. 5, pp. 963–971, 2021.

58. Kolosnitsyn V. S., E. V. Karaseva, E. V. Kuzmina, and A. L. Ivanov, “Reasons for the Effect of the Amount of Electrolyte on the Performance of Lithium–Sulfur Cells”, *Russian Journal of Electrochemistry*, Vol. 52, No. 3, pp. 273–282, 2016.

59. Kumaresan K., Y. Mikhaylik, and R. E. White, “A Mathematical Model for a Lithium–Sulfur Cell”, *Journal of Electrochemical Society*, Vol. 155, No. 8, p. A576, 2008.

60. Zhang T., M. Marinescu, L. O’Neill, M. Wild, and G. Offer, “Modeling the Voltage Loss Mechanisms in Lithium-Sulfur Cells: The Importance of Electrolyte Resistance and Precipitation Kinetics”, *Physical Chemistry Chemical Physics*, Vol. 17, No. 35, pp. 22581–22586, 2015.

61. Ghaznavi M., and P. Chen, “Sensitivity Analysis of a Mathematical Model of Lithium-Sulfur Cells Part I: Applied Discharge Current and Cathode Conductivity”, *Journal of Power Sources*, Vol. 257, pp. 394–401, 2014.

62. Ghaznavi M., and P. Chen, “Sensitivity Analysis of a Mathematical Model of Lithium-Sulfur Cells: Part II: Precipitation Reaction Kinetics and Sulfur Content”, *Journal of Power Sources*, Vol. 257, pp. 402–411, 2014.

63. Ghaznavi M., and P. Chen, “Analysis of a Mathematical Model of Lithium-Sulfur Cells Part III: Electrochemical Reaction Kinetics, Transport Properties and Charging”, *Electrochim Acta*, Vol. 137, pp. 575–585, 2014.

64. Abdulkadiroglu B., H. Bektas, and D. Eroglu, “How to Model the Cathode Area in Lithium-Sulfur Batteries?”, *ChemElectroChem*, Vol. 9, No. 4, 2022.

65. He Q., Y. Gorlin, M. U. M. Patel, H. A. Gasteiger, and Y.-C. Lu, “Unraveling the Correlation between Solvent Properties and Sulfur Redox Behavior in Lithium-Sulfur Batteries”, *Journal of the Electrochemical Society*, Vol. 165, No. 16, pp. A4027–A4033, 2018.

66. Elabd A., J. Kim, D. Sethio, S. Kang, T. Kang, J. W. Choi, and A. Coskun, “Dual Functional High Donor Electrolytes for Lithium-Sulfur Batteries under Lithium Nitrate Free and Lean Electrolyte Conditions”, *ACS Energy Letters*, Vol. 7, No. 8, pp. 2459–2468, 2022.

67. Shin H., M. Baek, A. Gupta, K. Char, A. Manthiram, and J. W. Choi, “Recent Progress in High Donor Electrolytes for Lithium–Sulfur Batteries”, *Advanced Energy Materials*, Vol. 10, No. 27, 2020.

68. Kong L., L. Yin, F. Xu, J. Bian, H. Yuan, Z. Lu, and Y. Zhao, “Electrolyte Solvation Chemistry for Lithium–Sulfur Batteries with Electrolyte-Lean Conditions”, *Journal of Energy Chemistry*, Vol. 55, pp. 80–91, 2021.

69. Kaiser M. R., S. Chou, H. K. Liu, S. X. Dou, C. Wang, and J. Wang, “Structure–Property Relationships of Organic Electrolytes and Their Effects on Li/S Battery Performance”, *Advanced Materials*, Vol. 29, No. 48, 2017.

70. Baek M., H. Shin, K. Char, and J. W. Choi, “New High Donor Electrolyte for Lithium–Sulfur Batteries”, *Advanced Materials*, Vol. 32, No. 52, 2020.

APPENDIX

A. Sample of the Linearization

$$\frac{\partial \varepsilon C_{S^{2-}}}{\partial t} = -\frac{\partial}{\partial x}\left[\left(-D_{S^{2-},0} \times \varepsilon^{b}\right)\frac{\partial C_{S^{2-}}}{\partial x} - z_{S^{2-}}\frac{\left(D_{S^{2-},0} \times \varepsilon^{b}\right)}{RT}F\, C_{S^{2-}}\,\frac{\partial \phi_e}{\partial x}\right]$$
$$+\left[-\alpha_0 \times \left(\frac{\varepsilon}{\varepsilon_0}\right)^{\xi} \times \left(\frac{i_5}{F}\right)\right] - \gamma_{S^{2-},Li_2S}$$
$$\times \left[k_{Li_2S} \times \varepsilon_{Li_2S} \times \left\{\left(C_{Li^+}{}^{\gamma_{Li^+,Li_2S}} \times C_{S^{2-}}{}^{\gamma_{S^{2-},Li_2S}}\right) - K_{sp,Li_2S}\right\}\right]. \quad (A.1)$$

In Equation (A. 1), $\gamma_{S^{2-},Li_2S} = 1\ and\ \gamma_{Li^+,Li_2S} = 2$ then,

$$\frac{\partial \varepsilon}{\partial t}C_{S^{2-}} + \frac{\partial C_{S^{2-}}}{\partial t}\varepsilon = D_{S^{2-},0}\frac{\partial}{\partial x}\left(\varepsilon^{b}\frac{\partial C_{S^{2-}}}{\partial x}\right) + \frac{z_{S^{2-}}D_{S^{2-},0}F}{RT}\frac{\partial}{\partial x}\left(\varepsilon^{b}C_{S^{2-}}\frac{\partial \phi_e}{\partial x}\right)$$
$$+\frac{-a_0}{\varepsilon_0^{\xi}F}\varepsilon^{\xi} i_5 - \left[k_{Li_2S} \times \varepsilon_{Li_2S} \times \left\{\left(C_{Li^+}{}^2 \times C_{S^{2-}}\right) - K_{sp,Li_2S}\right\}\right], \quad (A.2)$$

$$\frac{\partial \varepsilon}{\partial t}C_{S^{2-}} + \frac{\partial C_{S^{2-}}}{\partial t}\varepsilon = D_{S^{2-},0}\frac{\partial}{\partial x}\left(\frac{\partial \varepsilon^{b}}{\partial x}\frac{\partial C_{S^{2-}}}{\partial x} + \frac{\partial^2 C_{S^{2-}}}{\partial x^2}\varepsilon^{b}\right)$$
$$+\frac{z_{S^{2-}}D_{S^{2-},0}F}{RT}\left(\frac{\partial \varepsilon^{b}}{\partial x}C_{S^{2-}}\frac{\partial \phi_e}{\partial x} + \frac{\partial C_{S^{2-}}}{\partial x}\varepsilon^{b}\frac{\partial \phi_e}{\partial x} + \frac{\partial^2 \emptyset_e}{\partial x^2}\varepsilon^{b}C_{S^{2-}}\right)$$
$$+\frac{-a_0}{\varepsilon_0^{\xi}F}\varepsilon^{\xi} i_5 - \left[k_{Li_2S} \times \varepsilon_{Li_2S} \times \left\{\left(C_{Li^+}{}^2 \times C_{S^{2-}}\right) - K_{sp,Li_2S}\right\}\right]. \quad (A.3)$$

The variables are expanded by the Taylor series, given Equations A.4 - A.13

$$C_{S^{2-}} = C_{S^{2-},prev} + \Delta C_{S^{2-}}, \quad (A.4)$$
$$\varepsilon = \varepsilon_{prev} + \Delta\varepsilon, \quad (A.5)$$
$$\varepsilon^{b} = \varepsilon_{prev}^{b} + b\varepsilon_{prev}^{b-1} + \Delta\varepsilon, \quad (A.6)$$
$$\varepsilon^{\xi} = \varepsilon_{prev}^{\xi} + \xi\varepsilon_{prev}^{\xi-1} + \Delta\varepsilon, \quad (A.7)$$
$$\varepsilon_{Li_2S} = \varepsilon_{Li_2S,prev} + \Delta\varepsilon_{Li_2S}, \quad (A.8)$$
$$\emptyset_e = \emptyset_{e,prev} + \Delta\emptyset_e, \quad (A.9)$$
$$i_5 = i_{5,prev} + \Delta i_5, \quad (A.10)$$
$$C_{Li^+}^2 = C_{Li^+,prev}^2 + 2C_{Li^+,prev}\,\Delta C_{Li^+}, \quad (A.11)$$

$$\frac{\partial \varepsilon}{\partial t} = \frac{\Delta \varepsilon}{\Delta t}, \tag{A. 12}$$

$$\frac{\partial C_{S^{2-}}}{\partial t} = \frac{\Delta C_{S^{2-}}}{\Delta t}. \tag{A. 13}$$

All these equations are used into the Equation A.3, and left-hand side of the equation is

$$\frac{\partial \varepsilon}{\partial \mathrm{t}}\left(\mathrm{C}_{\mathrm{S}^{2-},\mathrm{prev}} + \Delta \mathrm{C}_{\mathrm{S}^{2-}}\right) + \frac{\partial \mathrm{C}_{\mathrm{S}^{2-}}}{\partial \mathrm{t}}\left(\varepsilon_{\mathrm{prev}} + \Delta\varepsilon\right). \tag{A. 14}$$

And then, right-hand side of the equation is

$$\begin{aligned}
&\mathrm{D}_{\mathrm{S}^{2-},0}\left\{\left(\mathrm{b}\varepsilon_{\mathrm{prev}}^{\mathrm{b}-1} + \mathrm{b}(\mathrm{b}-1)\varepsilon_{\mathrm{prev}}^{\mathrm{b}-2}\Delta\varepsilon\right)\left(\frac{\partial \varepsilon_{\mathrm{prev}}}{\partial \mathrm{x}} + \frac{\partial \Delta\varepsilon}{\partial \mathrm{x}}\right)\left(\frac{\partial \mathrm{C}_{\mathrm{S}^{2-}_{\mathrm{prev}}}}{\partial \mathrm{x}} + \frac{\partial \Delta C_{S^{2-}}}{\partial \mathrm{x}}\right)\right.\\
&\left.+\left(\frac{\partial^2 \mathrm{C}_{\mathrm{S}^{2-}_{\mathrm{prev}}}}{\partial \mathrm{x}^2} + \frac{\partial^2 \Delta \mathrm{C}_{\mathrm{S}^{2-}}}{\partial \mathrm{x}^2}\right)\left(\varepsilon_{\mathrm{prev}}^{\mathrm{b}} + \mathrm{b}\varepsilon_{\mathrm{prev}}^{\mathrm{b}-1} + \Delta\varepsilon\right)\right\}\\
&+\frac{\mathrm{z}_{\mathrm{S}^{2-}}\mathrm{D}_{\mathrm{S}^{2-},0}\mathrm{F}}{\mathrm{RT}}\left\{\left[\begin{array}{l}\left(\mathrm{b}\varepsilon_{\mathrm{prev}}^{\mathrm{b}-1} + \mathrm{b}(\mathrm{b}-1)\varepsilon_{\mathrm{prev}}^{\mathrm{b}-2}\Delta\varepsilon\right)\left(\frac{\partial \varepsilon_{\mathrm{prev}}}{\partial \mathrm{x}} + \frac{\partial \Delta\varepsilon}{\partial \mathrm{x}}\right)\\ \left(\mathrm{C}_{\mathrm{S}^{2-},\mathrm{prev}} + \Delta \mathrm{C}_{\mathrm{S}^{2-}}\right)\left(\frac{\partial \emptyset_{\mathrm{e,prev}}}{\partial \mathrm{x}} + \frac{\partial \Delta \emptyset_{\mathrm{e}}}{\partial \mathrm{x}}\right)\end{array}\right]\right.\\
&+\left[\left(\varepsilon_{\mathrm{prev}}^{\mathrm{b}} + \mathrm{b}\varepsilon_{\mathrm{prev}}^{\mathrm{b}-1} + \Delta\varepsilon\right)\left(\frac{\partial \mathrm{C}_{\mathrm{S}^{2-}_{\mathrm{prev}}}}{\partial \mathrm{x}} + \frac{\partial \Delta C_{S^{2-}}}{\partial \mathrm{x}}\right)\left(\frac{\partial \emptyset_{\mathrm{e,prev}}}{\partial \mathrm{x}} + \frac{\partial \Delta \emptyset_{\mathrm{e}}}{\partial \mathrm{x}}\right)\right]\\
&\left.+\left[\left(\varepsilon_{\mathrm{prev}}^{\mathrm{b}} + \mathrm{b}\varepsilon_{\mathrm{prev}}^{\mathrm{b}-1} + \Delta\varepsilon\right)\left(\frac{\partial^2 \emptyset_{\mathrm{e,prev}}}{\partial \mathrm{x}^2} + \frac{\partial^2 \Delta \emptyset_{\mathrm{e}}}{\partial \mathrm{x}^2}\right)\left(\mathrm{C}_{\mathrm{S}^{2-},\mathrm{prev}} + \Delta \mathrm{C}_{\mathrm{S}^{2-}}\right)\right]\right\}\\
&+\frac{-a_0}{\varepsilon_0^{\xi} F}\left(\varepsilon_{\mathrm{prev}}^{\xi} + \xi\varepsilon_{\mathrm{prev}}^{\xi-1} + \Delta\varepsilon\right)\left(i_{5,prev} + \Delta i_5\right)\\
&-\left\{k_{Li_2S}\left(\varepsilon_{Li_2S,prev} + \Delta\varepsilon_{Li_2S}\right)\left[\left(C_{Li^+,prev}^2 + 2C_{Li^+,prev}\,\Delta C_{Li^+}\right)\left(\mathrm{C}_{\mathrm{S}^{2-},\mathrm{prev}} + \Delta \mathrm{C}_{\mathrm{S}^{2-}}\right)\right.\right.\\
&\left.\left.- K_{sp,Li_2S}\right]\right\}.
\end{aligned} \tag{A. 15}$$

Nonlinear terms are neglected and then equation rearranged according to the Equation 4.145. Therefore, left-hand side of the equation becomes,

$$\left(D_{S^{2-},0}\,\varepsilon_{prev}^{b}\right)\frac{\partial \Delta C_{S^{2-}}}{\partial x}+\left(\frac{z_{S^{2-}}D_{S^{2-},0}F}{RT}\varepsilon_{prev}^{b}C_{S^{2-},prev}\right)\frac{\partial^2 \Delta \emptyset_e}{\partial x^2}$$
$$+\left(D_{S^{2-},0}b\varepsilon_{prev}^{b-1}\frac{\partial \varepsilon_{prev}}{\partial x}+\frac{z_{S^{2-}}D_{S^{2-},0}F}{RT}\varepsilon_{prev}^{b}\frac{\partial \emptyset_{e,prev}}{\partial x}\right)\frac{\partial \Delta C_{S^{2-}}}{\partial x}$$
$$+\frac{z_{S^{2-}}D_{S^{2-},0}F}{RT}\left(b\varepsilon_{prev}^{b-1}\frac{\partial \varepsilon_{prev}}{\partial x}C_{S^{2-},prev}+\varepsilon_{prev}^{b}\frac{\partial C_{S_{prev}^{2-}}}{\partial x}\right)\frac{\partial \Delta \emptyset_e}{\partial x}$$
$$+\left(D_{S^{2-},0}b\varepsilon_{prev}^{b-1}\frac{\partial C_{S_{prev}^{2-}}}{\partial x}+\frac{z_{S^{2-}}D_{S^{2-},0}F}{RT}b\varepsilon_{prev}^{b-1}C_{S^{2-},prev}\frac{\partial \emptyset_{e,prev}}{\partial x}\right)\frac{\partial \Delta \varepsilon}{\partial x}$$
$$+\left(-\frac{\varepsilon_{prev}}{\Delta t}+\frac{z_{S^{2-}}D_{S^{2-},0}F}{RT}\left[b\varepsilon_{prev}^{b-1}\frac{\partial \varepsilon_{prev}}{\partial x}\frac{\partial \emptyset_{e,prev}}{\partial x}+\varepsilon_{prev}^{b}\frac{\partial^2 \emptyset_{e,prev}}{\partial x^2}\right]\right.$$
$$\left.-k_{Li_2S}\,\varepsilon_{Li_2S,prev}C_{Li^+,prev}^{2}\right)\Delta C_{S^{2-}}$$
$$+\left(-2k_{Li_2S}\,\varepsilon_{Li_2S,prev}C_{Li^+,prev}\,C_{S^{2-},prev}\right)\Delta C_{Li^+}$$
$$+\left(-\frac{C_{S^{2-},prev}}{\Delta t}+D_{S^{2-},0}b(b-1)\varepsilon_{prev}^{b-2}\frac{\partial \varepsilon_{prev}}{\partial x}\frac{\partial C_{S_{prev}^{2-}}}{\partial x}+D_{S^{2-},0}\frac{\partial C_{S_{prev}^{2-}}}{\partial x}b\varepsilon_{prev}^{b-1}\right.$$
$$+\frac{z_{S^{2-}}D_{S^{2-},0}F}{RT}\begin{bmatrix} b(b-1)\varepsilon_{prev}^{b-2}\frac{\partial \varepsilon_{prev}}{\partial x}C_{S^{2-},prev}\frac{\partial \emptyset_{e,prev}}{\partial x} \\ +b\varepsilon_{prev}^{b-1}\frac{\partial C_{S_{prev}^{2-}}}{\partial x}\frac{\partial \emptyset_{e,prev}}{\partial x}+b\varepsilon_{prev}^{b-1}\frac{\partial^2 \emptyset_{e,prev}}{\partial x^2}C_{S^{2-},prev}\end{bmatrix}$$
$$\left.+\frac{-a_0}{\varepsilon_0^{\xi}F}\,\xi\varepsilon_{prev}^{\xi-1}i_{5,prev}\right)\Delta\varepsilon$$
$$+\left(\frac{-a_0}{\varepsilon_0^{\xi}F}\varepsilon_{prev}^{\xi}\right)\Delta i_5+k_{Li_2S}\left(K_{sp,Li_2S}-C_{Li^+,prev}^{2}C_{S^{2-},prev}\right)\Delta\varepsilon_{Li_2S}. \qquad (A.16)$$

Then, right-hand side of the equation is

$$-\left(D_{S^{2-},0}b\varepsilon_{prev}^{b-1}\frac{\partial \varepsilon_{prev}}{\partial x}\frac{\partial C_{S_{prev}^{2-}}}{\partial x}+D_{S^{2-},0}\frac{\partial^2 C_{S_{prev}^{2-}}}{\partial x^2}\,\varepsilon_{prev}^{b}\right.$$
$$+\frac{z_{S^{2-}}D_{S^{2-},0}F}{RT}\left[b\varepsilon_{prev}^{b-1}\frac{\partial \varepsilon_{prev}}{\partial x}C_{S^{2-},prev}\frac{\partial \emptyset_{e,prev}}{\partial x}+\varepsilon_{prev}^{b}\frac{\partial C_{S_{prev}^{2-}}}{\partial x}\frac{\partial \emptyset_{e,prev}}{\partial x}\right.$$
$$\left.+\varepsilon_{prev}^{b}\frac{\partial^2 \emptyset_{e,prev}}{\partial x^2}C_{S^{2-},prev}\right]+\frac{-a_0}{\varepsilon_0^{\xi}F}\varepsilon_{prev}^{\xi}i_{5,prev}$$
$$\left.-k_{Li_2S}\,\varepsilon_{Li_2S,prev}C_{Li^+,prev}^{2}C_{S^{2-},prev}+k_{Li_2S}\,\varepsilon_{Li_2S,prev}K_{sp,Li_2S}\right). \qquad (A.17)$$

After the linearization the linearization coefficients are

$$a_{7,7} = \mathrm{D}_{\mathrm{S}^{2-},0}\,\varepsilon_{\mathrm{prev}}^{\mathrm{b}}\,, \tag{A.18}$$

$$a_{7,15} = \frac{\mathrm{z}_{\mathrm{S}^{2-}}\mathrm{D}_{\mathrm{S}^{2-},0}\mathrm{F}}{\mathrm{RT}}\varepsilon_{\mathrm{prev}}^{\mathrm{b}}\mathrm{C}_{\mathrm{S}^{2-},\mathrm{prev}}\,, \tag{A.19}$$

$$b_{7,7} = \mathrm{D}_{\mathrm{S}^{2-},0}\mathrm{b}\varepsilon_{\mathrm{prev}}^{\mathrm{b}-1}\frac{\partial\varepsilon_{\mathrm{prev}}}{\partial\mathrm{x}} + \frac{\mathrm{z}_{\mathrm{S}^{2-}}\mathrm{D}_{\mathrm{S}^{2-},0}\mathrm{F}}{\mathrm{RT}}\varepsilon_{\mathrm{prev}}^{\mathrm{b}}\frac{\partial\emptyset_{\mathrm{e,prev}}}{\partial\mathrm{x}}\,, \tag{A.20}$$

$$b_{7,15} = \frac{\mathrm{z}_{\mathrm{S}^{2-}}\mathrm{D}_{\mathrm{S}^{2-},0}\mathrm{F}}{\mathrm{RT}}\left(\mathrm{b}\varepsilon_{\mathrm{prev}}^{\mathrm{b}-1}\frac{\partial\varepsilon_{\mathrm{prev}}}{\partial\mathrm{x}}\mathrm{C}_{\mathrm{S}^{2-},\mathrm{prev}} + \varepsilon_{\mathrm{prev}}^{\mathrm{b}}\frac{\partial\mathrm{C}_{\mathrm{S}_{\mathrm{prev}}^{2-}}}{\partial\mathrm{x}}\right), \tag{A.21}$$

$$b_{7,18} = \mathrm{D}_{\mathrm{S}^{2-},0}\mathrm{b}\varepsilon_{\mathrm{prev}}^{\mathrm{b}-1}\frac{\partial\mathrm{C}_{\mathrm{S}_{\mathrm{prev}}^{2-}}}{\partial\mathrm{x}} + \frac{\mathrm{z}_{\mathrm{S}^{2-}}\mathrm{D}_{\mathrm{S}^{2-},0}\mathrm{F}}{\mathrm{RT}}\mathrm{b}\varepsilon_{\mathrm{prev}}^{\mathrm{b}-1}\mathrm{C}_{\mathrm{S}^{2-},\mathrm{prev}}\frac{\partial\emptyset_{\mathrm{e,prev}}}{\partial\mathrm{x}}, \tag{A.22}$$

$$d_{7,7} = -\frac{\varepsilon_{\mathrm{prev}}}{\Delta\mathrm{t}} + \frac{\mathrm{z}_{\mathrm{S}^{2-}}\mathrm{D}_{\mathrm{S}^{2-},0}\mathrm{F}}{\mathrm{RT}}\left[\mathrm{b}\varepsilon_{\mathrm{prev}}^{\mathrm{b}-1}\frac{\partial\varepsilon_{\mathrm{prev}}}{\partial\mathrm{x}}\frac{\partial\emptyset_{\mathrm{e,prev}}}{\partial\mathrm{x}} + \varepsilon_{\mathrm{prev}}^{\mathrm{b}}\frac{\partial^2\emptyset_{\mathrm{e,prev}}}{\partial\mathrm{x}^2}\right] - \mathrm{k}_{\mathrm{Li_2S}}\,\varepsilon_{\mathrm{Li_2S,prev}}\mathrm{C}_{\mathrm{Li}^+,\mathrm{prev}}^2 \tag{A.23}$$

$$d_{7,1} = -2\mathrm{k}_{\mathrm{Li_2S}}\,\varepsilon_{\mathrm{Li_2S,prev}}\mathrm{C}_{\mathrm{Li}^+,\mathrm{prev}}\,\mathrm{C}_{\mathrm{S}^{2-},\mathrm{prev}}\,, \tag{A.24}$$

$$d_{7,13} = \frac{-\mathrm{a}_0}{\varepsilon_0^{\xi}\mathrm{F}}\varepsilon_{\mathrm{prev}}^{\xi}\,, \tag{A.25}$$

$$\begin{aligned} d_{7,18} = {} & -\frac{\mathrm{C}_{\mathrm{S}^{2-},\mathrm{prev}}}{\Delta\mathrm{t}} + \mathrm{D}_{\mathrm{S}^{2-},0}\mathrm{b}(\mathrm{b}-1)\varepsilon_{\mathrm{prev}}^{\mathrm{b}-2}\frac{\partial\varepsilon_{\mathrm{prev}}}{\partial\mathrm{x}}\frac{\partial\mathrm{C}_{\mathrm{S}_{\mathrm{prev}}^{2-}}}{\partial\mathrm{x}} \\ & + \mathrm{D}_{\mathrm{S}^{2-},0}\frac{\partial\mathrm{C}_{\mathrm{S}_{\mathrm{prev}}^{2-}}}{\partial\mathrm{x}}\mathrm{b}\varepsilon_{\mathrm{prev}}^{\mathrm{b}-1} + \frac{\mathrm{z}_{\mathrm{S}^{2-}}\mathrm{D}_{\mathrm{S}^{2-},0}\mathrm{F}}{\mathrm{RT}} \\ & \times\left[\mathrm{b}(\mathrm{b}-1)\varepsilon_{\mathrm{prev}}^{\mathrm{b}-2}\frac{\partial\varepsilon_{\mathrm{prev}}}{\partial\mathrm{x}}\mathrm{C}_{\mathrm{S}^{2-},\mathrm{prev}}\frac{\partial\emptyset_{\mathrm{e,prev}}}{\partial\mathrm{x}}\right. \\ & \left. + \mathrm{b}\varepsilon_{\mathrm{prev}}^{\mathrm{b}-1}\frac{\partial\mathrm{C}_{\mathrm{S}_{\mathrm{prev}}^{2-}}}{\partial\mathrm{x}}\frac{\partial\emptyset_{\mathrm{e,prev}}}{\partial\mathrm{x}} + \mathrm{b}\varepsilon_{\mathrm{prev}}^{\mathrm{b}-1}\frac{\partial^2\emptyset_{\mathrm{e,prev}}}{\partial\mathrm{x}^2}\mathrm{C}_{\mathrm{S}^{2-},\mathrm{prev}}\right] \\ & + \frac{-\mathrm{a}_0}{\varepsilon_0^{\xi}\mathrm{F}}\,\xi\varepsilon_{\mathrm{prev}}^{\xi-1}i_{5,\mathrm{prev}}\,, \end{aligned} \tag{A.26}$$

$$d_{7,19} = \mathrm{k}_{\mathrm{Li_2S}}\left(\mathrm{K}_{\mathrm{sp,Li_2S}} - \mathrm{C}_{\mathrm{Li}^+,\mathrm{prev}}^2\mathrm{C}_{\mathrm{S}^{2-},\mathrm{prev}}\right), \tag{A.27}$$

$$g_7 = -\Bigg(D_{S^{2-},0} b \varepsilon_{prev}^{b-1} \frac{\partial \varepsilon_{prev}}{\partial x} \frac{\partial C_{S^{2-}_{prev}}}{\partial x} + D_{S^{2-},0} \frac{\partial^2 C_{S^{2-}_{prev}}}{\partial x^2} \varepsilon_{prev}^{b}$$

$$+ \frac{z_{S^{2-}} D_{S^{2-},0} F}{RT} \Bigg[b \varepsilon_{prev}^{b-1} \frac{\partial \varepsilon_{prev}}{\partial x} C_{S^{2-},prev} \frac{\partial \emptyset_{e,prev}}{\partial x} + \varepsilon_{prev}^{b} \frac{\partial C_{S^{2-}_{prev}}}{\partial x} \frac{\partial \emptyset_{e,prev}}{\partial x}$$

$$+ \varepsilon_{prev}^{b} \frac{\partial^2 \emptyset_{e,prev}}{\partial x^2} C_{S^{2-},prev} \Bigg] + \frac{-a_0}{\varepsilon_0^{\xi} F} \varepsilon_{prev}^{\xi} i_{5,prev}$$

$$- k_{Li_2S} \varepsilon_{Li_2S,prev} C_{Li^+,prev}^2 C_{S^{2-},prev} + k_{Li_2S} \varepsilon_{Li_2S,prev} K_{sp,Li_2S} \Bigg). \qquad (A.28)$$